98-69-7423
MOTC-IOT-97-H2DA006-1

沈箱受碎波波力作用之初始運動模態評估準則

交 通 部 運 輸 研 究 所
中華民國 98 年 5 月

98-69-7423
MOTC-IOT-97-H2DA006-1

沈箱受碎波波力作用之初始運動模態評估準則

著者：董啟超、林炤圭、邱永芳

交 通 部 運 輸 研 究 所
中華民國 98 年 5 月

98

沈箱受碎波波力作用之初始運動模態評估準則

交通部運輸研究所

GPN:1009801341
定價 200 元

沈箱受碎波波力作用之初始運動模態評估準則

著　　者：董啓超、林炤圭、邱永芳
出版機關：交通部運輸研究所
地　　址：10548 臺北市敦化北路 240 號
網　　址：www.ihmt.gov.tw (中文版＞中心出版品)
電　　話：(04)26587176
出版年月：中華民國 98 年 5 月
印 刷 者：良機事務機器有限公司
版(刷)次冊數：初版一刷 110 冊
本書同時登載於交通部運輸研究所網站
定　　價： 200 元
展 售 處：
交通部運輸研究所運輸資訊組•電話：(02)23496880
國家書店松江門市：10485 臺北市中山區松江路 209 號 F1•電話：(02) 25180207
五南文化廣場：40042 臺中市中山路 6 號•電話：(04)22260330

GPN：1009801341　　　　ISBN：978-986-01-8721-2 (平裝)

交通部運輸研究所自行研究計畫出版品摘要表

<table>
<tr><td colspan="4">出版品名稱：沉箱受碎波波力作用之初始運動模態評估準則</td></tr>
<tr><td>國際標準書號（或叢刊號）
ISBN 978-986-01-8721-2（平裝）</td><td>政府出版品統一編號
1009801341</td><td>運輸研究所出版品編號
98-69-7423</td><td>計畫編號
97-H2DA006-1</td></tr>
<tr><td colspan="3">主辦單位：港灣技術研究中心
主管：邱永芳
總計劃主持人：董啟超
計劃主持人：林炤圭、邱永芳
研究人員：
聯絡電話：886-4-26587101
傳真號碼：886-4-26571329</td><td>研究期間
自 97 年 01 月
至 97 年 12 月</td></tr>
<tr><td colspan="4">關鍵詞：靜止、滑動、搖晃、搖晃且滑動</td></tr>
<tr><td colspan="4">摘要：
本報告探討一個假設放置在粗糙底床的理想化剛性沈箱在且受到如碎波波力的短時間作用的集中力以及上揚力作用下發生不同型態運動(靜止、滑動、搖晃、以及搖晃且滑動)的啟動條件。分析的方法與董等人(2005)「自由剛性塊體受水平力作用下的行為模式」報告相同，僅是該研究並未考慮上揚力的作用。雖然分析的方法是很直截了當，但由於包含了許多種狀況，使得相當地分析過程複雜且冗長，因此本報告僅探討碎波波力作用於沈箱的質量中心以上的狀況。</td></tr>
</table>

<table>
<tr><td>出版日期</td><td>頁數</td><td>定價</td><td>本 出 版 品 取 得 方 式</td></tr>
<tr><td>98 年 5 月</td><td>96</td><td>200</td><td>凡屬機密性出版品均不對外公開。普通性出版品，公營、公益機關團體及學校可函洽本所免費贈閱；私人及私營機關團體可按定價價購。</td></tr>
<tr><td colspan="4">機密等級：
□密□機密 □極機密 □絕對機密
（解密條件：□ 年 月 日解密，□公布後解密，□附件抽存後解密，
□工作完成或會議終了時解密，□另行檢討後辦理解密）
■普通</td></tr>
<tr><td colspan="4">備註：本研究之結論與建議不代表交通部之意見。</td></tr>
</table>

PUBLICATION ABSTRACTS OF RESEARCH PROJECTS
INSTITUTE OF TRANSPORTATION
MINISTRY OF TRANSPORTATION AND COMMUNICATIONS

TITLE: Criteria for the Initiation of Modes of a Caisson Subjected to a Breaking Wave Force			
ISBN (OR ISSN) ISBN978-986-01-8721-2 (pbk)	GOVERNMENT PUBLICATIONS NUMBER 1009801341	IOT SERIAL NUMBER 98-69-7423	PROJECT NUMBER 97-H2DA006-1
DIVISION: HARBOR & MARINE TECHNOLOGY CENTER DIVISION DIRECTOR: Chiu Yung-fang PROJECT ADVISOR: Chi-Chao Tun g PRINCIPAL INVESTIGATOR: Jaw-Guei Lin, Yung-Fang Chiu PROJECT STAFF: PHONE: 886-4-26587101 FAX: 886-4-26571329			PROJECT PERIOD FROM January 2008 TO December 2008
KEY WORDS: rest, slide, rock and rock slide			

ABSTRACT:

In this report, the conditions for the initiation of various (rest, slide, rock and rock slide) modes of motions of an idealized caisson are obtained analytically. The caisson is modeled as a rigid body placed on a frictional base under the action of a concentrated force of short duration representing a breaking wave force as well as the action of an accompanying uplift force. The method of analysis is the same as that of a previous study in which the effect of uplift force was not included. The analysis, though straightforward, involves many cases and is therefore complex and lengthy. For this reason, this report considers only the situation of a breaking wave force applied above but not below the center of mass of the caisson.

DATE OF PUBLICATION	NUMBER OF PAGES	PRICE	CLASSIFICATION
May 2009	96	200	☐RESTRICTED ☐CONFIDENTIAL ☐SECRET ☐TOP SECRET ■UNCLASSIFIED

The views expressed in this publication are not necessarily those of the Ministry of Transportation and Communications.

Content

Figures

Symbols

a = quantity defined in (21)

a’ = quantity defined in (45)

B = half-width of caisson

b = quantity defined in (22)

C = center of mass of caisson

c = quantity defined in (23)

c’ = quantity defined in (46)

d = quantity defined in (24)

E = empty space in $k-\mu$ plane

e = quantity defined in (27)

e’ = quantity defined in (28)

F = horizontal applied force

FF = free-flight space in $k-\mu$ plane

f_x = horizontal reaction

f_y = vertical reaction

g = gravitational acceleration

H = half-height of caisson

h = distance between line of action of F and center of mass C

I = mass moment of inertia of caisson about center of mass C

k = quantity used to express magnitude of force F in terms of weight of caisson

k' = quantity used to express distance of force F from center of mass C in terms of h

k_A	= quantity defined in (7)
k_C	= quantity defined in (35)
k_D	= quantity defined in (14)
k_E	= quantity defined in (47)
k_F	$= d/c'$
$k_{F'}$	$= (1+\gamma^2)/\left[3\gamma k' + q(2+\gamma^2)\right]$
k_G	= quantity defined in (52)
m	= total mass of caisson
q	= quantity used to express magnitude of uplift force U in terms of applied force F
q_1	$= 3k'/\gamma$
q_2	= quantity defined in (47)
q_4	$= \left[-\left(4+\gamma^2\right)/2\gamma\right] + 3\gamma k'/2$
q_G	= quantity defined in (52)
RE	= symbol used to represent region of rest mode
RO	= symbol used to represent region of rock about point O mode
RO'	= symbol used to represent region of rock about point O' mode
SL	= symbol used to represent region of slide mode
SRO_-	= symbol used to represent region of slide-rock about point O mode with $\ddot{x}_O \leq 0$
SRO_+	= symbol used to represent region of slide-rock about point O mode with $\ddot{x}_O \geq 0$

SRO'_- = symbol used to represent region of slide-rock about point O' mode with $\ddot{x}_O \le 0$

x = horizontal displacement of center of mass C

x_O = horizontal displacement of O at base of caisson

$x_{O'}$ = horizontal displacement of O' at base of caisson

y = vertical displacement of center of mass C

γ = H/B, aspect ratio of caisson

θ = rotation of caisson

μ = coefficient of friction between caisson and base

μ_A = quantity defined in (8)

μ_C = quantity defined in (35)

$\mu_O(k)$ = curve defined in (6)

$\mu_1(k)$ = curve defined in (13)

$\mu_2(k)$ = $(a'k-b)/(d-c'k)$

$\mu^*(k)$ = curve defined in (26)

$\mu^{**}(k)$ = curve defined in (51)

ξ = distance between line of action of f_y and center of mass C

$|\ |$ = absolute value sign

Over-dot = differentiation with respect to time

I. Introduction

In a previous study (see Refs.1, 2) we obtained conditions for the initiation of various (rest, slide, rock and slide-rock) modes of motion of a rigid body placed on a frictional base under the action of a concentrated force of short duration. The study was motivated by our desire to better understand the behavior of a caisson due to a breaking wave force.

Since there had not been previous work done on the subject as described in Refs.1, 2, and in anticipation that the work would be rather involved, the uplift force acting at the bottom of a caisson that normally accompanies a breaking wave was not included in the study. Indeed, our investigation (see Refs.1, 2) shows that the analysis is complex and a caisson behaves rather differently depending on whether the force is applied above or below the center of mass of the body.

In the present study, the uplift force is included. The approach of the analysis follows that in the previous work (see Refs.1, 2). The analysis, though straight forward, involves many cases and is therefore complex and lengthy. For this reason, this report considers only the situation of a breaking wave force applied above but not below the center of mass of the body. The presentation is necessarily brief; only the essentials of the analysis are given.

The report begins with a section ‘Models’ which describes the models employed for the caisson, the breaking wave force and the uplift force. This is followed by sections of derivations of the criteria for the initiation of the various modes.

II. Models

Consider a plane rigid body, partially immersed in water, of uniform mass distribution, the total mass in water being m (see Fig.1). The body is rectangular in elevation and footprint whose height is $2H$, width $2B$ and depth equal to unity. It rests on a horizontal frictional base. The friction between the base and the body is of the Coulomb type with coefficient of static friction μ. The body is initially at rest and is subjected to a breaking wave which imparts pressures on the seaward side of the vertical wall. The resultant of the pressures is the horizontal force F which is assumed to act on the body only for a short duration. The force is expressed in terms of the weight of the body in water as $F = mgk$ where g is gravitational acceleration and k is a non-dimensional coefficient. In this study, we consider only the case in which F is applied above, and at a distance h from the center of mass of the body where $h = k'H$ and $0 \le k' \le 1$. The breaking wave also induces pressures on the bottom of the body whose distribution along the width of the body is assumed to be triangular, decreasing from maximum on the seaward side to zero on the landward side. The resultant of the pressures is denoted by $U = qF = mgkq$ where the quantity q is a non-dimensional coefficient. The motion of the plane body is specified by the horizontal and vertical displacements of the center of mass C of the body and its rotation, θ, considered positive in the counterclockwise direction. The horizontal and vertical displacements of C are x and y, considered positive to the right and upwards respectively as shown in Fig.1. The reaction forces are f_x and f_y, positive to the right and upwards respectively. f_y acts at a distance ξ from C. The uplift force U acts at a distance $B/3$ from C.

III. Rest (RE)

When the body is at rest, the equations of equilibrium are:

$$f_x = F = mgk \quad \text{(1)}$$

$$f_y = mg - U = mg(1 - qk) \quad \text{(2)}$$

and, by taking moment of the forces about C,

$$f_x H + f_y \xi + Fh + UB/3 = 0 \quad \text{(3)}$$

By substituting (1) and (2) into (3), we get

$$\xi = -\frac{Bk[\gamma(1+k') + q/3]}{1 - qk} \quad \text{(4)}$$

where $\gamma = H/B$ is the aspect ratio of the body.

For the body to be in contact with the base, f_y must be greater than or equal to zero, or

$$k \le \frac{1}{q} \quad \text{(5)}$$

For the body to be at rest, f_x must be smaller than or equal to the limiting Coulomb friction force μf_y. That is,

$$\mu \ge \frac{f_x}{f_y} = \frac{k}{1 - qk} \equiv \mu_0(k) \quad \text{(6)}$$

Finally, f_y must remain within the base (OO') of the body; i.e. $|\xi| \le B$. From (4), for the condition to be satisfied, it requires

$$k \le \frac{1}{\gamma(1+k') + 4q/3} \equiv k_A \quad \text{(7)}$$

It may be verified that $k_A \le 1/q$. The above conditions (6) and (7) constitute the criteria for the body to remain at rest under the action of F and U, the resultants of the distributed short duration pressures due to a breaking wave. These conditions may be conveniently presented graphically as a region using the parameters k and μ as the horizontal and the vertical axes respectively as shown in Fig.2.

The curve OA or $\mu_0(k)$ and the line AH or $k = k_A$ intersect at point A with coordinates $k = k_A$ and

$$\mu = \mu_A = \frac{1}{\gamma(1+k')+q/3} \geq k_A \quad \text{...} (8)$$

The region that represents the rest mode is shaded and denoted by the symbol RE in Fig.2.

It may be seen from (7) and (8) and Fig.2 that the larger the values of γ, k' and q, the closer is the line AH to the μ axis, the narrower is the rest region and the less likely is the body to remain at rest. Also, when $q = 0$, the result agrees with those obtained earlier in Refs.1, 2.

IV. Slide (SL)

The equations of motion for the initiation of a slide mode are the same as those for a rest mode except the equation in the x-direction. They are:

$$m\ddot{x} = f_x - F \quad \text{..........(9)}$$

$$f_y = mg - U = mg(1-qk) \quad \text{..........(10)}$$

and,

$$f_x H + f_y \xi + Fh + UB/3 = 0 \quad \text{..........(11)}$$

Here and hereafter, over-dot denotes differentiation with respect to time. The conditions for a slide mode to occur are $f_y \geq 0$, $f_x = \mu f_y$ and $|\xi| \leq B$. The condition $f_y \geq 0$ gives, from (10), $k \leq 1/q$. Equation (11) gives

$$\xi = -\frac{k(k'H + qB/3) + \mu H(1-qk)}{1-qk} \quad \text{..........(12)}$$

For $k \leq 1/q$, ξ is always smaller than or equal to zero. The condition $|\xi| \leq B$ therefore requires,

$$\mu \leq \frac{(1/\gamma) - k[k' + (4q/3\gamma)]}{1-qk} \equiv \mu_1(k) \quad \text{..........(13)}$$

The curve $\mu_1(k)$ is sketched in Fig.3 in the $k-\mu$ plane; it intersects $\mu_0(k)$ at point A, and the horizontal k axis at D where the abscissa is

$$k_D = \frac{1}{\gamma k' + 4q/3} \quad \text{..........(14)}$$

Beyond k_D, the curve μ_1 is negative and goes to negative infinity as k approaches $1/q$.

The region corresponding to a slide mode is the shaded area OAD in Fig.3. The symbol SL is used to denote the slide mode. In region OAM, the rest mode governs because the horizontal reaction force f_x in a rest mode is smaller than the horizontal reaction force f_x in the slide mode. From (9), we have $\ddot{x} = (1 - qk)(\mu - \mu_0)$. In the region of slide mode, (OAD), $k \le 1/q$ and $\mu \le \mu_0$; thus, $\ddot{x} \le 0$. Since the body is originally at rest, $\dot{x} \le 0$ and $x \le 0$. That is, the body slides to the left under the action of F, as expected.

V. Rock about point O (RO)

When a body is about to rock about point O, the equations of motion are:

$$m\ddot{x} = f_x - F \quad \text{.......(15)}$$

$$m\ddot{y} = f_y - mg + U \quad \text{.......(16)}$$

and, noting that f_y acts at point O (see Fig.1) about which the body rotates,

$$I\ddot{\theta} = f_x H - f_y B + Fh + UB/3 \quad \text{.......(17)}$$

Here, $I = \frac{1}{3}m(B^2 + H^2)$ is mass moment of inertia of the body about its center of mass C.

The accelerations $\ddot{x}$ and $\ddot{y}$ of point C are related to the angular acceleration $\ddot{\theta}$ of the body as $\ddot{x} = -H\ddot{\theta}$ and $\ddot{y} = B\ddot{\theta}$. Equation (17) gives

$$\ddot{\theta} = \frac{3g}{4B(1+\gamma^2)}\left(\frac{k}{k_A} - 1\right) \quad \text{.......(18)}$$

where k_A is given in (7).

Equations (15) and (16) give respectively

$$f_x = \frac{mg}{4(1+\gamma^2)}(ak + b) \quad \text{.......(19)}$$

and

$$f_y = \frac{mg}{4(1+\gamma^2)}(ck + d) \quad \text{.......(20)}$$

where

$$a = 4 + \gamma^2 - 3\gamma^2 k' - 4\gamma q \quad \text{.......(21)}$$

$$b = 3\gamma \quad \text{.......(22)}$$

$$c = 3\gamma(1 + k') - 4\gamma^2 q \quad \text{.......(23)}$$

and

$$d = 1 + 4\gamma^2 \quad (24)$$

It is noted that both f_x and f_y are either positive or negative since the quantities a and c may be positive or negative. For the case of $c \geq 0$, f_y is always greater than or equal to zero. For the case of $c \leq 0$, $f_y = -|c|k + d$, in which case, $f_y \geq 0$ for $k \leq d/|c|$. For $k \geq d/|c|$, the body is in a free-flight mode.

For the body to rock about point O, $\ddot{\theta}$ must be greater than or equal to zero. This means, from (18),

$$k \geq k_A \quad (25)$$

For a rock mode to be initiated, f_x must not exceed the limiting friction force. That is, $|f_x| \leq \mu f_y$, or,

$$\mu \geq \frac{|ak + b|}{ck + d} \equiv \mu^*(k) \quad (26)$$

The function $\mu^*(k)$ behaves in a variety of ways depending on the signs of the quantities a, c and f_x. There are altogether six cases that must be considered. They are:

Case I: $a \geq 0, c \geq 0, f_x \geq 0, \mu^* = (ak + b)/(ck + d), 0 \leq k \leq \infty$

Case II: $a \geq 0,\ c \leq 0,\ f_x \geq 0,\ \mu^* = (ak + b)/(-|c|k + d),\ 0 \leq k \leq d/|c|$; for $d/|c| \leq k \leq \infty$, the body is in a free-flight mode

Case III: $a \leq 0, c \geq 0, f_x \geq 0, \mu^* = (-|a|k + b)/(ck + d), 0 \leq k \leq b/|a|$

Case IV: $a \leq 0, c \leq 0, f_x \geq 0, \mu^* = (-|a|k + b)/(-|c|k + d), 0 \leq k \leq b/|a|, 0 \leq k \leq d/|c|$; for $d/|c| \leq k \leq \infty$, the body is in a free-flight mode

Case V: $a \leq 0, c \geq 0, f_x \leq 0, \mu^* = \left|-|a|k + b\right|/(ck + d), b/|a| \leq k \leq \infty$

Case VI: $a \le 0, c \le 0, f_x \le 0, \mu^* = \left|-|a|k + b\right| / (-|c|k + d), b/|a| \le k \le \infty, k \le d/|c|$; for $d/|c| \le k \le \infty$ the body is in a free-flight mode

Properties of $\mu^*(k)$ are examined for each of the above six cases.

Case I:

The curve $\mu^*(k) = (ak + b)/(ck + d)$ passes point A (see Fig.2). As k approaches infinity, $\mu^* = (a/c) \ge 0$ The slope of $\mu^*(k)$ is $d\mu^*/dk = (ad - bc)/(ck + d)^2$ where $ad - bc = 4(1 + \gamma^2)e$ is independent of k; here

$$e = 1 + \gamma^2 - 3\gamma^2 k' - \gamma q \qquad (27)$$

which may be greater or smaller than zero. Thus the slope of $\mu^*(k)$ is a decreasing function of k and approaches zero as k approaches infinity. Also, the slope of $\mu^*(k)$ at point A is equal to $e/4(1+\gamma^2)$. Since the quantity e may be greater or smaller than zero, distinction must be made between two sub-cases: sub-case 1 is for $e \ge 0$, denoted by case I1 and sub-case 2 is for $e \le 0$ denoted by case I2. Figs. 4a and 4b show, from (25) and (26), the regions for rock mode to occur for cases I1 and I2 respectively.

For values of γ, k' and q, if k (force) and μ (coefficient of friction) correspond to a point in the $k - \mu$ plane that falls in the region to the right of the vertical line AH and above the curve $\mu = \mu^*(k)$ in Figs. 4a and 4b, a rock mode would ensue. Here the region corresponding to a rock (about point O) mode is shaded and the symbol RO is used to denote the case of rock (about point O) mode.

Case II:

In this case, $\mu^* = (ak + b)/(-|c|k + d)$ passes the point A and the expression of its slope is the same as that in case I. For $k \le d/|c|$, μ^* is greater than or equal to zero and approaches infinity at $k = d/|c|$. Thus, the slope of μ^* is greater than or equal to zero and consequently the quantity e is either greater than or equal to zero. It may be verified that $d/|c| \ge 1/q$. The region corresponding to a rock mode is identified in Fig. 5 as that to the right of AH above μ^* and to the left of the line PQ($k \le d/|c|$), shaded and denoted by RO. For $k \ge d/|c|$, the body would be lifted off the base in a free-flight mode denoted by the symbol FF.

Case III:

In this case, $\mu^* = (-|a|k + b)/(ck + d), 0 \le k \le b/|a|$. Again, $\mu^*(k)$ passes point A and is equal to zero at $k = b/|a|$; the expression of its slope is the same as that in case I and hence $e \le 0$. It may be verified that $(b/|a|) - (1/q) = e'/|a|q$ where

$$e' = e + 3 = 4 + \gamma^2 - 3\gamma^2 k' - \gamma q \quad \text{...(28)}$$

which may be greater or smaller than zero. Thus, case III is sub-divided into two cases: case III1 is for $e' \ge 0$ and case III2 is for $e' \le 0$. The regions corresponding to these two sub-cases are shown respectively in Figs. 6a and 6b to the right of line AH, left of line NL and above the curve $\mu = \mu^*(k)$. These regions are shaded as shown. The symbol E is used to mean that the region is 'empty', not covered by the cases III1 and III2.

Case IV:

In this case, $\mu^* = (-|a|k + b)/(-|c|k + d)$ for $k \le d/|c|$ and $k \le b/|a|$. By comparing $d/|c|$, $b/|a|$ and $1/q$, we see that $d/|c| - b/|a| = -[4(1+\gamma^2)e]/|ac|$, $b/|a| - 1/q = e'/(|a|q)$ and $d/|c| - 1/q = [q + 3\gamma(1 + k')]/(|c|q)$ which is always greater than zero. Thus, case IV has three sub-cases: sub-case IV1 is for $e \ge 0$, $e' \ge 0$ in which case $b/|a| \ge d/|c|$ and $b/|a| \ge 1/q$; sub-case IV2 is for $e \le 0$, $e' \ge 0$ in which case $b/|a| \le d/|c|$ and $b/|a| \ge 1/q$; finally, sub-case IV3 is for $e \le 0$, $e' \le 0$ in which case $b/|a| \le d/|c|$ and $b/|a| \le 1/q$.

In case IV1, the characteristics of μ^* are the same as those in case II. In cases IV2 and IV3, μ^* passes point A; since for these cases, $e \le 0$, the slope of μ^* decreases as k increases. Also, at $k = b/|a|$, $\mu^* = 0$.

The shaded regions shown in Figs. 7a, 7b and 7c correspond respectively to a rock mode for these cases.

Case V:

In this case, $a \le 0, c \ge 0, f_x \le 0, \mu^* = |-|a|k + b|/(ck + d)$ and $b/|a| \le k \le \infty$. The characteristics of μ^* are: at $k = b/|a|$, $\mu^* = 0$; as k approaches infinity, $\mu^* = |a|/c \ge 0$, and its slope approaches zero. Since $\mu^* \ge 0$, its slope must be greater than or equal to zero as well. Thus the quantity e must be less than zero. Since $b/|a| - 1/q = e'/(|a|q)$ which may be greater or smaller than zero, two sub-cases must be considered. In case V1, $e' \geq 0$, $b/|a| \geq 1/q$ and in case V2, $e' \leq 0$, $b/|a| \leq 1/q$. The curves μ^* are sketched in Figs. 8a and 8b respectively and a rock mode is marked as the shaded regions above the curve μ^* for $k \geq b/|a|$ to the right of line NL.

Case VI:

In this case, $a \leq 0, c \leq 0, f_x \leq 0, \mu^* = \left|-|a|k + b\right|/(-|c|k + d), b/|a| \leq k \leq \infty,$ and $k \leq d/|c|$. It is seen that at $k = b/|a|$, $\mu^* = 0$ and μ^* approaches infinity at $k = d/|c|$. Since the slope of μ^* is equal to $d\mu^*/dk = -4(1+\gamma^2)e/(-|c|k + d)^2$ and must be greater than or equal to zero, we conclude that $e \leq 0$ indicating that $b/|a| \leq d/|c|$; however, since $b/|a|$ may be greater or smaller than $1/q$, two sub-cases arise. The characteristics of μ^* are such that μ^* starts at zero at $k = b/|a|$ and slopes up and approaches infinity at $k = d/|c|$ as shown in Figs. 9a and 9b for $b/|a| \geq 1/q$ and $b/|a| \leq 1/q$ respectively. In both Figs. 9a and 9b, the shaded regions to the right of the line NL and above μ^* correspond to a rock mode. For $k \geq d/|c|$ the body is in a free-flight mode.

The six cases are divided based on the sign of a and c and that of f_x. In the analysis, it is seen that the sub-cases also depend on the sign of the quantities e and e'. Since these quantities are all functions of γ, k' and q, we identify these cases in a k'–q plane with γ as the parameter as shown in Fig. 10. The lines $a = 0$, $c = 0$, $e = 0$ and $e' = 0$ are indicated.

VI. Slide-rock about point O (SRO)

When a body is on the verge of sliding and rocking about point O simultaneously, f_y acts at O and the equations of motion are:

$$m\ddot{x} = f_x - F \quad (29)$$

$$m\ddot{y} = f_y - mg + U \quad (30)$$

and

$$I\ddot{\theta} = f_x H - f_y B + Fh + UB/3 \quad (31)$$

These equations are the same as (15), (16) and (17), those governing the initiation of a rocking motion about point O. The difference is that in the case of a rock mode, $\ddot{x} = -H\ddot{\theta}$ and $|f_x| \le \mu f_y$. In the present case, $\ddot{x}$ is not equal to $-H\ddot{\theta}$ although the relation $\ddot{y} = B\ddot{\theta}$ is still valid, and f_x is either equal to μf_y or $-\mu f_y$. In the following, the two cases of $f_x = \mu f_y$ and $f_x = -\mu f_y$ are treated separately. In a rock about point O mode, the cases I, II, III, and IV correspond to $f_x \ge 0$ and the cases V and VI are for $f_x \le 0$. The study of slide-rock about point O mode is also divided into these six cases.

Case I: $a \ge 0, c \ge 0, f_x = \mu f_y$

For $f_x = \mu f_y$, from (31),

$$\ddot{\theta} = \frac{3g}{B(4+\gamma^2-3\mu\gamma)}\{\mu\gamma - 1 + k[k'\gamma + q(\frac{4}{3} - \mu\gamma)]\} \quad (32)$$

and, from (30)

$$f_y = \frac{mg}{4+\gamma^2-3\mu\gamma}[1+\gamma^2 - k\gamma(q\gamma - 3k')] \quad (33)$$

For the case under consideration, $f_x \ge 0$, so that the velocity at point O, denoted $\dot{x}_O$, of the body about which rotation takes place is less than or equal to zero. It suffices to examine the acceleration $\ddot{x}_O$ of point O when a slide-rock mode of motion is impending, the body being initially at rest. Noting that $\ddot{x}_O = \ddot{x} + H\ddot{\theta}$ and $\ddot{x}$ is given by (29), we get

$$\ddot{x}_O = \frac{g}{4+\gamma^2-3\mu\gamma}[\mu(ck+d)-(ak+b)] \text{ ....}(34)$$

For a slide-rock (about point O) mode to occur, we must have $\ddot{\theta} \geq 0$, $f_y \geq 0$ and, with $f_x = \mu f_y \geq 0$, $\dot{x}_O \leq 0$.

Case I has two sub-cases: I1 for $e \geq 0$ and I2 for $e \leq 0$. These sub-cases are discussed below.

Case I1: ($e \geq 0$). The condition $f_y \geq 0$ is satisfied provided, from (33), (a) $\mu \leq \mu_c$ and $k \leq k_C$, and, (b) $\mu \geq \mu_c$ and $k \geq k_C$.

Here,

$$\mu_c \equiv (4+\gamma^2)/3\gamma, \quad k_C \equiv (1+\gamma^2)/\gamma(q\gamma - 3k') \text{ ....}(35)$$

Depending on whether $q\gamma \geq 3k'$ or $q\gamma \leq 3k'$, k_C may be greater or smaller than zero. Sub-case I1 is therefore further divided into cases I1,1 and I1,2 for $q\gamma \geq 3k'$ and $q\gamma \leq 3k'$ respectively.

To visualize these requirements, reference is made to Figs. 11a and 11b for $q\gamma \geq 3k'$ ($k_C \geq 0$) (case I1,1) and $q\gamma \leq 3k'$ ($k_C \leq 0$) (case I1,2) respectively. It is noted that μ_C intersects μ^* (see Figs. 4a and 4b) at $k = k_C$ for $k_C \geq 0$ or, equivalently, $q\gamma \geq 3k'$. For $q\gamma \leq 3k'$, μ_C and μ^* do not intersect.

In Fig. 11a, the shaded region to the left of SR and below μ_C and the shaded region to the right of SR and above μ_C are the regions in which the condition $f_y \geq 0$ is satisfied. In Fig. 11b, the shaded region below μ_C corresponds to the condition $f_y \geq 0$; otherwise, the body is in a state of free-flight.

Similarly, the regions corresponding to $\ddot{x}_O \leq 0$ are (a) $\mu \leq \mu_c$ and $\mu \leq \mu^*$, and, (b) $\mu \geq \mu_c$ and $\mu \geq \mu^*$. These regions are shown in Fig. 12a for $q\gamma \geq 3k'$ and Fig.12b for $q\gamma \leq 3k'$ as shaded regions.

Finally, the condition $\ddot{\theta} \geq 0$ is satisfied provided: for $k \leq 1/q$, (a) $\mu \leq \mu_c$, $\mu \geq \mu_1$, and, (b) $\mu \geq \mu_c$, $\mu \leq \mu_1$; for $k \geq 1/q$, (a) $\mu \leq \mu_c$, $\mu \leq \mu_1$ and (b) $\mu \geq \mu_c$, $\mu \geq \mu_1$. Here, μ_1 is defined in (13) in the slide (SL) section. A branch of μ_1 is added for $k \geq 1/q$. The regions corresponding to $\ddot{\theta} \geq 0$

are shown in Figs. 13a and 13b for the cases I1,1 ($q\gamma \geq 3k'$) and I1,2 ($q\gamma \leq 3k'$) respectively.

By combining the conditions $f_y \geq 0$, $\ddot{x}_O \leq 0$ and $\ddot{\theta} \geq 0$, the regions for a slide-rock (about point O) mode are shown as shaded in Figs. 14a and 14b for the cases of I1,1 and I1,2 respectively. The symbol SRO_- is used to represent slide-rock (about point O) mode. The subscript refers to the situation of $\dot{x}_O \leq 0$.

As is done for the case of rock about point O where the various cases (I to VI) are shown as regions in $k'\!-\!q$ plane in Fig. 10, the same is done for the cases of the slide-rock about point O in Fig. 15.

Case I2: ($e \leq 0$). In this case, $q\gamma \leq 3k'$. The conditions $f_y \geq 0$, $\ddot{x}_O \leq 0$, and $\ddot{\theta} \geq 0$ are represented by the shaded regions in Figs. 16, 17 and 18 respectively. By combining the regions satisfying these conditions, the regions corresponding to a slide-rock (about point O) mode with $\dot{x}_O \leq 0$, denoted SRO_-, for the case I2 are given in Fig.18.

Case II:

In this case, $a \geq 0, c \leq 0, f_x = \mu f_y$, and $q\gamma \geq 3k'$.The regions for $f_y \geq 0$, $\ddot{x}_O \leq 0$ and $\ddot{\theta} \geq 0$ are represented by the shaded areas in Figs. 20, 21 and 22 respectively. An additional branch of μ^* is added for $k \geq d/|c|$. The regions for a slide-rock (about point O) mode for case II are given in Fig. 23.

Case III:

In this case, $a \leq 0, c \geq 0, f_x = \mu f_y, e \leq 0$, and $q\gamma \leq 3k'$ ($k_C \leq 0$). Recall that for case III in the case of rock about point O, distinction is made between case III1 for $e' \geq 0$ ($b/|a| \geq 1/q$) and case III2 for $e' \leq 0$ ($b/|a| \leq 1/q$). Such distinction is similarly made for the case of slide-rock (about point O). The regions corresponding to $f_y \geq 0$ are given in Figs. 24a and 24b. The regions corresponding to $\ddot{x}_O \leq 0$ are given in Figs. 25a and 25b and those corresponding to $\ddot{\theta} \geq 0$ are given in Figs. 26a and 26b.

The regions of a slide-rock about point O mode for cases III1 and III2 are given in Figs. 27a and 27b.

Case IV:

In this case, $a \le 0$, $c \le 0$, $f_x = \mu f_y$. In the case of rock about point O, case IV is divided into three sub-cases: case IV1 for $e \ge 0$, $e' \ge 0$, $b/|a| \ge d/|c|$, $b/|a| \ge 1/q$, case IV2, for $e \le 0$, $e' \ge 0$, $b/|a| \le d/|c|$, $b/|a| \ge 1/q$ and case IV3, for $e \le 0$, $e' \le 0$, $b/|a| \le d/|c|$, $b/|a| \le 1/q$.

Now in the case of slide-rock about point O, for IV1, $q\gamma$ is greater than or equal to $3k'$, and for IV2 and IV3, both $q\gamma \ge 3k'$ and $q\gamma \le 3k'$ can happen so that IV2 is further divided into IV2,1 (for $q\gamma \ge 3k'$) and IV2,2 (for $q\gamma \le 3k'$). Similarly, IV3 is further divided into IV3,1 (for $q\gamma \ge 3k'$) and IV3,2 (for $q\gamma \le 3k'$).

For IV1, the regions corresponding to $f_y \ge 0$, $\ddot{x}_O \le 0$ and $\ddot{\theta} \ge 0$ are given respectively in Figs. 28, 29 and 30. The regions corresponding to a slide-rock about point O mode for case IV1 are shown in Fig. 31. An additional branch for μ^* is added for $k \ge d/|c|$.

For IV2,1, the regions corresponding to $f_y \ge 0$, $\ddot{x}_O \le 0$ and $\ddot{\theta} \ge 0$ are given respectively in Figs. 32a, 33a and 34a, and the regions for the case IV2,1 are given in Fig. 35a.

Similarly, for case IV2,2 the regions corresponding to $f_y \ge 0$, $\ddot{x}_O \le 0$ and $\ddot{\theta} \ge 0$ are given respectively in Figs. 32b, 33b and 34b, and the regions for the case of IV2,2 are given in Fig. 35b.

In much the same way, case IV3 is sub-divided into IV3,1 and IV3,2. The regions corresponding to $f_y \ge 0$, $\ddot{x}_O \le 0$ and $\ddot{\theta} \ge 0$ are given respectively in Figs. 36a, 36b, 37a, 37b, 38a and 38b. The regions for these sub-cases are given in Figs. 39a and 39b.

Case V:

In this case, $a \le 0, c \ge 0, f_x = -\mu f_y, e \le 0,$ and $q\gamma \le 3k'$ as can be seen from Fig. 15. Since $f_x = -\mu f_y$, the results are anticipated to be quite different from the case of $f_x = \mu f_y$ although the equations of motion for both cases are the same in form. The expressions of $\ddot{\theta}$, f_y and $\ddot{x}_O$ are obtained from (32), (33) and (34) by replacing μ by $-\mu$. That is,

$$\ddot{\theta} = \frac{3g}{B(4+\gamma^2+3\mu\gamma)}\{-\mu\gamma - 1 + k[\gamma k' + q((4/3)+\mu\gamma)]\} \quad \text{.............................(36)}$$

$$f_y = \frac{mg}{4+\gamma^2+3\mu\gamma}[1+\gamma^2 - k\gamma(q\gamma - 3k')] \quad \text{...(37)}$$

$$\ddot{x}_O = \frac{-g}{4+\gamma^2+3\mu\gamma}[\mu(ck+d) - \left|-|a|k+b\right|] \quad \text{...(38)}$$

As in case V for the case of rock (about point O), two sub-cases: V1 (for $e' \geq 0$) and V2 (for $e' \leq 0$) must be considered.

The condition $f_y \geq 0$ is always satisfied since $q\gamma \leq 3k'$. Therefore, no figure is given for this condition. The condition $\ddot{x}_O \geq 0$ is represented by the shaded areas in Figs. 40a and 40b for the two sub-cases: V1 and V2 respectively. The condition $\ddot{\theta} \geq 0$ is represented by the shaded areas in Figs. 41a and 41b respectively. The regions corresponding to a slide-rock about O mode with $\ddot{x}_O \geq 0$ are given in Figs. 42a and 42b. The symbol SRO_+ is used to represent a slide-rock about O mode where $\ddot{x}_O \geq 0$.

Case VI:

In this case, $a \leq 0, c \leq 0, f_x = -\mu f_y$, and $e \leq 0$. For the cases of $e' \geq 0$ ($b/|a| \leq 1/q$) and $e' \leq 0$ ($b/|a| \geq 1/q$), the case VI is sub-divided into cases VI1 and VI2. Furthermore, since $q\gamma$ may be greater or smaller than $3k'$, these two sub-cases are further divided into VI1,1 and VI2,1 (for the case of $q\gamma \geq 3k'$) and VI1,2 and VI2,2 (for the case of $q\gamma \leq 3k'$).

For the cases of VI1,1 and VI2,1, Figs. 43a and 43b are for the condition $f_y \geq 0$, Figs. 44a and 44b are for the condition $\ddot{x}_O \geq 0$, and Figs. 45a and 45b are for the condition $\ddot{\theta} \geq 0$. Figs. 46a and 46b are for VI1,1 and VI2,1 when all three conditions are satisfied.

For the cases of VI1,2 and VI2,2 ($q\gamma \leq 3k'$), the condition $f_y \geq 0$ is always satisfied and the regions for the conditions $\ddot{x}_O \geq 0$ and $\ddot{\theta} \geq 0$ are the same as in Figs. 44a, 44b and 45a, 45b and the regions corresponding to a slide-rock about point O mode for the cases of VI1,2 and VI2,2 (for $q\gamma \leq 3k'$) are given in Figs. 47a and 47b respectively.

VII. Rock about point O' (RO')

The equations of motion are:

$$m\ddot{x} = f_x - F \quad (39)$$

$$m\ddot{y} = f_y - mg + U \quad (40)$$

and, noting that f_y acts at the point O' (see Fig.1) about which the body rotates,

$$I\ddot{\theta} = f_x H + f_y B + Fh + UB/3 \quad (41)$$

The relationships $\ddot{x} = -H\ddot{\theta}$ and $\ddot{y} = B\ddot{\theta}$ still hold. From these equations, we get

$$\ddot{\theta} = \frac{3g}{4B(1+\gamma^2)}(1 - \frac{k}{k_E}) \quad (42)$$

$$f_x = \frac{mg}{4(1+\gamma^2)}(a'k - b) \quad (43)$$

and

$$f_y = \frac{mg}{4(1+\gamma^2)}(d - c'k) \quad (44)$$

where

$$a' = 4 + \gamma^2 - 3\gamma^2 k' + 2q\gamma \quad (45)$$

$$c' = 3\gamma(1+k') + 2q(1+2\gamma^2) \quad (46)$$

and

$$k_E = \frac{3}{2(q - q_2)}; q_2 = \frac{3}{2}\gamma(1+k') \quad (47)$$

The conditions to be satisfied for a rock about point O' mode to occur are $\ddot{\theta} \le 0$, $f_y \ge 0$ and $\mu \ge |f_x|/f_y$. It is seen that while $c' \ge 0$, a' may be greater or smaller than zero. Since a' is a function of k' and q, we plot the line $a' = 0$

or $q = -[(4+\gamma^2)/(2\gamma)] + [(3/2)\gamma k'] \equiv q_4$ on the $k' - q$ diagram in Fig.15. The region below the line $a' = 0$ corresponds to the case of $a' \leq 0$, $(q \leq q_4)$. Now we turn our attention to the condition for a rock about point O' mode to occur. From (42), it is seen that for $\ddot{\theta} \leq 0$, k_E must be greater than or equal to zero. This means, from (47), that $q \geq q_2$. The line $q = q_2$ is parallel to and lies above the line $q = q_4$ ($a' = 0$). Thus $\ddot{\theta}$ can not be smaller than or equal to zero for the cases III2 and V2 in the region which corresponds to $a' \leq 0$. For $q \geq q_2$ ($a' \geq 0$), the condition $\ddot{\theta} \leq 0$ is satisfied provided, from (42), $k \geq k_E$. It may be verified that $k_E \geq 1/q$ and the region corresponding to $\ddot{\theta} \leq 0$ is shown shaded as in Fig. 48. The condition $f_y \geq 0$ requires $k \leq d/c' \equiv k_F$ where $k_F \leq 1/q$ as can be verified. In the $k - \mu$ plane, the region corresponding to $f_y \geq 0$ is shown in Fig.49. Before examining the condition $\mu \geq |f_x|/f_y$ we note that f_x cannot be less than zero. This is because, from (39), $f_x \leq 0$ implies $\ddot{x} \leq 0$ which in turn implies $\ddot{\theta} \geq 0$ on account of the fact that $\ddot{x} = -H\ddot{\theta}$. Since $\ddot{\theta}$ must be less than zero, a rock (about point O') mode cannot be realized. Thus, the region $0 \leq k \leq b/a' \leq k_E$ is empty as shown in Fig.50. The last condition to be satisfied is therefore written as $\mu \geq f_x/f_y \equiv \mu_2 = (a'k - b)/(d - c'k)$. Since, for $a' \geq 0$, d/c' may be greater or smaller than b/c' depending on the sign of the quantity e since $(d/c') - (b/a') = [4(1+\gamma^2)e]/a'c'$. Let us first consider the case of $e \geq 0$ ($d/c' \geq b/a'$). The curve μ_2 is as shown in Fig. 51 where an additional branch of μ_2 for $k \geq k_F$ is added. The region corresponding to the condition $\mu \geq f_x/f_y$ is the shaded area in Fig.51. For $k \geq k_F$, f_y is less than zero, the body is in free-flight mode and the condition $\mu \geq f_x/f_y$ has no meaning. Since the regions corresponding to the conditions $\ddot{\theta} \leq 0$ and $\mu \geq f_x/f_y$ are disjoint, no rock about point O' mode can happen for $e \geq 0$. It may be similarly shown that no rock about point O' mode for the case of $e \leq 0$ can be initiated.

This concludes the discussion of rock about O' mode. In the following, the mode of slide-rock about O' is examined.

VIII. Slide-rock about point O' (SRO')

The equations of motion are the same as those governing rock about O mode, namely equations (38), (39) and (40), except that $\ddot{x} = -H\ddot{\theta}$ no longer holds but $\ddot{y} = B\ddot{\theta}$ is still valid. We now consider first the case in which $f_x = \mu f_y \geq 0$ (the symbol used for this case is SRO'_-; the subscript refers to the case in which $\ddot{x}_{O'} \leq 0$). Solutions of the equations of motion are:

$$\ddot{\theta} = \frac{3g}{B(4+\gamma^2+3\mu\gamma)}\{\mu\gamma + 1 + k[\gamma k' - q((2/3)+\mu\gamma)]\} \quad (48)$$

$$f_y = \frac{mg}{4+\gamma^2+3\mu\gamma}\{1+\gamma^2 - k[3k' + q(2+\gamma^2)]\} \quad (49)$$

and

$$\ddot{x}_O = \frac{g}{4+\gamma^2 - +3\mu\gamma}[\mu(d-ck') - (a'k-b)] \quad (50)$$

The conditions for a slide-rock about point O' mode to occur are: $\ddot{\theta} \leq 0$, $f_y \geq 0$ and $\ddot{x}_{O'} \leq 0$. The condition $f_y \geq 0$ requires, from (49), $k \leq (1+\gamma^2)/[3\gamma k' + q(2+\gamma^2)] \equiv k_{F'} \leq 1/q$. This condition is shown in Fig. 52. The condition for $\ddot{x}_{O'} \leq 0$ is, from (50), $\mu(d-c'k) \leq (a'k-b)$ or, $\mu \leq \mu_2$ where $\mu_2 = (a'k-b)/(d-c'k)$. As is done in the case of rock about point O' mode, distinction is made between the cases of $e \geq 0$, $d/c' \geq b/a'$ and $e \leq 0$, $d/c' \leq b/a'$. The condition $\ddot{x}_{O'} \leq 0$ is shown for these two cases respectively in Figs. 53a and 53b. The condition $\ddot{\theta} \leq 0$ is expressed as $\mu(1-kq) \leq -(1/\gamma) + k[(2q/3\gamma) - k']$. We define

$$\mu^{**} = \{-(1/\gamma) + k[(2q/3\gamma) - k']\}/(1-kq) = (k-k_G)/[\gamma k_G(1-kq)] \quad (51)$$

where

$$k_G = 3/2(q-q_G), \text{ and } q_G = 3\gamma k'/2 \quad (52)$$

For $k \leq 1/q$ and $k \geq 1/q$, the two branches of μ^{**} are sketched in Fig.54. From (52), it is seen that if $q \geq q_G$ then $k_G \geq 0$ and $k_G \geq 1/q$; if $q \leq q_G$, then

$k_G \leq 0$. For ease of discussion, consider the specific case of I1,1 which is identified in the $k'-q$ diagram by the shaded regions sketched in Figs. 55a and 55b and in which the line $q = q_G = 3k'\gamma/2$ is drawn. Due to the fact that the slope of q_G may be greater or smaller than that of $q_1 = 3k'/\gamma$ depending on whether $\gamma \geq \sqrt{2}$ or $\gamma \leq \sqrt{2}$, two figures, Figs.55a and 55b, are given. The regions corresponding to $q \geq q_G$, $k_G \geq 0$ and $q \leq q_G$, $k_G \leq 0$ are also indicated. If a point falls in the region of $k_G \geq 0$, the condition for $\ddot{\theta} \leq 0$ is given by the following: (a) for $k \leq k_G$, $k \leq 1/q$, $\mu \leq \mu^{**}$ which is impossible, (b) for $k \leq k_G$, $k \geq 1/q$, $\mu \geq \mu^{**}$, and (c) for $k \geq 1/q$, $k \geq k_G$ which is always true. This is shown as shaded in Fig.56. If a point falls in the region of $q \leq q_G$, $k_G \leq 0$, the condition $\ddot{\theta} \leq 0$ can not be satisfied; the corresponding space in empty.

By combining the conditions $f_y \geq 0$, $\ddot{x}_{O'} \leq 0$ and $\ddot{\theta} \leq 0$, the region corresponding to a slide-rock about point O' mode with $\ddot{x}_{O'} \leq 0$ is shown in Fig.57. It is seen that, in a slide-rock about point O' mode, a caisson can only be in a free-flight mode

In case I1,1 and in other cases for which $q\gamma \geq 3k'$, we need to compare the relative magnitude of k_G and k_C. It may be verified that for $q \geq q_G$, $k_G \geq 0$, k_G may lie to the left or to the right of k_C depending on whether $\gamma \leq \sqrt{2}$ or $\gamma \geq \sqrt{2}$.

For the case of $f_x = -\mu f_y \leq 0$ ($\ddot{x}_{O'} \geq 0$, denoted SRO'_+) does not exist because $m\ddot{x} = f_x - F = -\mu f_y - F$ so that $\ddot{x} \leq 0$ always; since $\ddot{x}_{O'} = \ddot{x} + H\ddot{\theta}$ and $\ddot{\theta} \leq 0$, $\ddot{x}_{O'}$ can not be greater than zero.

IX. All modes combined

We now combine all the modes (RE, SL, RO, SRO, RO', SRO'). As we see in Ref.2, the various modes in the same region in the $k-\mu$ plane sometimes may overlap. To determine which mode governs in the overlapping region, we compare the horizontal forces f_x of the modes which overlap in that region; the mode which has the smaller f_x governs.

After combining all the modes, the final results are shown in Figs. 58 to 70. Since the region corresponding to the case of slide-rock about O' differ depending on whether $\gamma \geq \sqrt{2}$ or $\gamma \leq \sqrt{2}$, to save space, only the case of $\gamma \leq \sqrt{2}$ is presented.

Fig 58 is for I1,1 ($\gamma \leq \sqrt{2}$), Fig. 59 is for I1,2 ($\gamma \leq \sqrt{2}$), Fig. 60 is for I2 ($\gamma \leq \sqrt{2}$), Fig. 61 is for II ($\gamma \leq \sqrt{2}$), Fig. 62 is for III1 paired with V1 ($q\gamma \leq 3k'$), Fig. 63 is for III1 paired with V1 ($q\gamma \geq 3k'$, $\gamma \leq \sqrt{2}$), Fig. 64 is for III2 paired with V2 ($q\gamma \leq 3k'$), Fig. 65 is for III2 paired with V2 ($q\gamma \geq 3k'$, $\gamma \leq \sqrt{2}$), Fig. 66 is for IV1 ($q\gamma \geq 3k'$, $\gamma \leq \sqrt{2}$), Fig. 67 is for IV2 paired with VI1 ($q\gamma \geq 3k'$, $\gamma \leq \sqrt{2}$), Fig. 68 is for IV2' paired with VI1 ($q\gamma \leq 3k'$), Fig. 69 is for IV3 ($q\gamma \geq 3k'$, $\gamma \leq \sqrt{2}$) paired with VI2, Fig. 70 is for IV3' paired with VI2 ($q\gamma \leq 3k'$).

X. Discussion and concluding remarks

(1) If we let $q = 0$, the results of the present study, which includes uplift force, reduces to those in Refs.1,2 where uplift force is not considered. By letting $q = 0$, in the sections discussing RO and SRO modes, the cases of II, IV and VI are all no longer relevant since the quantity c is now greater than zero. Also, the cases involving $q\gamma \geq 3k'$ do not exist. For cases where $q\gamma \leq 3k'$ and $c \geq 0$, by letting $q = 0$, for example, case V1 does not exist but case V2 remains. It may be similarly verified that without an uplift force, a caisson can not be initiated into a RO' mode nor a SRO' mode.

(2) In reference to Figs. 10 and 15, since the caisson being considered is rectangular in its elevation and of uniform mass distribution, k' can not exceed unity. Thus, the regions to the right of $k' = 1$ is to be ignored; only the regions to the left of $k' = 1$ need be considered.

(3) To gain a sense of the behavior of a caisson, calculations should be made for a range of numerical values of γ, q, k', k and μ.

(4) The present study of the behavior of a caisson considering uplift force should be extended to cover the case of force F applied below point C.

(5) The results of this study as presented in Fig.15 and Fig.58 to Fig.70 can be used to determine the mode of motion of a caisson. For example, given the aspect ratio γ of a caisson, and knowledge of the location of the force F (k') and measure of the magnitude of the uplift force (q), Fig.15 can be used to determine the case (for example, case II) that governs the behavior of the caisson. The relevant figure in the $k - \mu$ plane can be identified from Fig. 58 to Fig.70 (for example, for case II, it is Fig. 61). Given the force and coefficient of friction, the mode that the caisson is to be initiation into is determined.

(6) The results of this study contribute to a better understanding of the behavior of a caisson under the action of an impact force. The study is not concerned with the problem of determining the actual response of

the caisson. For example, the study does not address the issue of the amount of sliding or rocking a caisson would undergo. The study, however, provides information based on which the engineer can make design decisions. For example, the configurations of the caisson may be adjusted to avoid it being initiated into a mode of response that is not considered desirable. More significantly, given the magnitude and location of the force F, the uplift force, and the coefficient of friction between the caisson and the base, one may, based on the region of rest (in the $k-\mu$ plane), determine the dimensions of the caisson so that the volume of the caisson is minimized.

Acknowledgements

The study is suggested and supported in part by the Harbor and Marine Technology Center, Institute of Transportation under the project entitled' A Study of Harbor Resonance of Hwa-Lien Harbor' of which J.G. Lin of National Taiwan Ocean University is the principal investigator.

References

Tung,C.C., Lin, J.G., and Chiu,Y.F. (2005). “Behavior of a freestanding rigid body subjected to a horizontal force.” Rep. No.HDL-003, National Taiwan Ocean University, Department of Harbor and River Engineering, Hydrodynamic Laboratory, Keelung, Taiwan

Tung,C.C. (2007). “Behavior of a Caisson subjected to a Horizontal Breaking Wave Force”, Volume 133, Number 12, Journal of Engineering Mechanics, American Society of Civil Engineers.

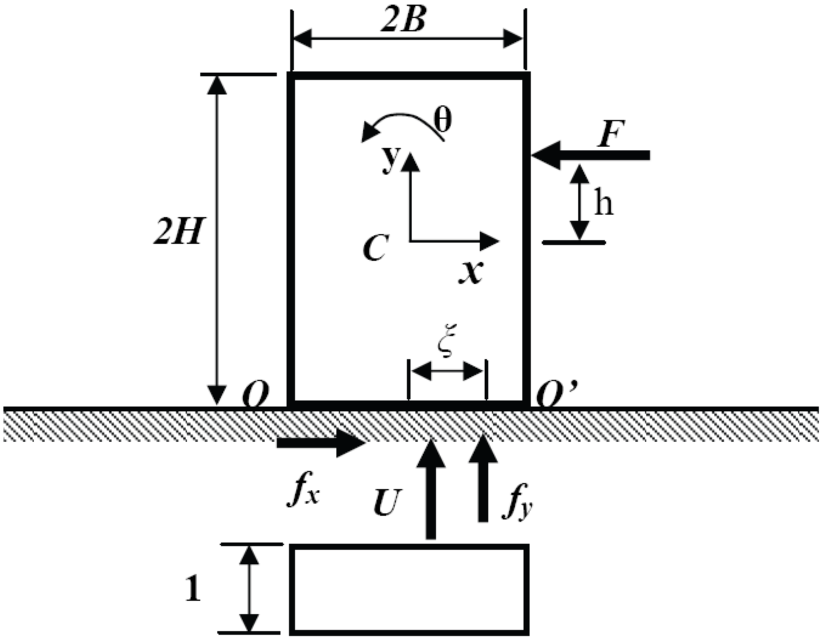

Fig. 1 Models

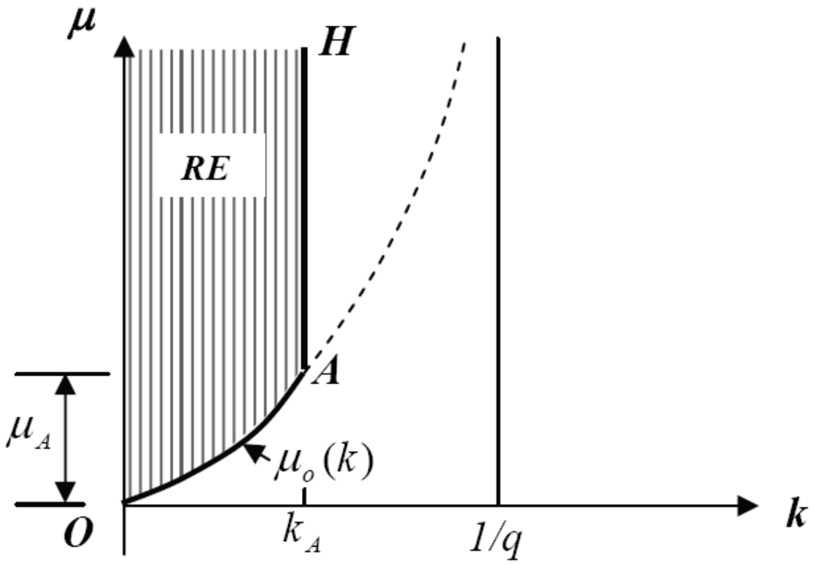

Fig. 2 Rest region

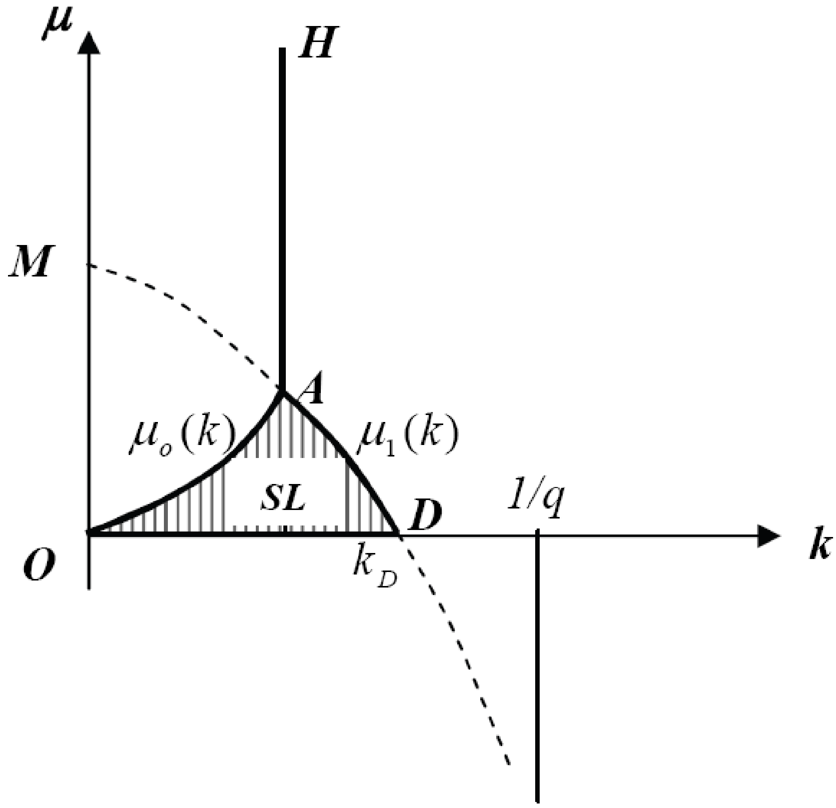

Fig. 3 Slide region

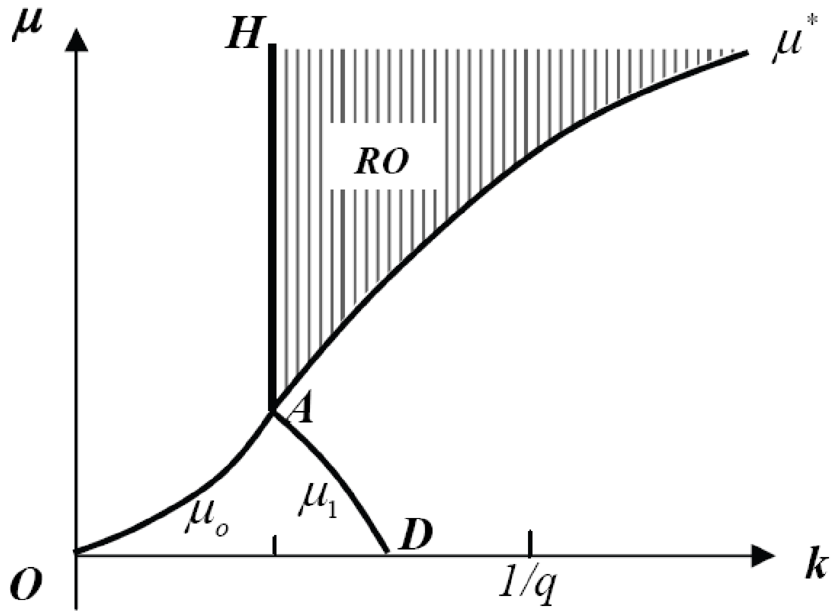

Fig. 4a Region of rock about point O mode , case I1 ($e \geq 0$)

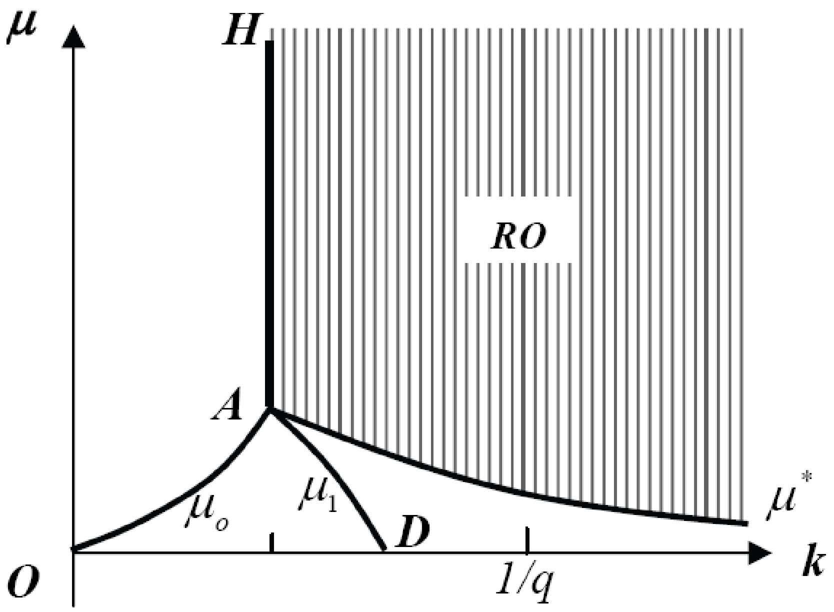

Fig. 4b Region of rock about point O mode, case I1 ($e \leq 0$)

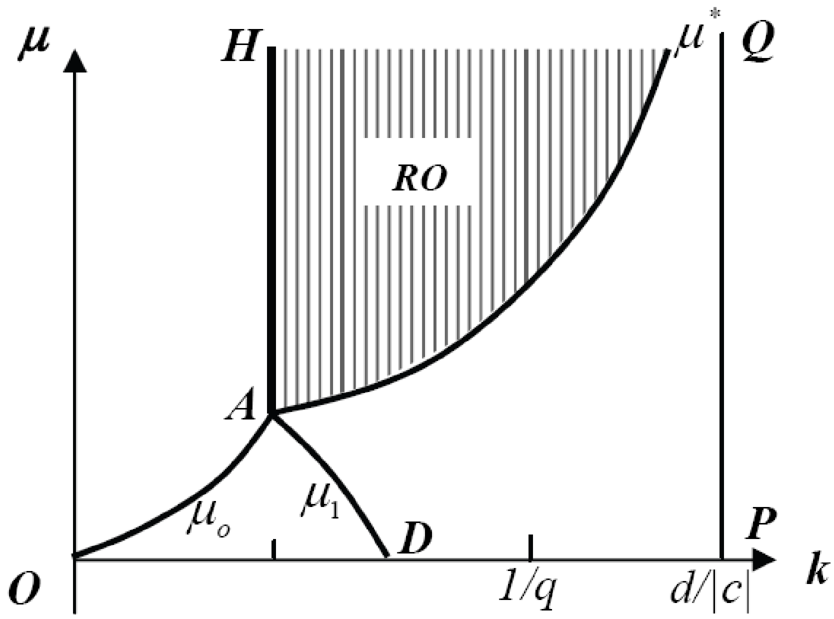

Fig. 5 Region of rock about point O mode, case II ($e \geq 0$)

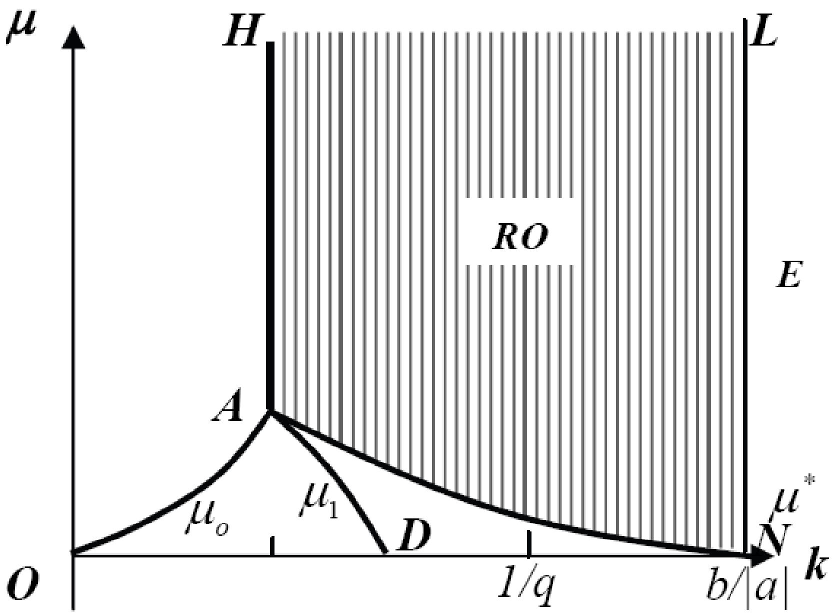

Fig. 6a Region of rock about point O mode, case III1 ($e \le 0, e' \ge 0$)

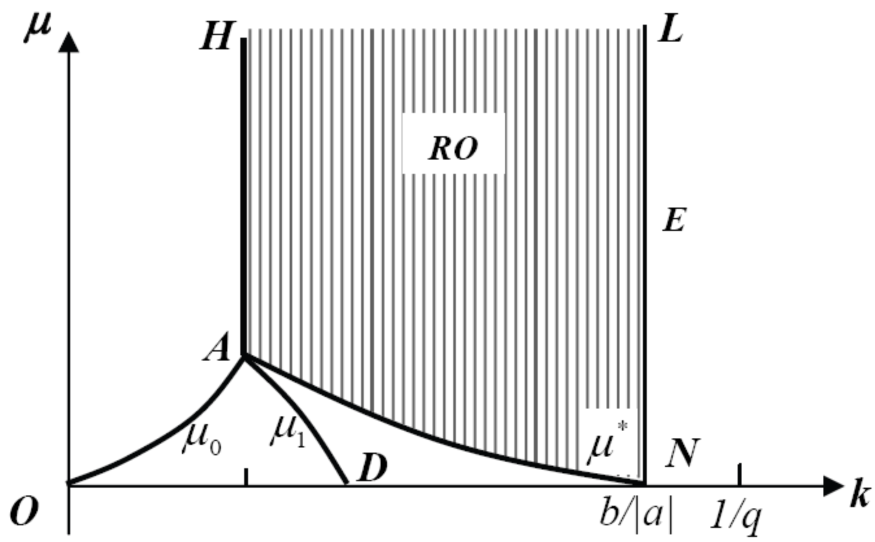

Fig. 6b Region of rock about point O mode, case III2 ($e \le 0, e' \le 0$)

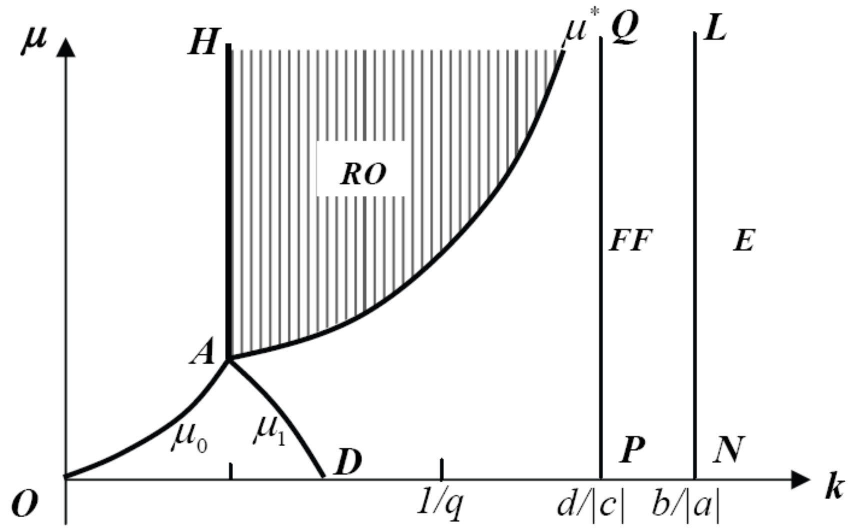

Fig. 7a Region of rock about point O mode, case IV1
$(e \geq 0, e' \geq 0, b/|a| \geq d/|c|, b/|a| \geq 1/q)$

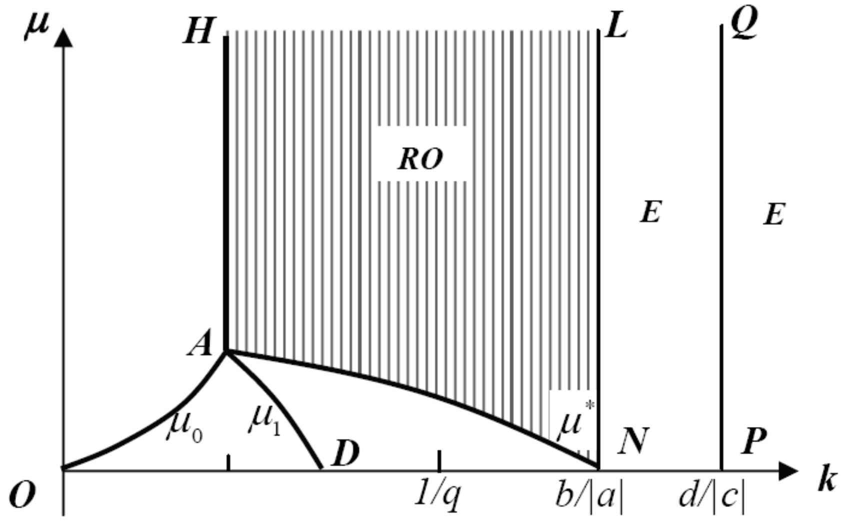

Fig. 7b Region of rock about point O mode, case IV2
$(e \leq 0, e' \geq 0, b/|a| \leq d/|c|, b/|a| \geq 1/q)$

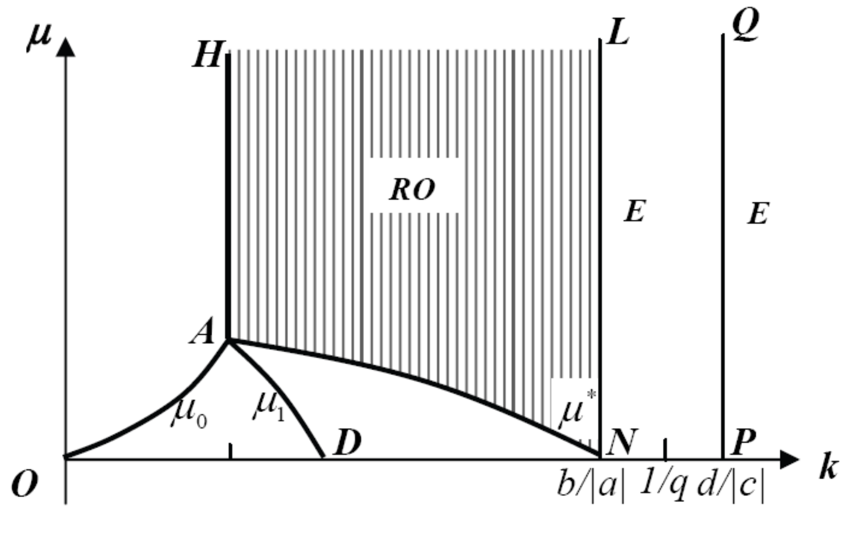

Fig. 7c Region of rock about point O mode, case IV3

($e \le 0, e' \le 0, b/|a| \le d/|c|, b/|a| \le 1/q$)

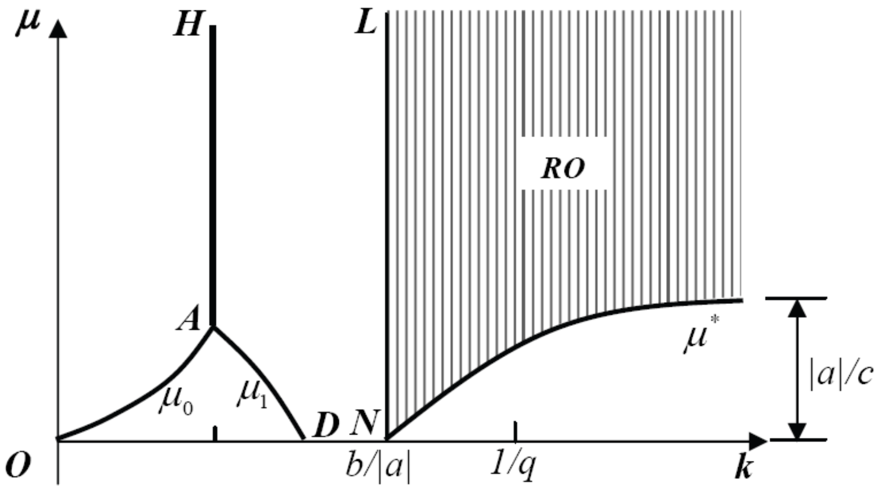

Fig. 8a Region of rock about point O mode, case V1
($e \le 0, e' \ge 0, b/|a| \ge 1/q$)

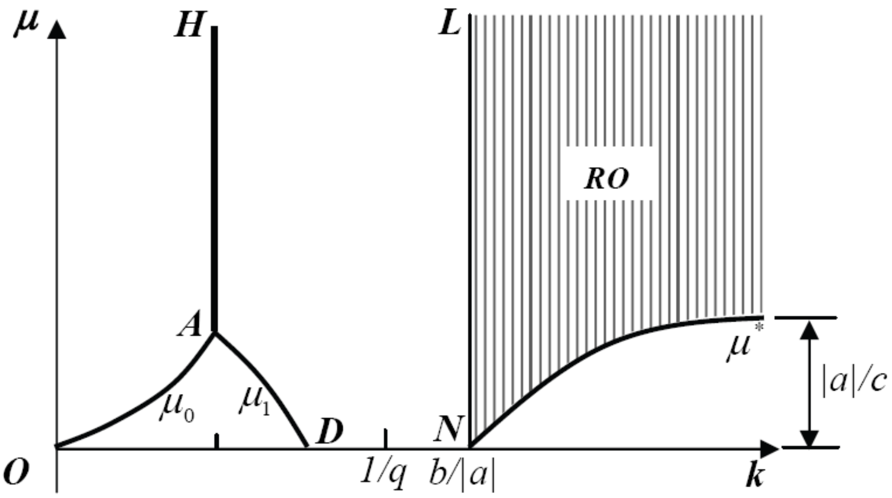

Fig. 8b Region of rock about point O mode, case V2
($e \le 0, e' \le 0, b/|a| \le 1/q$)

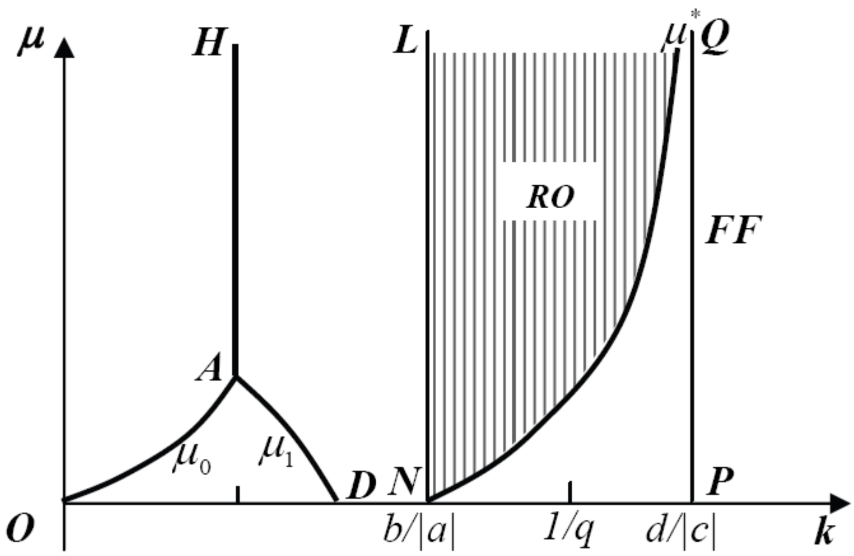

Fig. 9a Region of rock about point O mode, case VI1 ($e \le 0, e' \ge 0$)

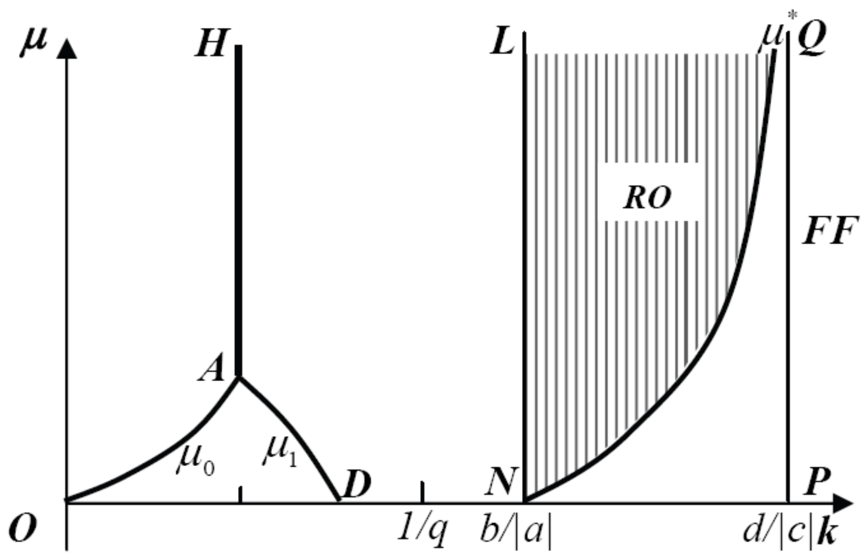

Fig. 9b Region of rock about point O mode, case VI2 ($e \le 0, e' \le 0$)

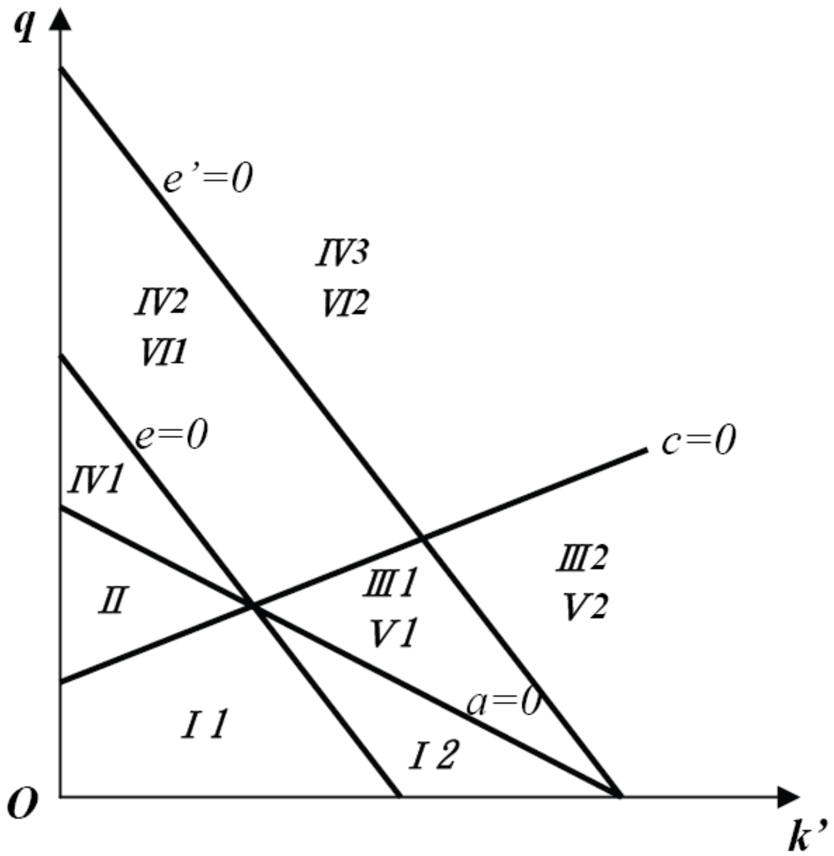

Fig. 10 Regions in k'–q plane for the six cases of rock about point O mode

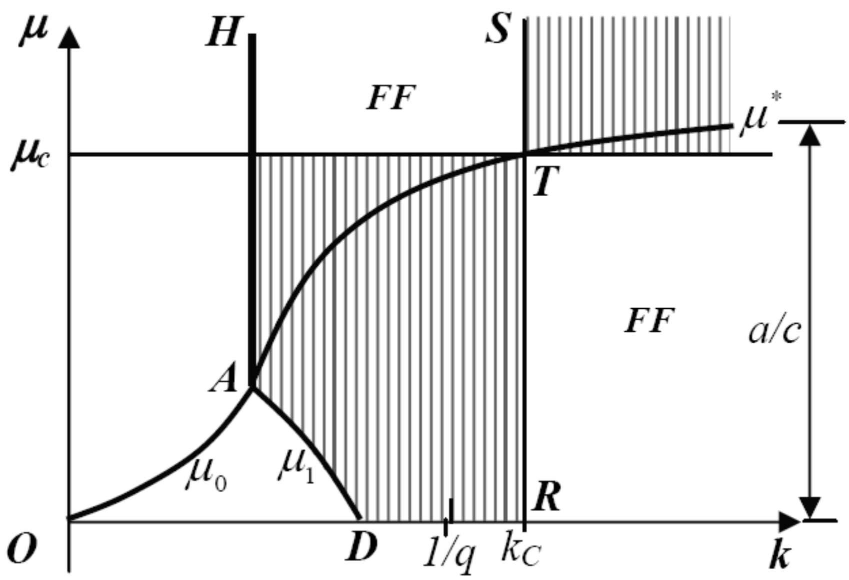

Fig. 11a Region of $f_y \geq 0$ for slide-rock about point O mode, case I1,1
($q\gamma \geq 3k'$)

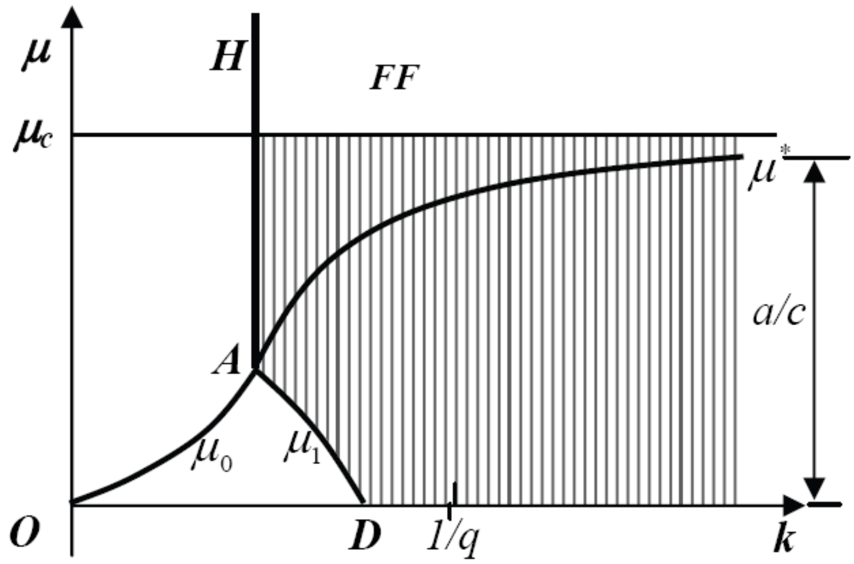

Fig. 11b Region of $f_y \geq 0$ for slide-rock about point O mode, case I1,2
($q\gamma \leq 3k'$)

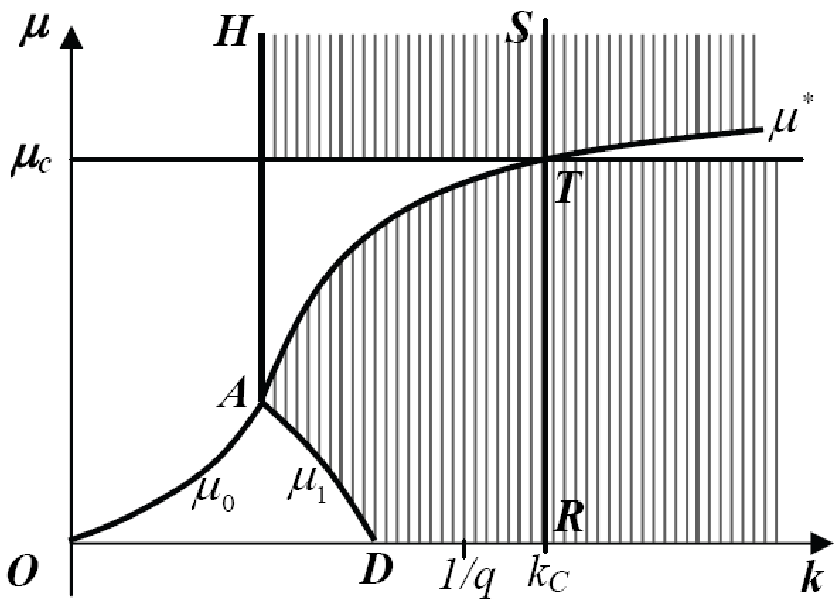

Fig. 12a Region of $\ddot{x}_O \le 0$ for slide-rock about point O mode, case I1,1
($q\gamma \ge 3k'$)

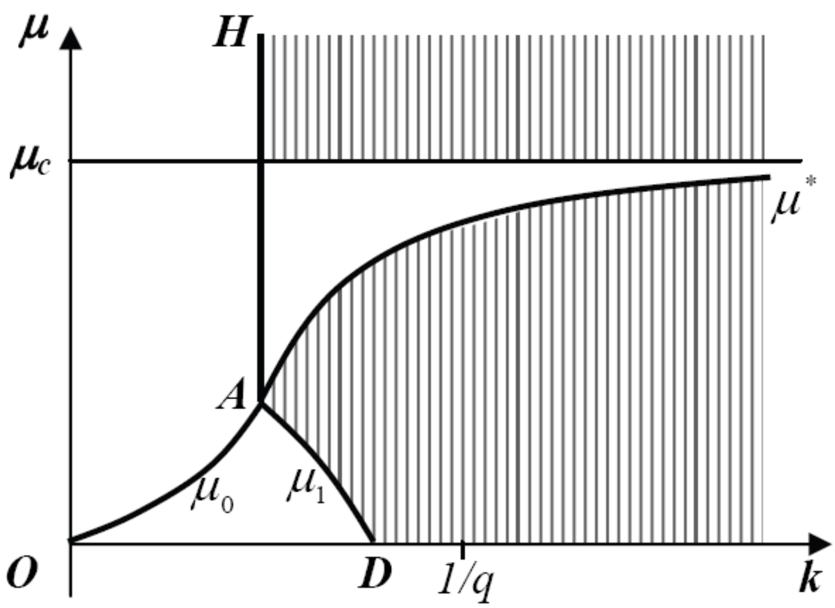

Fig. 12b Region of $\ddot{x}_O \le 0$ for slide-rock about point O mode, case I1,2
($q\gamma \le 3k'$)

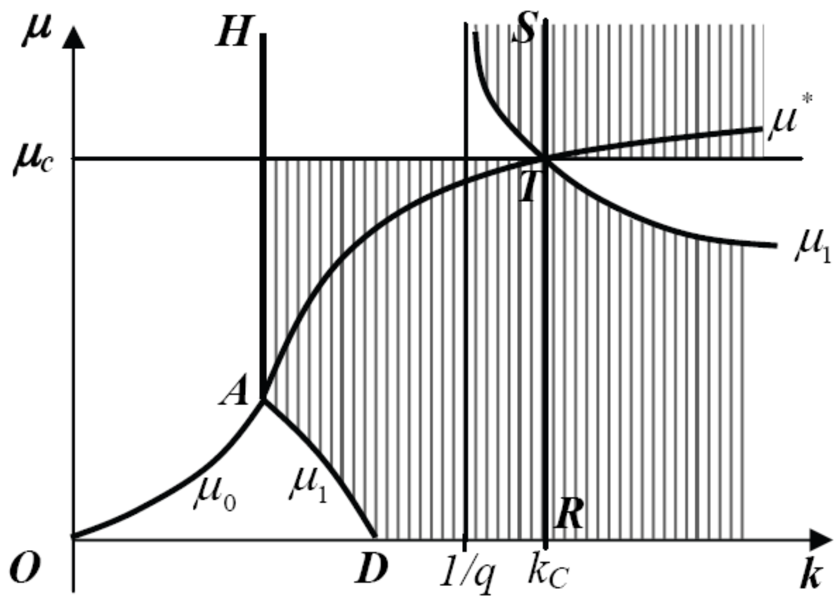

Fig. 13a Region of $\ddot{\theta} \geq 0$ for slide-rock about point O mode, case I1,1
($q\gamma \geq 3k'$)

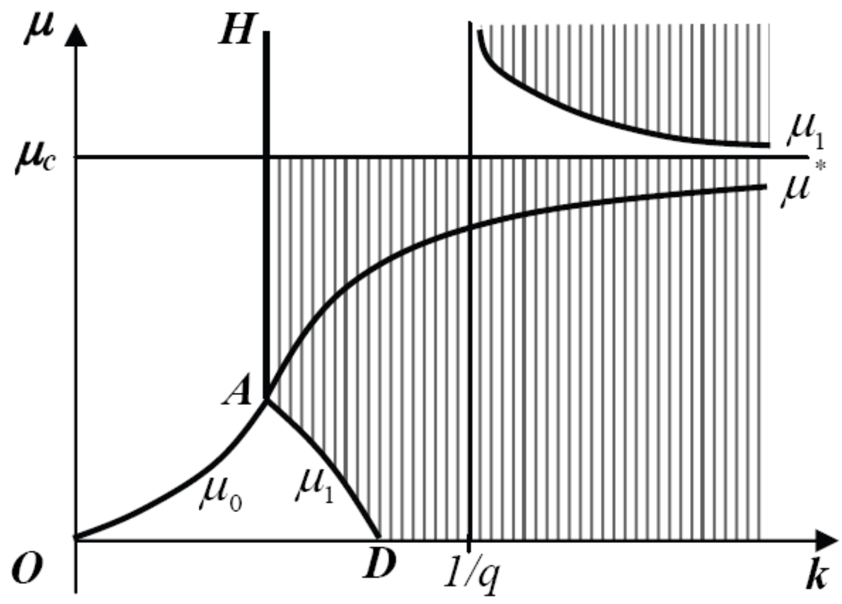

Fig. 13b Region of $\ddot{\theta} \geq 0$ for slide-rock about point O mode, case I1,2
($q\gamma \leq 3k'$)

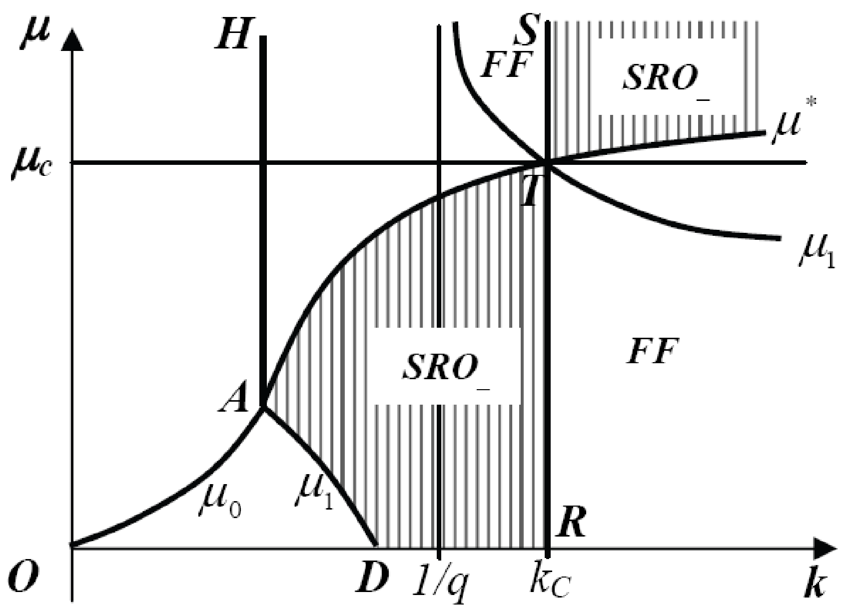

Fig. 14a Region of slide-rock about point O mode (SRO_-), case I1,1 ($q\gamma \geq 3k'$)

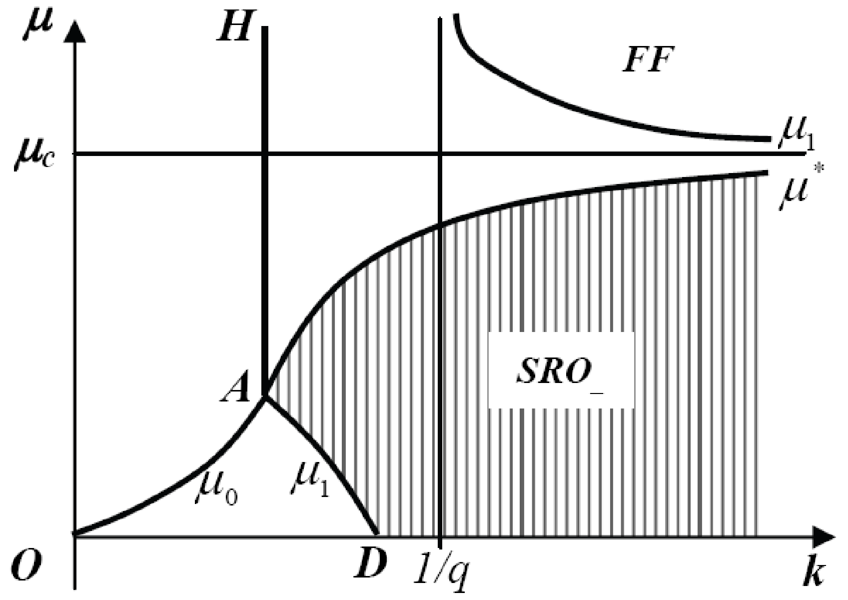

Fig. 14b Region of slide-rock about point O mode (SRO_-), case I1,2 ($q\gamma \leq 3k'$)

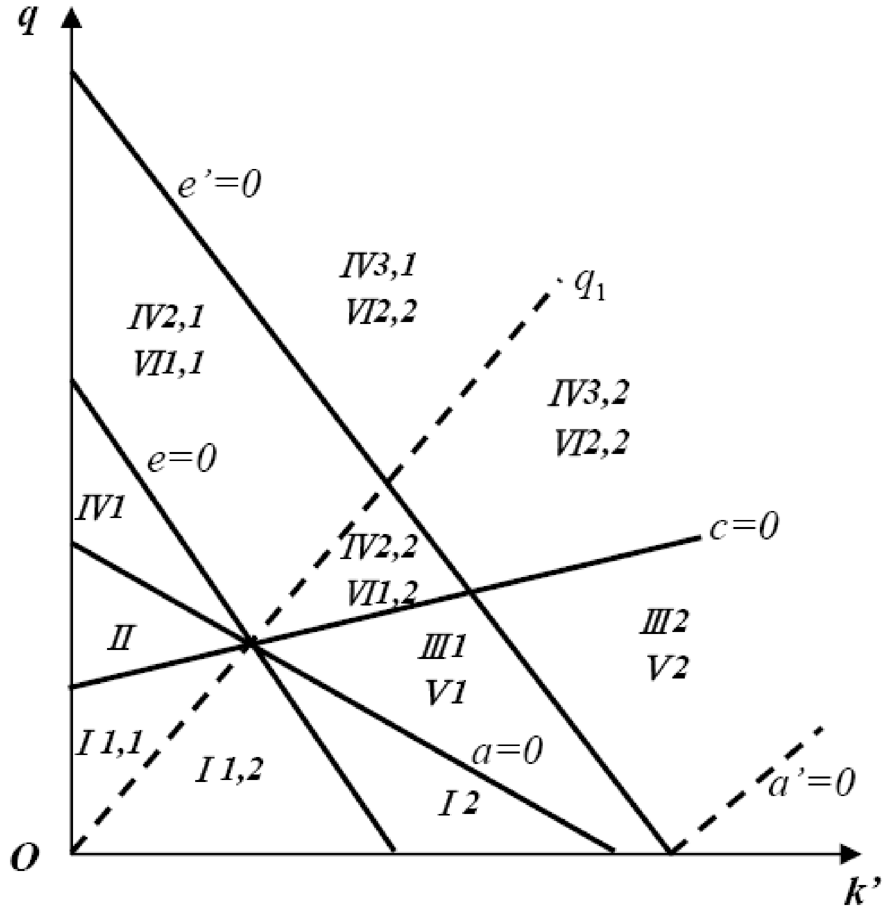

Fig. 15 Regions in k'–q plane for the six cases of slide-rock about point O mode

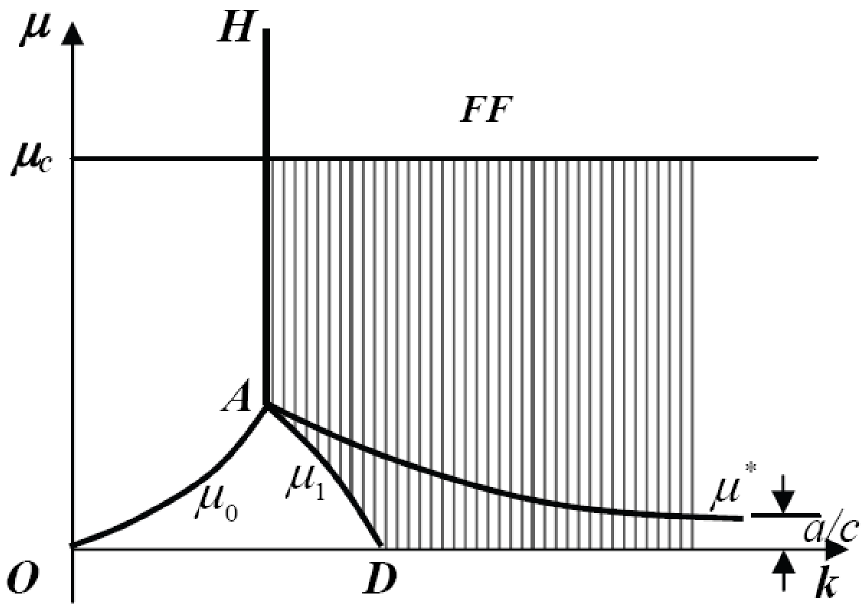

Fig. 16 Region of $f_y \geq 0$ for slide-rock about point O mode, case I2 ($q\gamma \leq 3k'$)

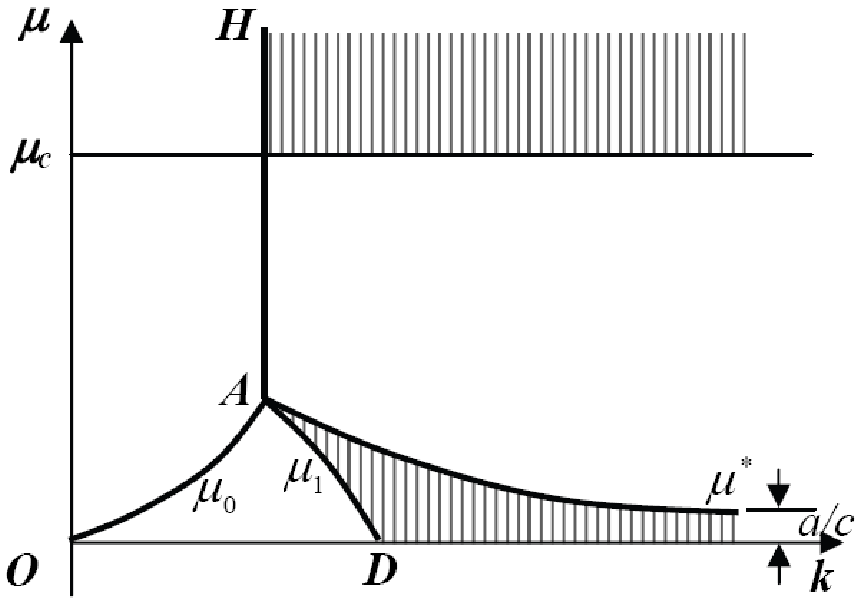

Fig. 17 Region of $\ddot{x}_O \leq 0$ for slide-rock about point O mode, case I2 ($q\gamma \leq 3k'$)

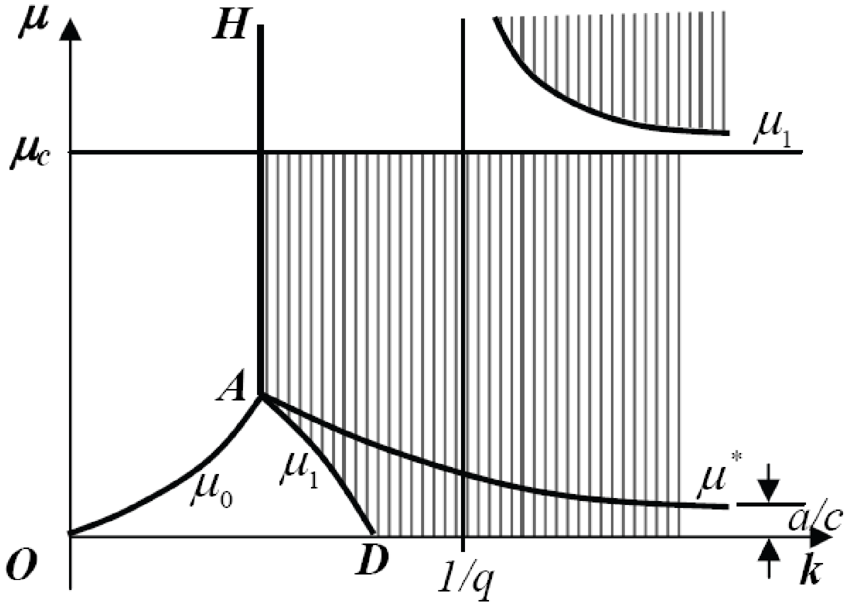

Fig. 18 Region of $\ddot{\theta} \geq 0$ for slide-rock about point O mode, case I2 ($q\gamma \leq 3k'$)

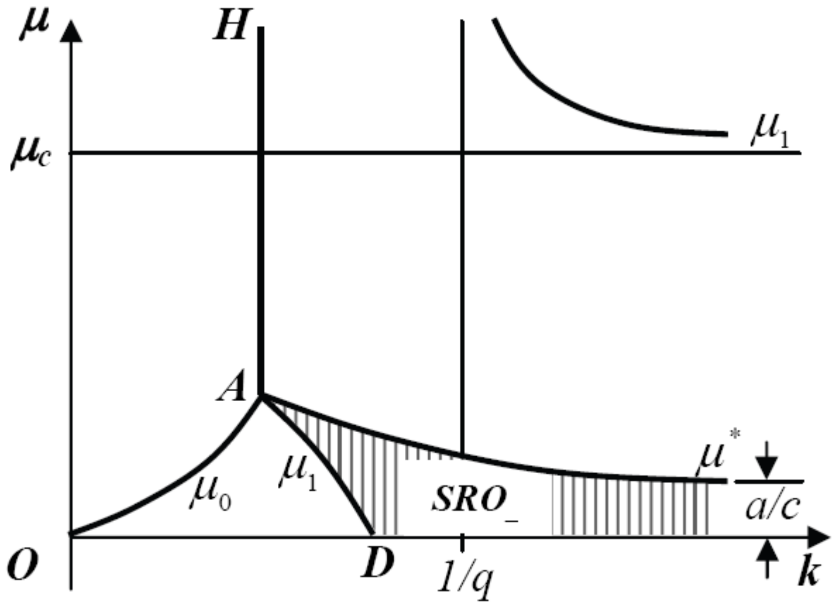

Fig. 19 Region of slide-rock about point O mode (SRO_-), case I2 ($q\gamma \leq 3k'$)

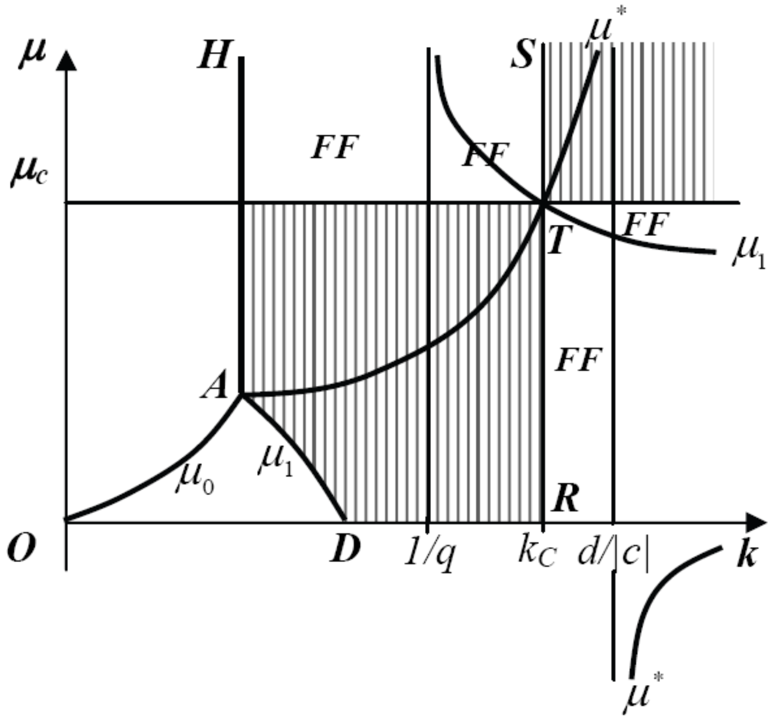

Fig. 20 Region of $f_y \geq 0$ for slide-rock about point O mode, case II ($q\gamma \geq 3k'$)

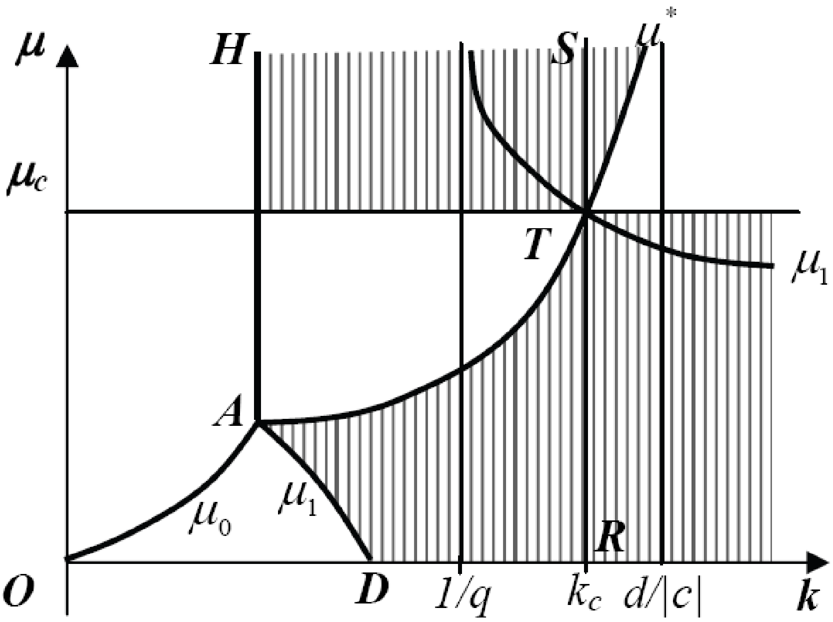

Fig. 21 Region of $\ddot{x}_O \leq 0$ for slide-rock about point O mode, case II ($q\gamma \geq 3k'$)

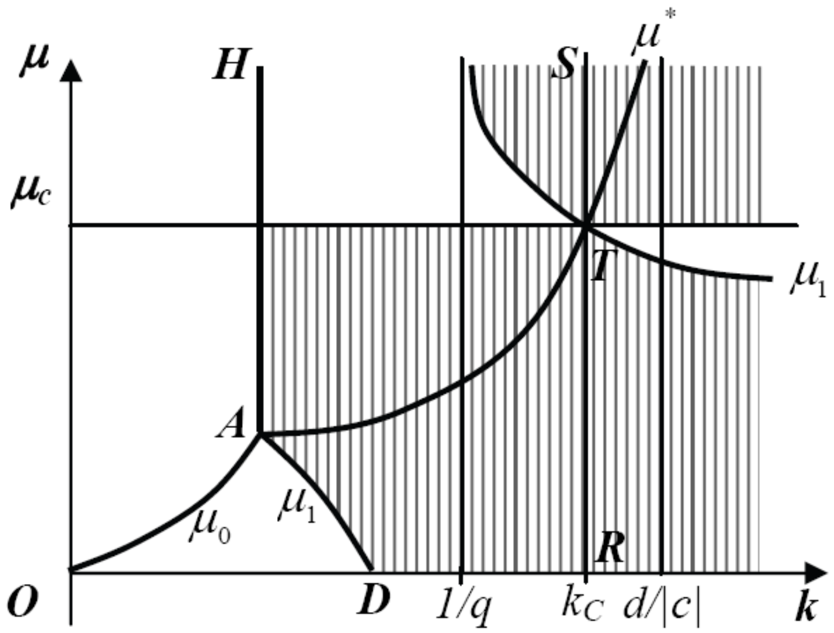

Fig. 22 Region of $\ddot{\theta} \geq 0$ for slide-rock about point O mode, case II ($q\gamma \geq 3k'$)

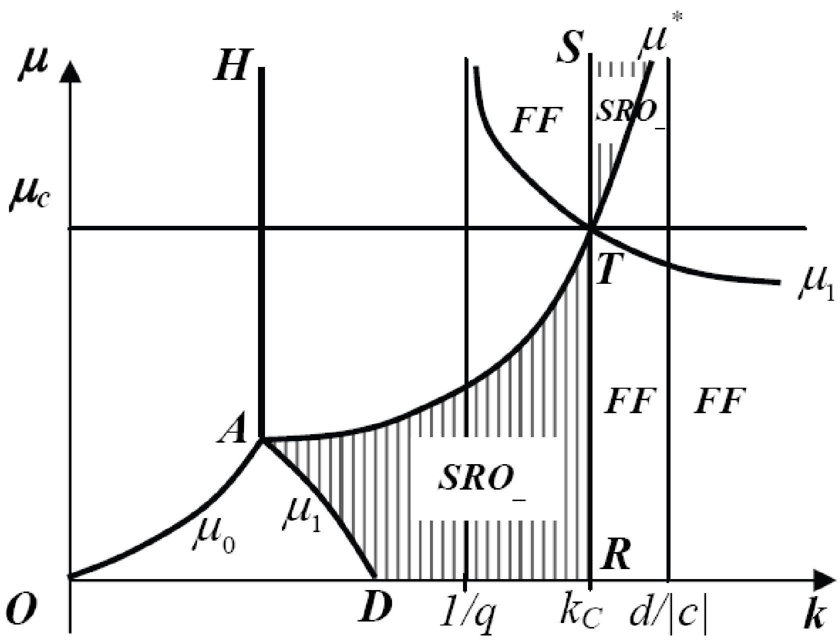

Fig. 23 Region of slide-rock about point O mode (SRO_-), case II ($q\gamma \geq 3k'$)

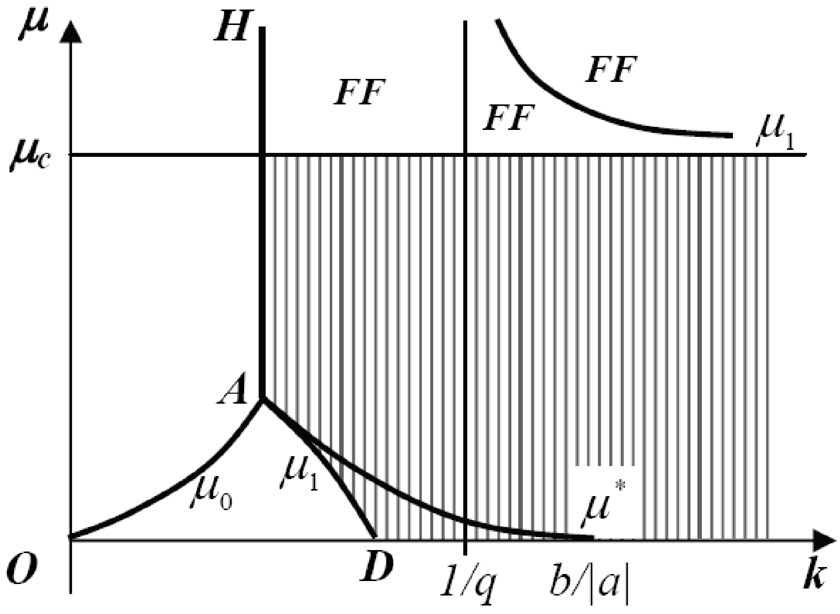

Fig. 24a Region of $f_y \geq 0$ for slide-rock about point O mode (SRO_-), case III1 ($q\gamma \leq 3k'$, $e' \geq 0$, $b/|a| \geq 1/q$)

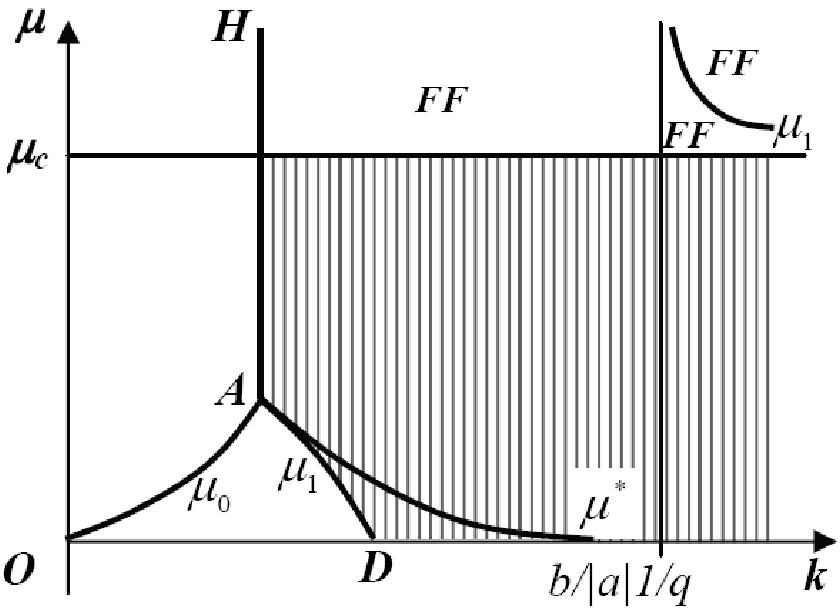

Fig. 24b Region of $f_y \geq 0$ for slide-rock about point O mode (SRO_-), case III1 ($q\gamma \leq 3k'$, $e' \leq 0$, $b/|a| \leq 1/q$)

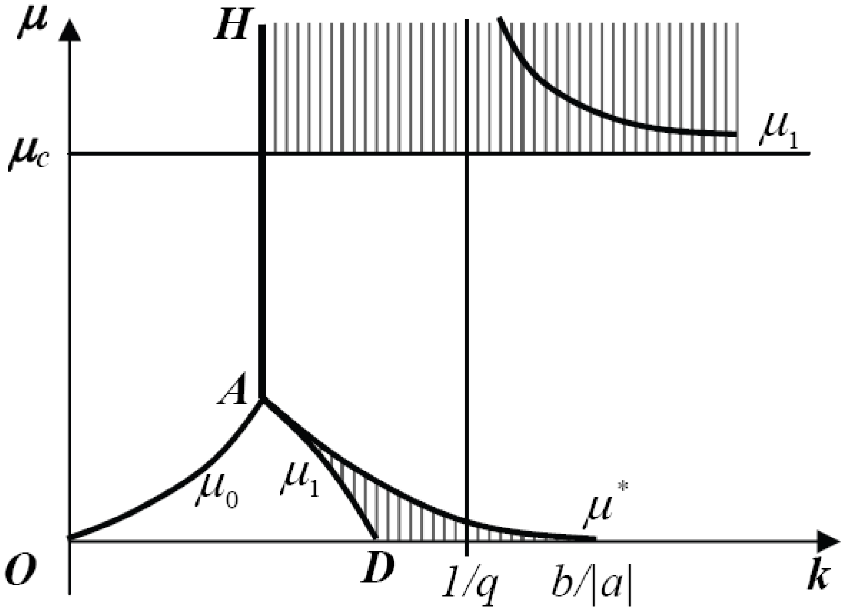

Fig. 25a Region of $\ddot{x}_O \leq 0$ for slide-rock about point O mode (SRO_-), case III1 ($q\gamma \leq 3k'$, $e' \geq 0$, $b/|a| \geq 1/q$)

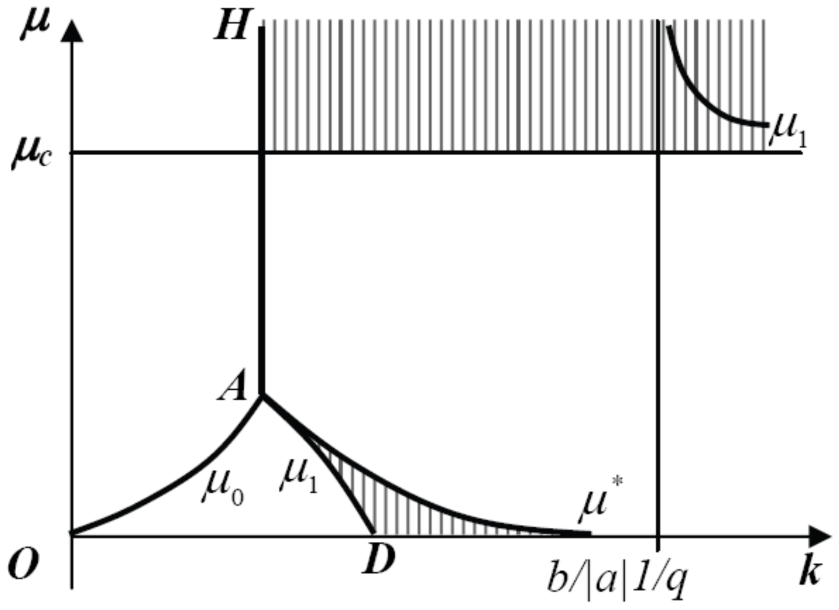

Fig. 25b Region of $\ddot{x}_O \leq 0$ for slide-rock about point O mode (SRO_-), case III1 ($q\gamma \leq 3k'$, $e' \leq 0$, $b/|a| \leq 1/q$)

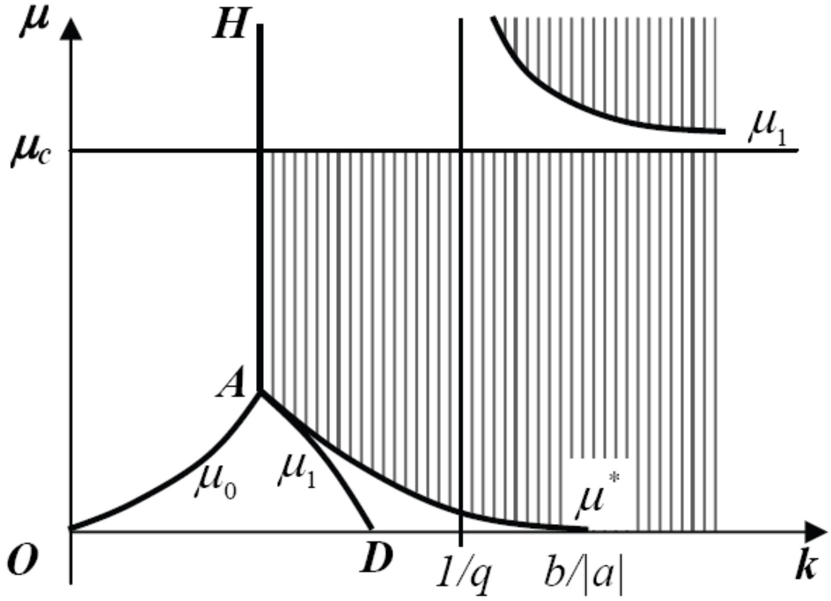

Fig. 26a Region of $\ddot{\theta} \geq 0$ for slide-rock about point O mode (SRO_-), case III1 ($q\gamma \leq 3k', e' \geq 0, b/|a| \geq 1/q$)

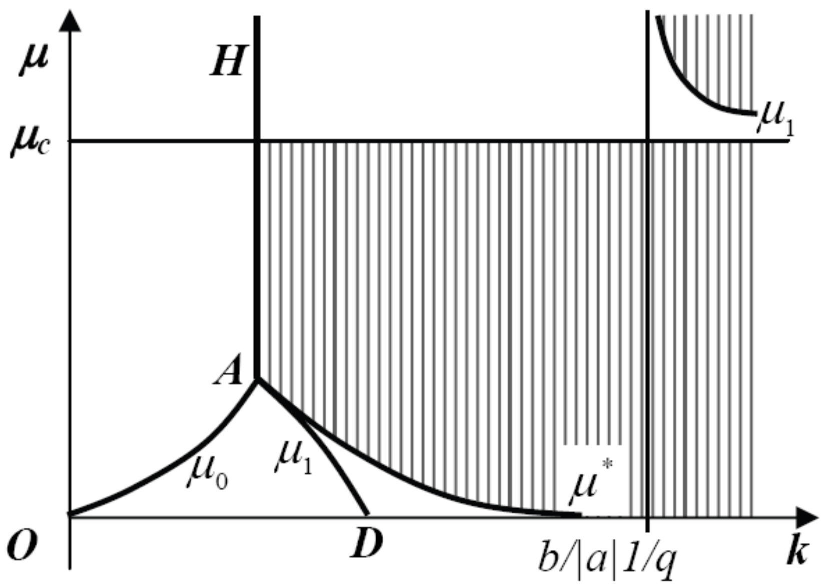

Fig. 26b Region of $\ddot{\theta} \geq 0$ for slide-rock about point O mode (SRO_-), case III1 ($q\gamma \leq 3k', e' \leq 0, b/|a| \leq 1/q$)

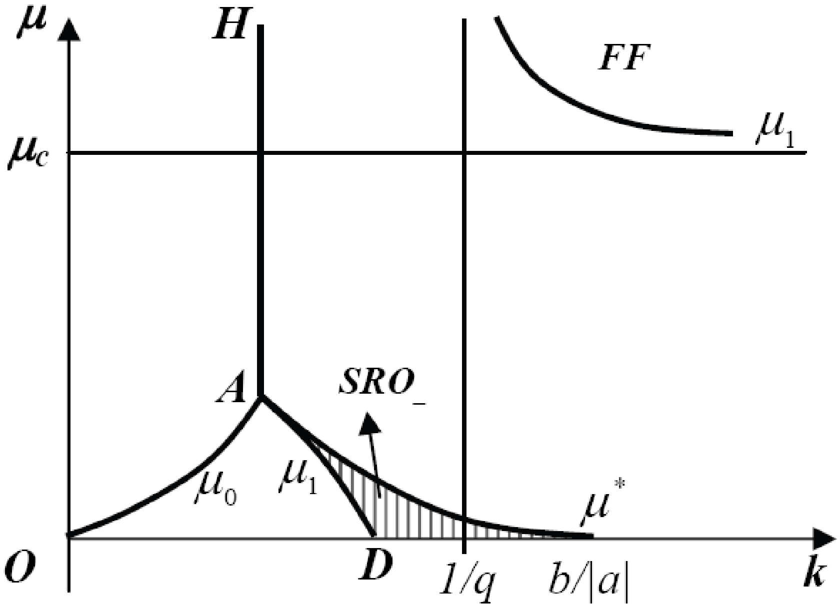

Fig. 27a Region of slide-rock about point O mode (SRO_-), case III1
($q\gamma \le 3k'$, $e' \ge 0$, $b/|a| \ge 1/q$)

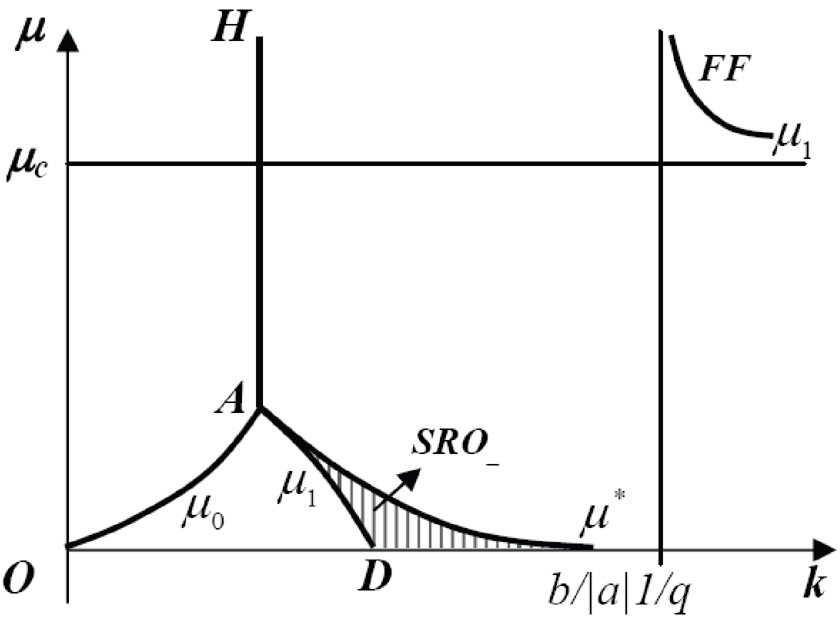

Fig. 27b Region of slide-rock about point O mode (SRO_-), case III1
($q\gamma \le 3k'$, $e' \le 0$, $b/|a| \le 1/q$)

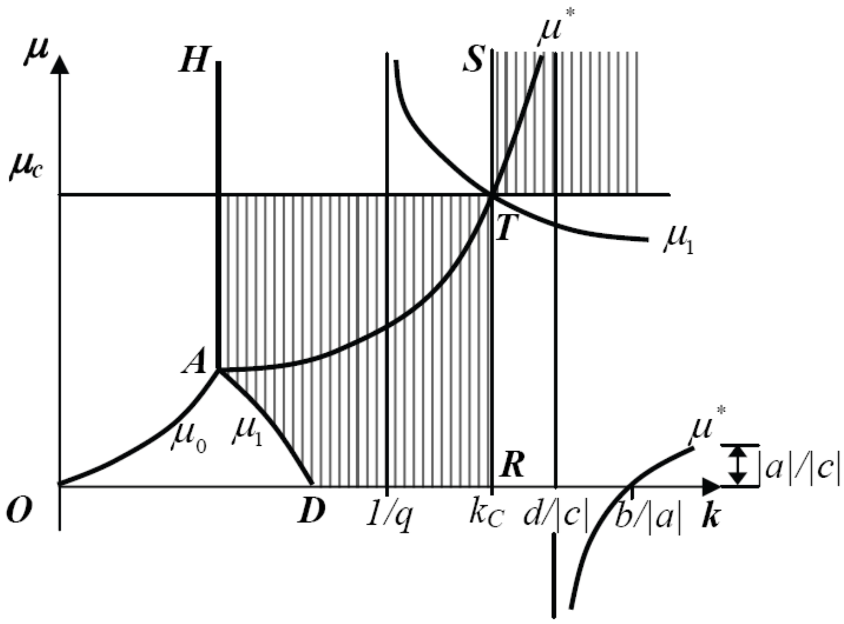

Fig. 28 Region of $f_y \geq 0$ for slide-rock about point O mode (SRO_-), case IV1 ($q\gamma \geq 3k', e \geq 0, e' \geq 0, b/|a| \geq d/|c|, b/|a| \geq 1/q$)

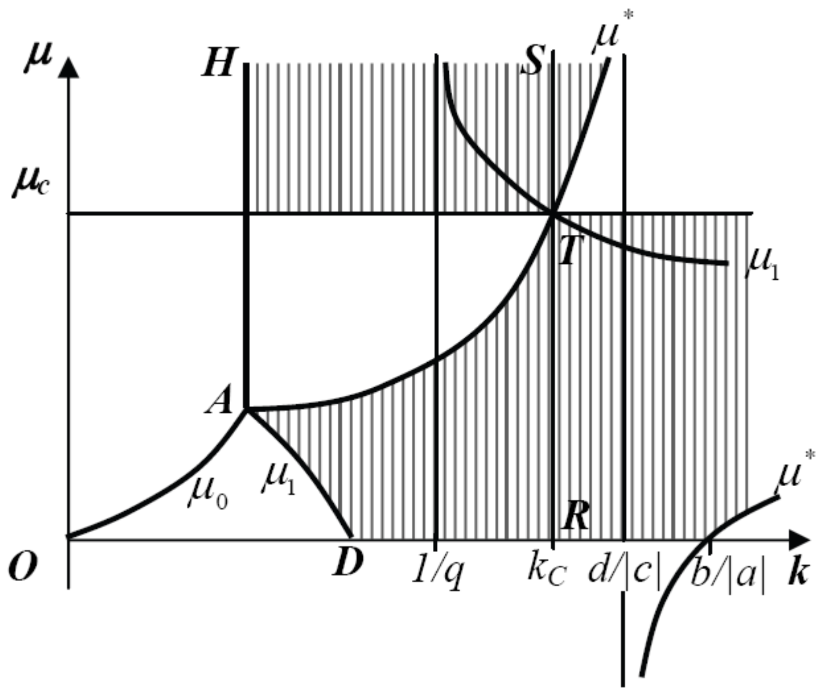

Fig. 29 Region of $\ddot{x}_O \leq 0$ for slide-rock about point O mode (SRO_-), case IV1 ($q\gamma \geq 3k', e \geq 0, e' \geq 0, b/|a| \geq d/|c|, b/|a| \geq 1/q$)

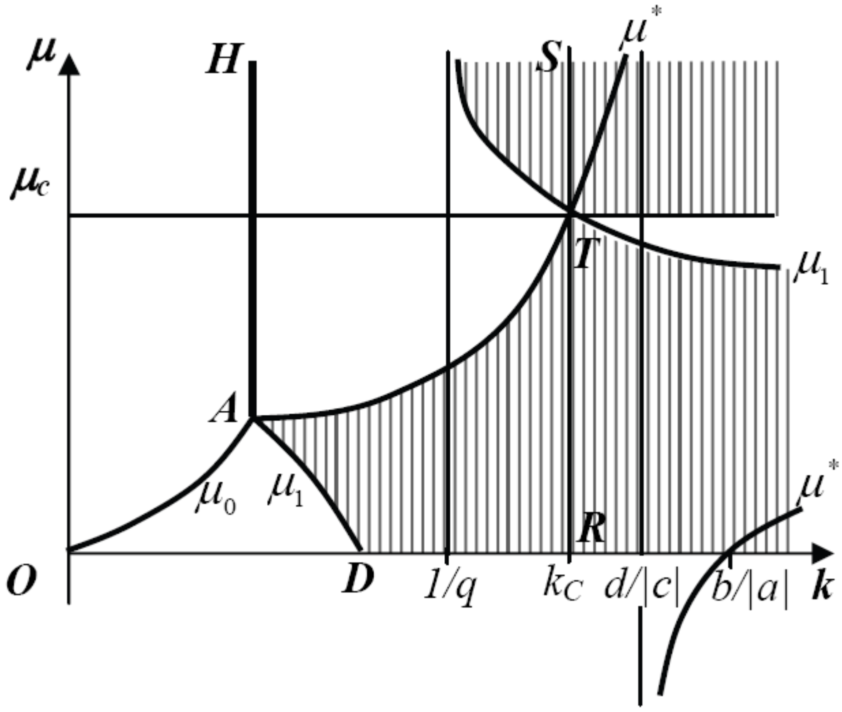

Fig. 30 Region of $\ddot{\theta} \ge 0$ for slide-rock about point O mode (SRO_{-}), case IV1 ($q\gamma \ge 3k'$, $e \ge 0$, $e' \ge 0$, $b/|a| \ge d/|c|$, $b/|a| \ge 1/q$)

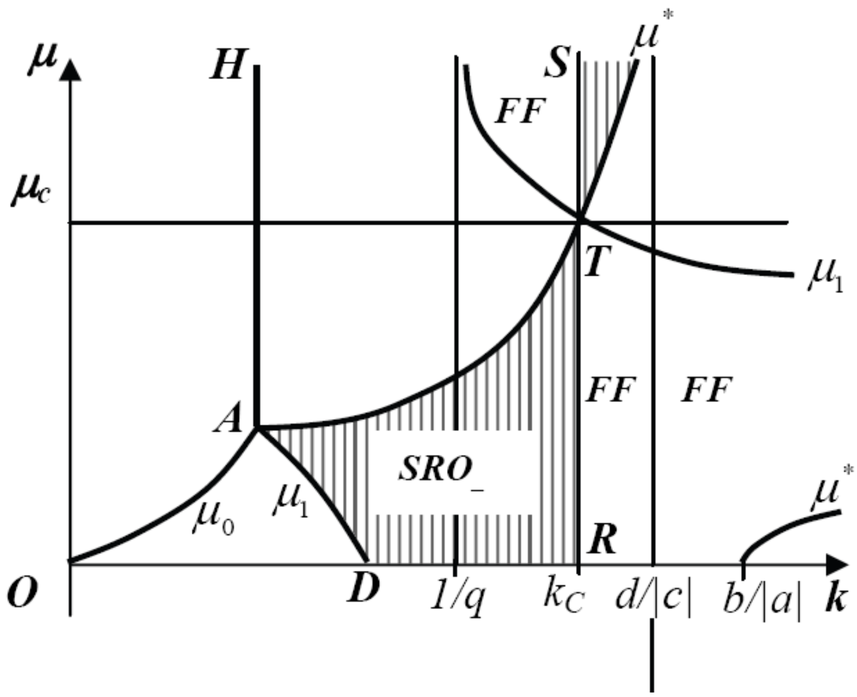

Fig. 31 Region of slide-rock about point O mode (SRO_{-}), case IV1 ($q\gamma \ge 3k'$, $e \ge 0$, $e' \ge 0$, $b/|a| \ge d/|c|$, $b/|a| \ge 1/q$)

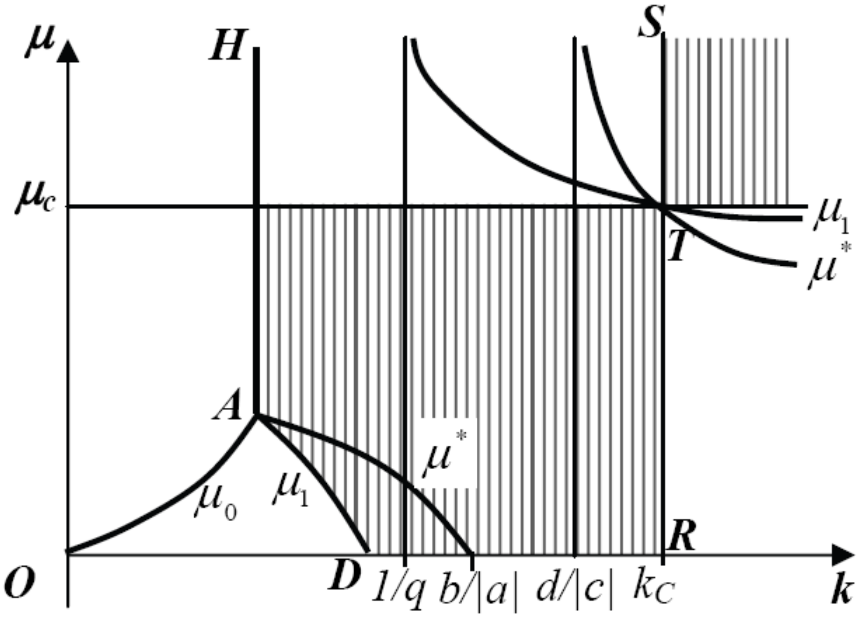

Fig. 32a Region of $f_y \geq 0$ for slide-rock about point O mode (SRO_-), case IV2,1 ($q\gamma \geq 3k'$, $e \leq 0$, $e' \geq 0$, $b/|a| \leq d/|c|$, $b/|a| \geq 1/q$)

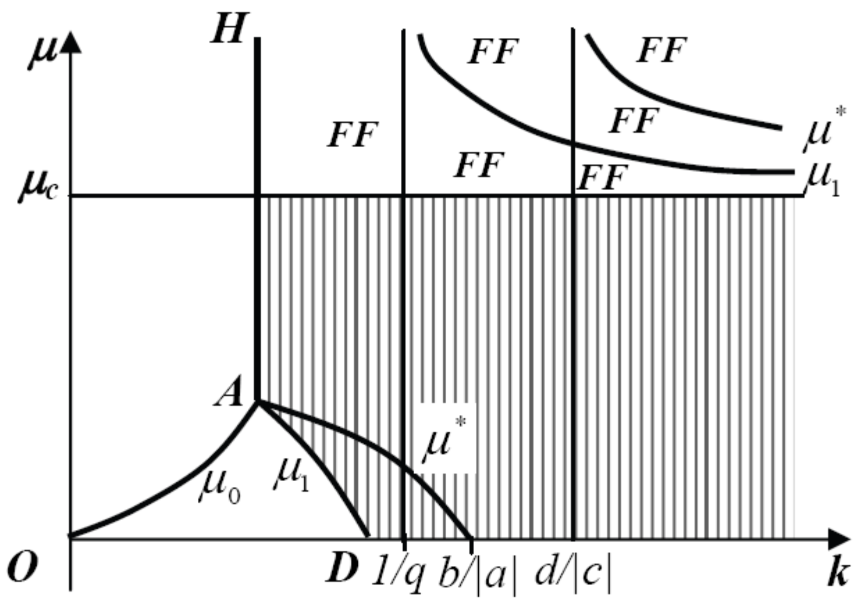

Fig. 32b Region of $f_y \geq 0$ for slide-rock about point O mode (SRO_-), case IV2,2 ($q\gamma \leq 3k'$, $e \leq 0$, $e' \geq 0$, $b/|a| \leq d/|c|$, $b/|a| \geq 1/q$)

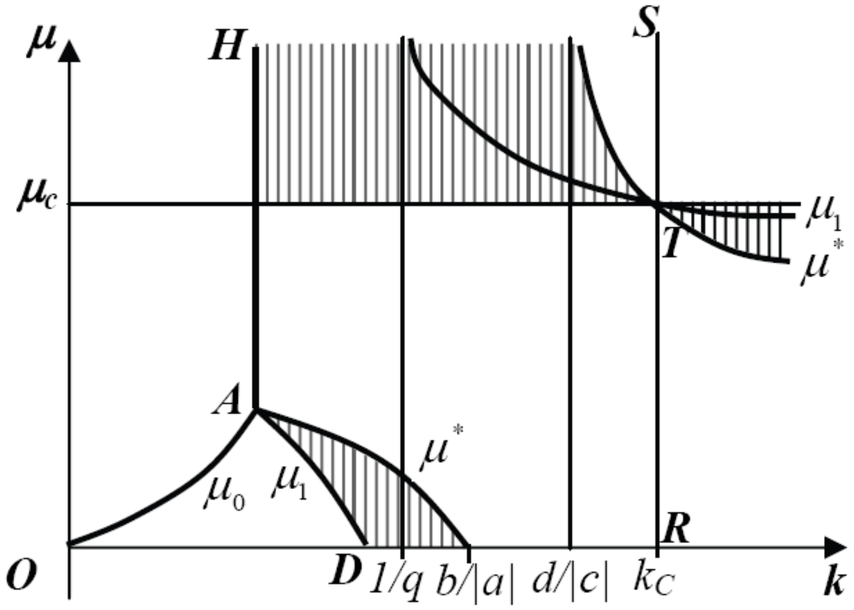

Fig. 33a Region of $\ddot{x}_O \le 0$ for slide-rock about point O mode (SRO_-), case IV2,1 ($q\gamma \ge 3k'$, $e \le 0$, $e' \ge 0$, $b/|a| \le d/|c|$, $b/|a| \ge 1/q$)

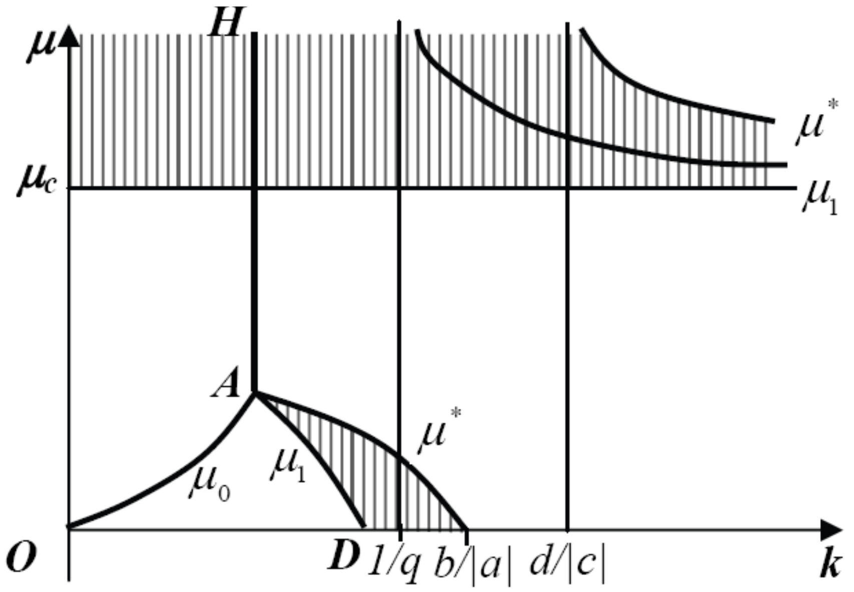

Fig. 33b Region of $\ddot{x}_O \le 0$ for slide-rock about point O mode (SRO_-), case IV2,2 ($q\gamma \le 3k'$, $e \le 0$, $e' \ge 0$, $b/|a| \le d/|c|$, $b/|a| \ge 1/q$)

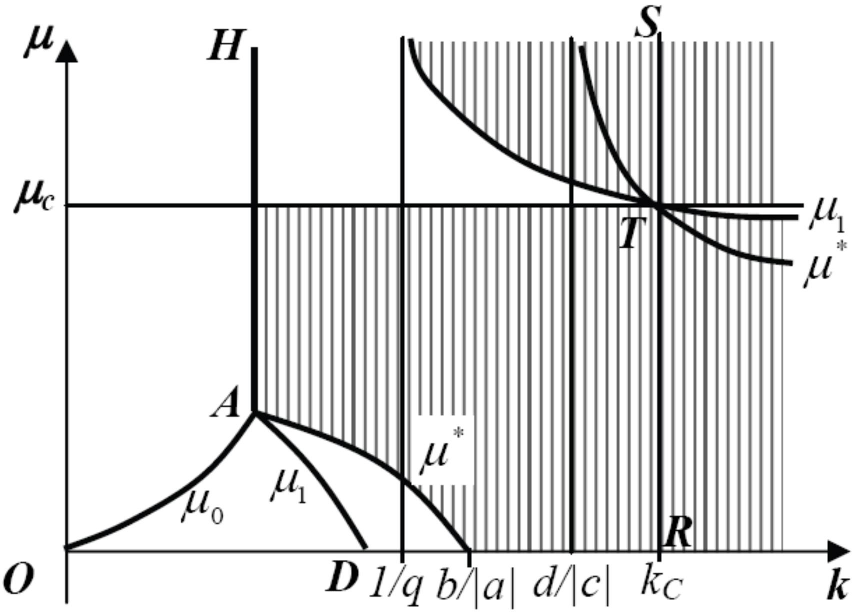

Fig. 34a Region of $\ddot{\theta} \geq 0$ for slide-rock about point O mode (SRO_{-}), case IV2,1 ($q\gamma \geq 3k'$, $e \leq 0$, $e' \geq 0$, $b/|a| \leq d/|c|$, $b/|a| \geq 1/q$)

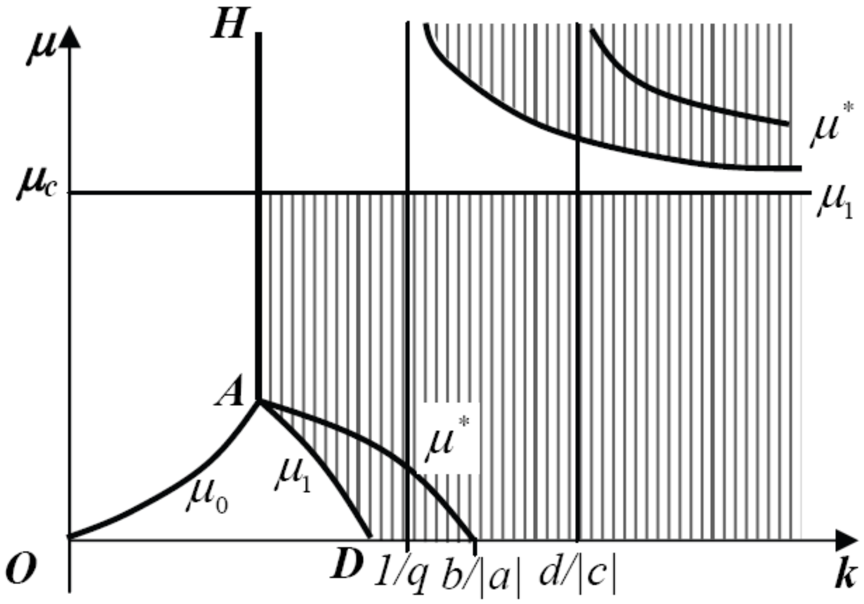

Fig. 34b Region of $\ddot{\theta} \geq 0$ for slide-rock about point O mode (SRO_{-}), case IV2,2 ($q\gamma \leq 3k'$, $e \leq 0$, $e' \geq 0$, $b/|a| \leq d/|c|$, $b/|a| \geq 1/q$)

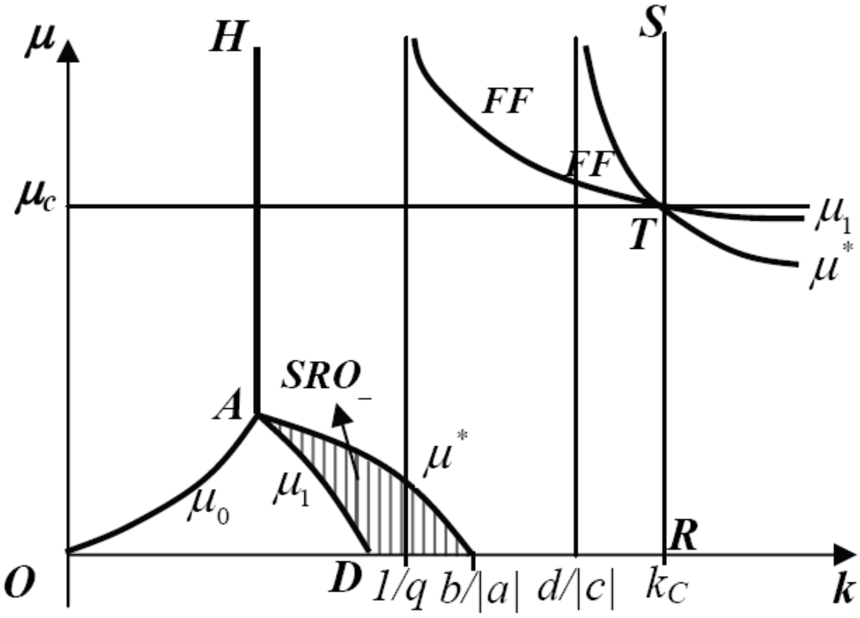

Fig. 35a Region of slide-rock about point O mode (SRO_{-}), case IV2,1

($q\gamma \geq 3k'$, $e \leq 0$, $e' \geq 0$, $b/|a| \leq d/|c|$, $b/|a| \geq 1/q$)

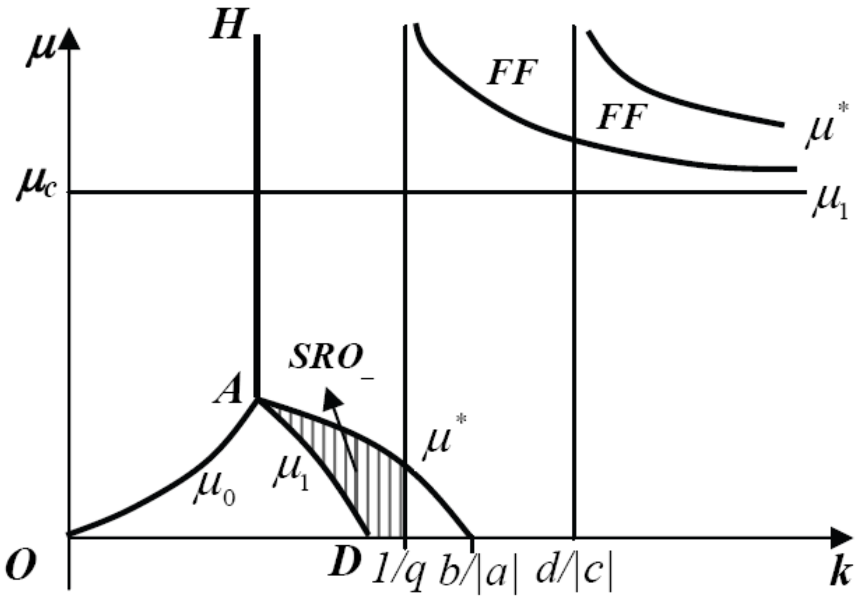

Fig. 35b Region of slide-rock about point O mode (SRO_{-}), case IV2,2

($q\gamma \leq 3k'$, $e \leq 0$, $e' \geq 0$, $b/|a| \leq d/|c|$, $b/|a| \geq 1/q$)

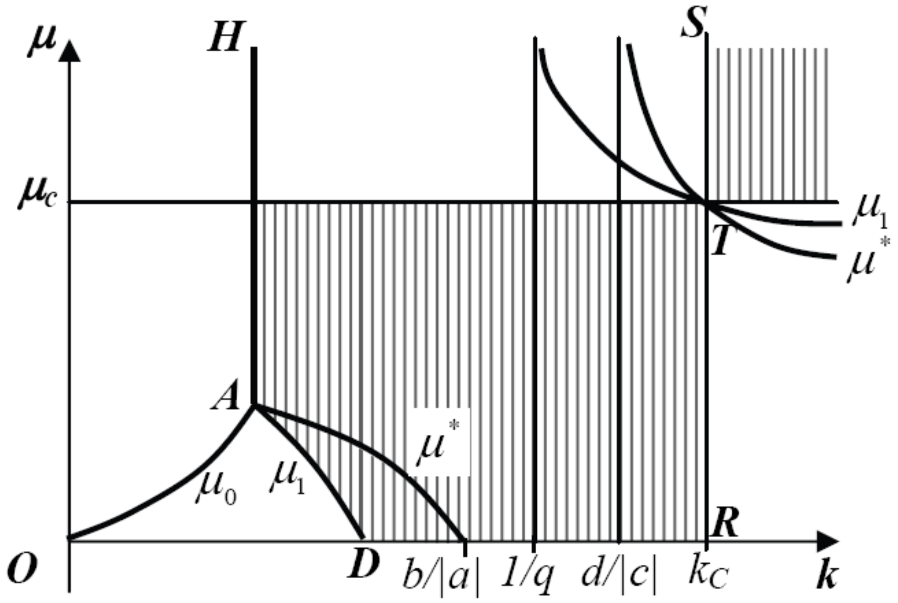

Fig. 36a Region of $f_y \geq 0$ for slide-rock about point O mode (SRO_-), case IV3,1 ($q\gamma \geq 3k', e \leq 0, e' \leq 0, b/|a| \leq d/|c|, b/|a| \leq 1/q$)

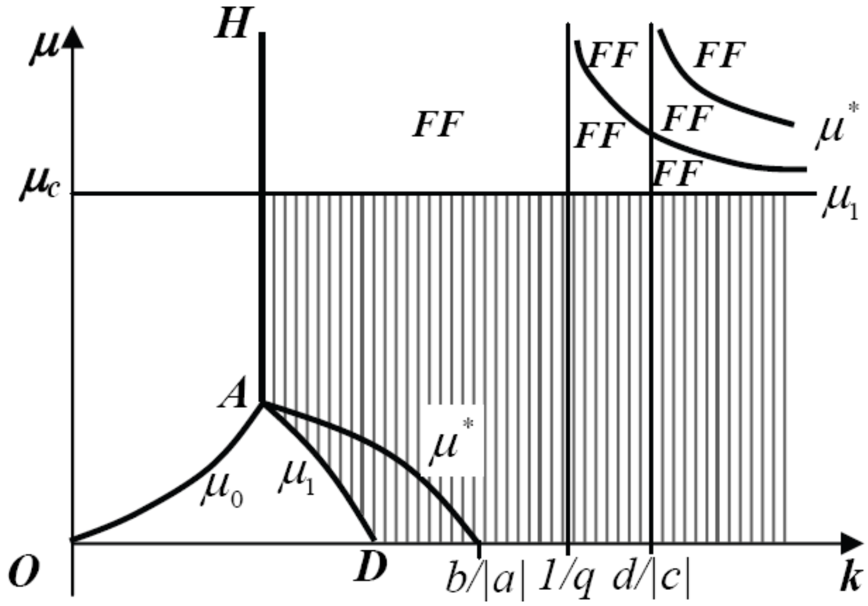

Fig. 36b Region of $f_y \geq 0$ for slide-rock about point O mode (SRO_-), case IV3,2 ($q\gamma \leq 3k', e \leq 0, e' \leq 0, b/|a| \leq d/|c|, b/|a| \leq 1/q$)

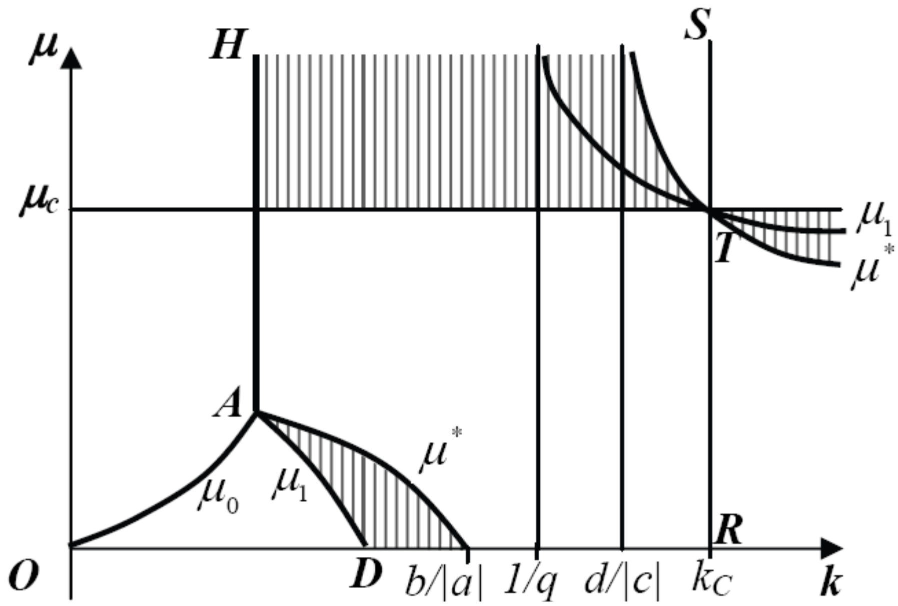

Fig. 37a Region of $\ddot{x}_O \le 0$ for slide-rock about point O mode (SRO_-), case IV3,1 ($q\gamma \ge 3k', e \le 0, e' \le 0, b/|a| \le d/|c|, b/|a| \le 1/q$)

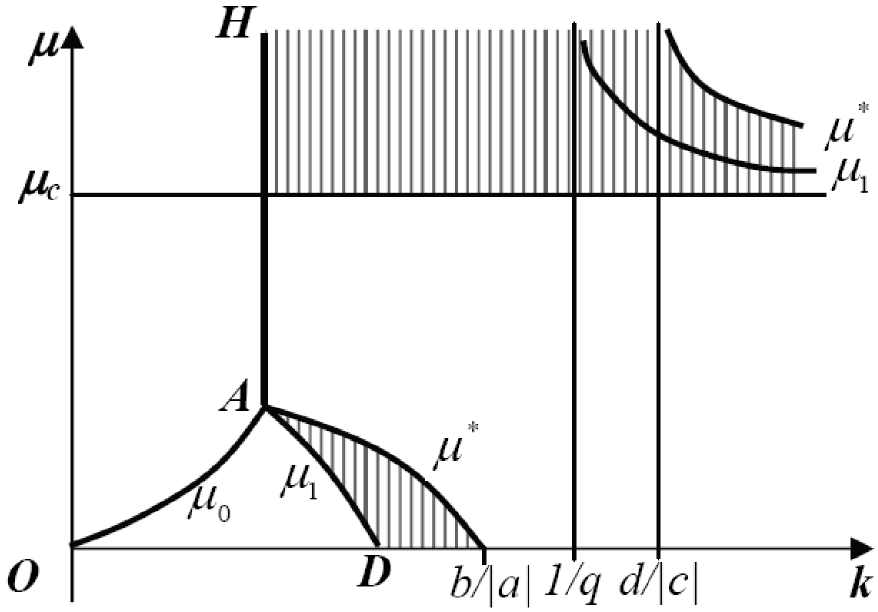

Fig. 37b Region of $\ddot{x}_O \le 0$ for slide-rock about point O mode (SRO_-), case IV3,2 ($q\gamma \le 3k', e \le 0, e' \le 0, b/|a| \le d/|c|, b/|a| \le 1/q$)

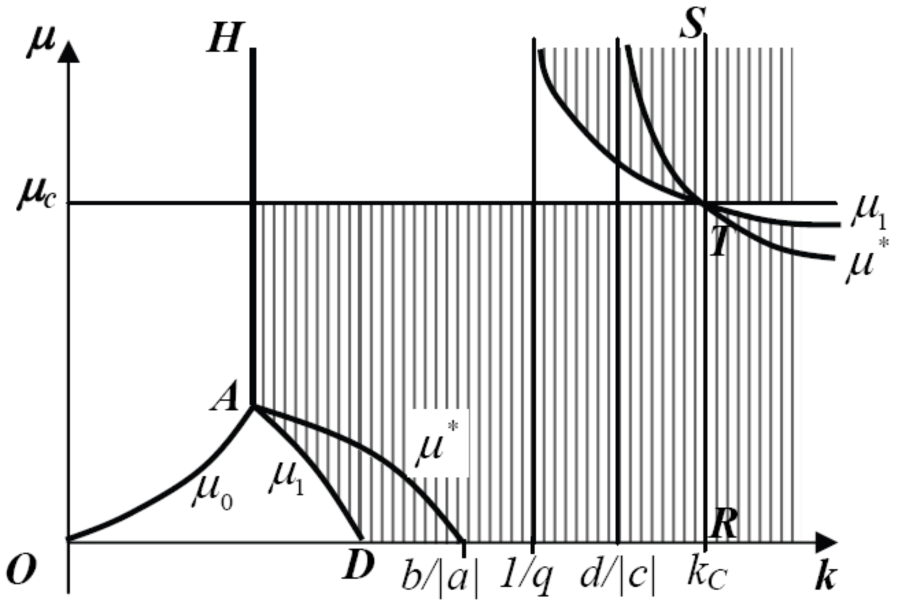

Fig. 38a Region of $\ddot{\theta} \geq 0$ for slide-rock about point O mode (SRO_{-}), case IV3,1 ($q\gamma \geq 3k', e \leq 0, e' \leq 0, b/|a| \leq d/|c|, b/|a| \leq 1/q$)

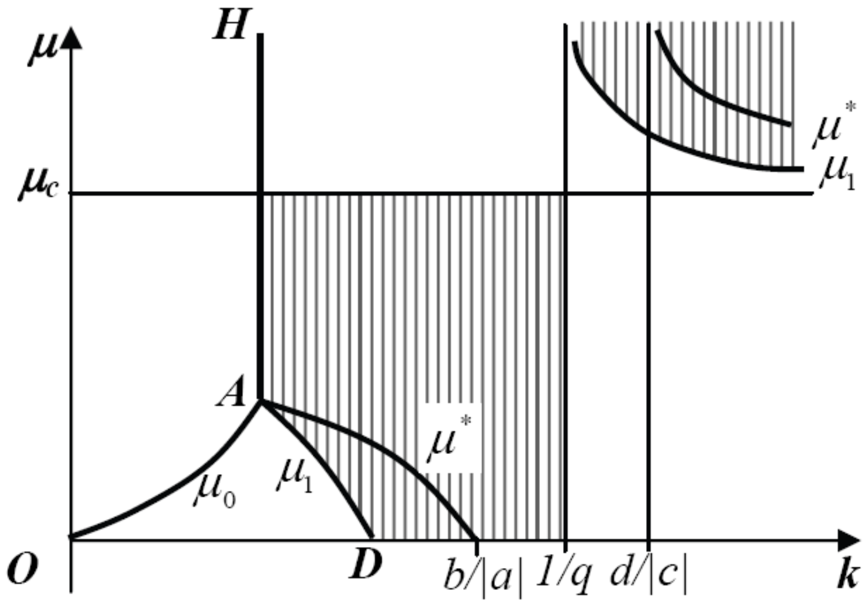

Fig. 38b Region of $\ddot{\theta} \geq 0$ for slide-rock about point O mode (SRO_{-}), case IV3,2 ($q\gamma \leq 3k', e \leq 0, e' \leq 0, b/|a| \leq d/|c|, b/|a| \leq 1/q$)

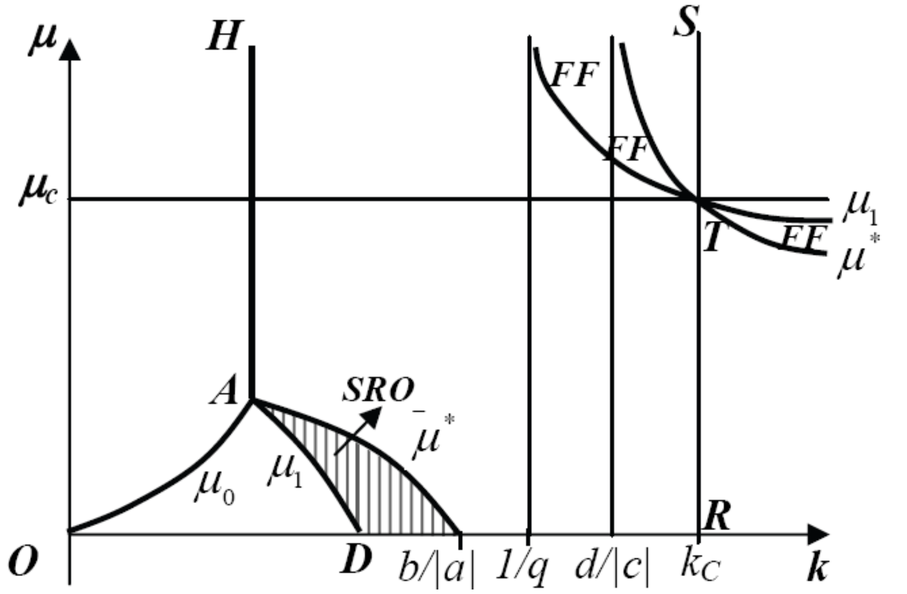

Fig. 39a Region of slide-rock about point O mode (SRO_-), case IV3,1

($q\gamma \geq 3k'$, $e \leq 0$, $e' \leq 0$, $b/|a| \leq d/|c|$, $b/|a| \leq 1/q$)

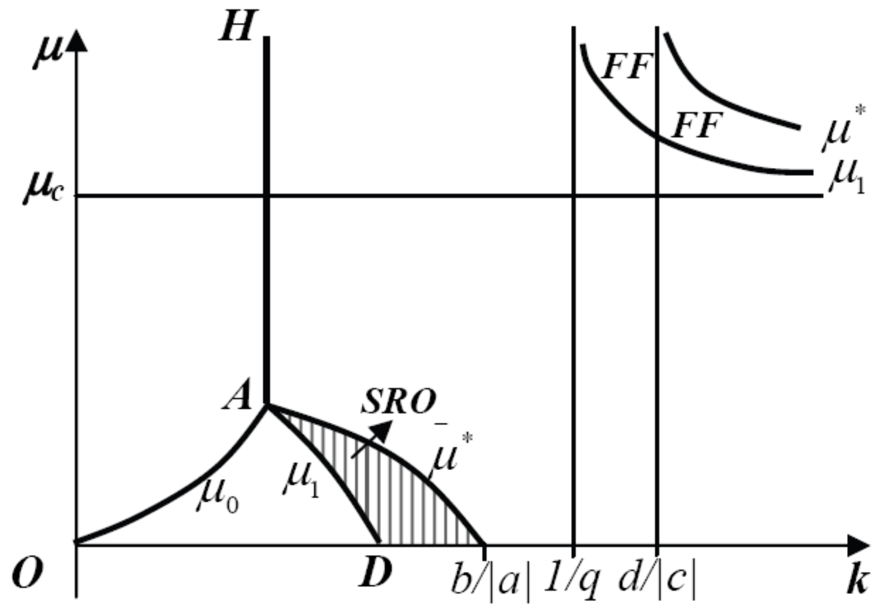

Fig. 39b Region of slide-rock about point O mode (SRO_-), case IV3,2

($q\gamma \leq 3k'$, $e \leq 0$, $e' \leq 0$, $b/|a| \leq d/|c|$, $b/|a| \leq 1/q$)

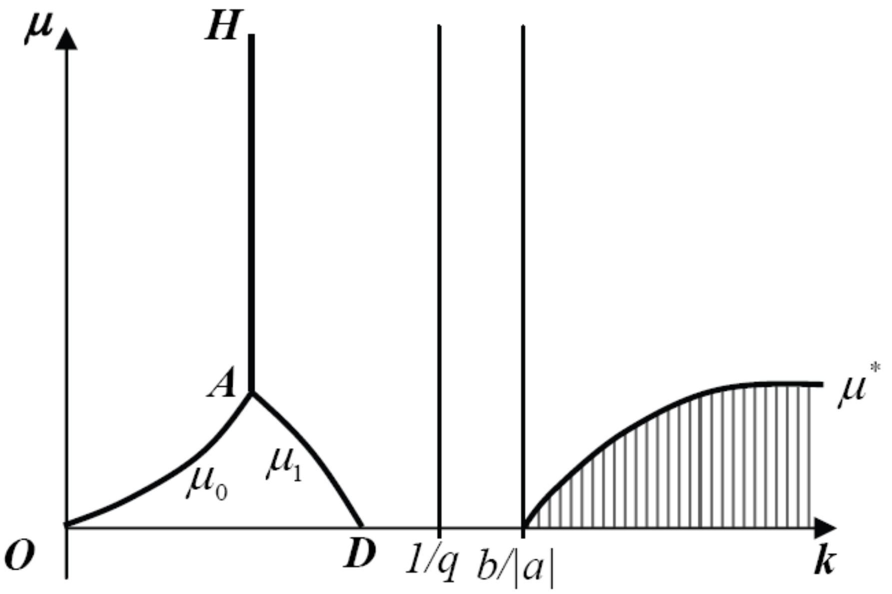

Fig. 40a Region of $\ddot{x}_O \geq 0$ for slide-rock about point O mode (SRO_+), case V1 ($q\gamma \leq 3k'$, $e \leq 0$, $e' \geq 0$)

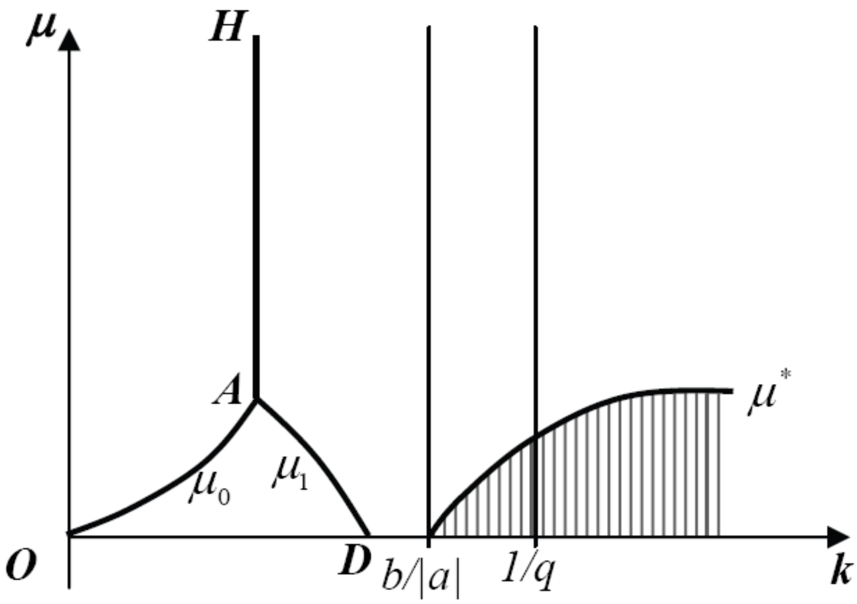

Fig. 40b Region of $\ddot{x}_O \geq 0$ for slide-rock about point O mode (SRO_+), case V2 ($q\gamma \leq 3k'$, $e \leq 0$, $e' \leq 0$)

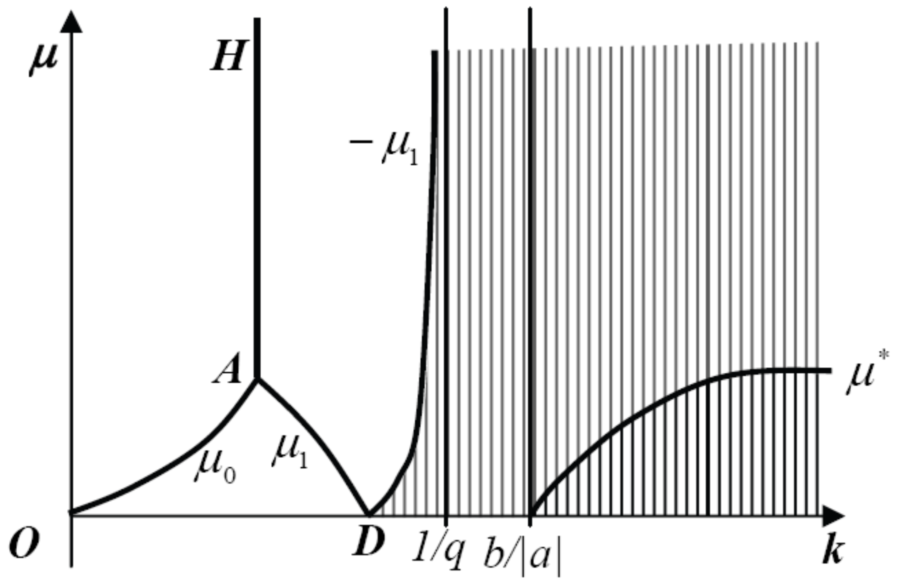

Fig. 41a Region of $\ddot{\theta} \geq 0$ for slide-rock about point O mode (SRO_+), case V1 ($q\gamma \leq 3k', e \leq 0, e' \geq 0$)

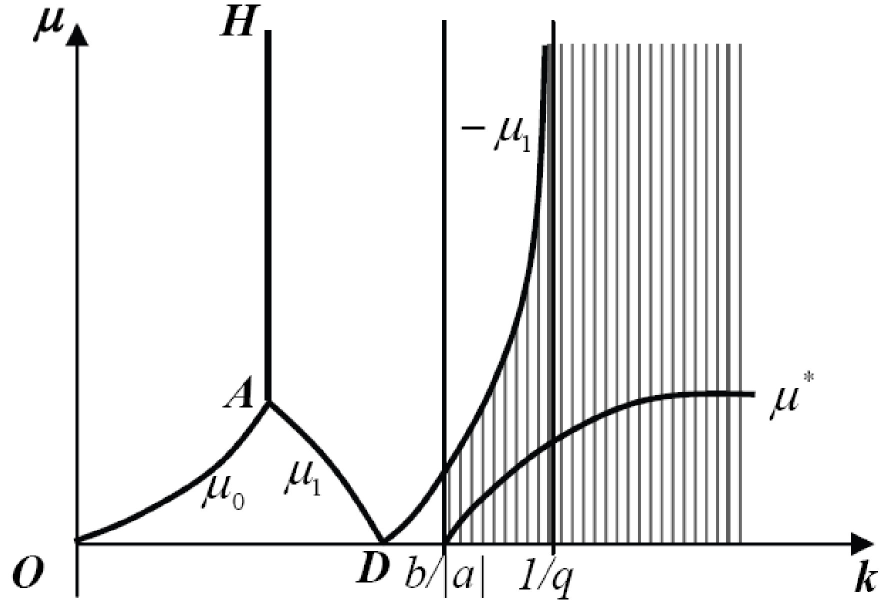

Fig. 41b Region of $\ddot{\theta} \geq 0$ for slide-rock about point O mode (SRO_+), case V2 ($q\gamma \leq 3k', e \leq 0, e' \leq 0$)

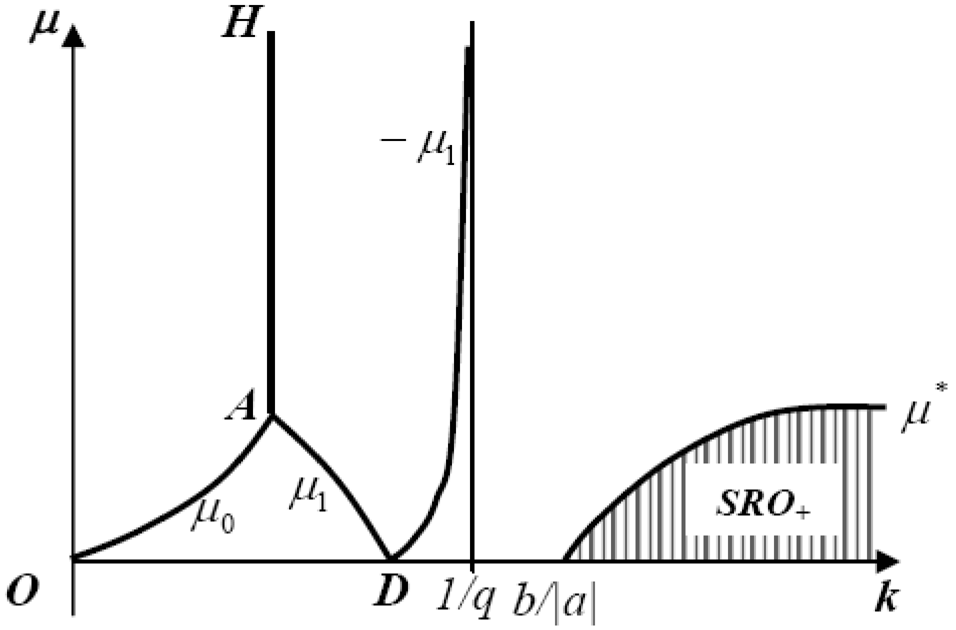

Fig. 42a Region of slide-rock about point O mode (SRO_+), case V1
($q\gamma \leq 3k'$, $e \leq 0$, $e' \geq 0$)

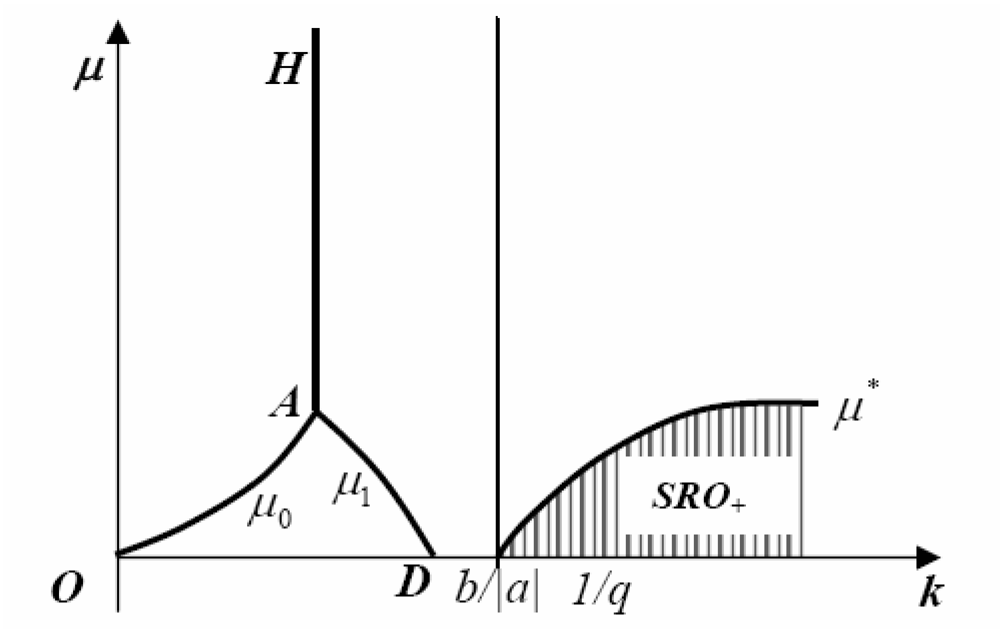

Fig. 42b Region of slide-rock about point O mode (SRO_+), case V2
($q\gamma \leq 3k'$, $e \leq 0$, $e' \leq 0$)

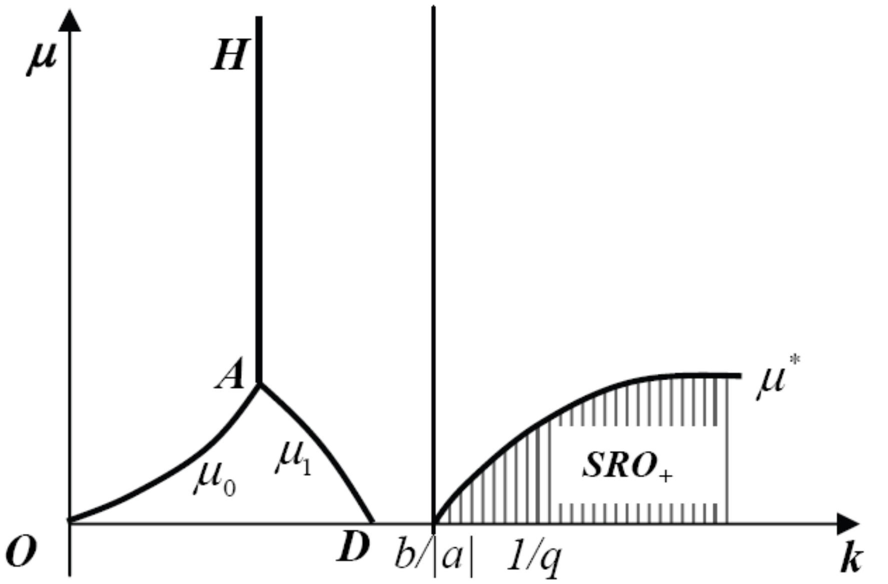

Fig. 43a Region of $f_y \geq 0$ for slide-rock about point O mode (SRO_+), case VI1,1 ($q\gamma \geq 3k', e \leq 0, e' \geq 0$)

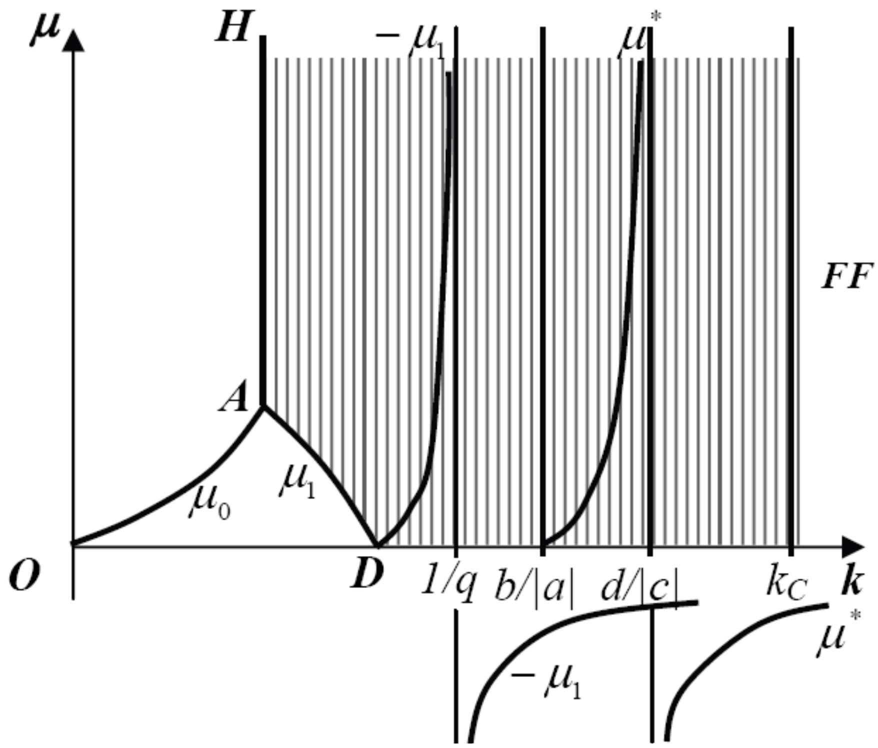

Fig. 43b Region of $f_y \geq 0$ for slide-rock about point O mode (SRO_+), case VI2,1 ($q\gamma \geq 3k', e \leq 0, e' \leq 0$)

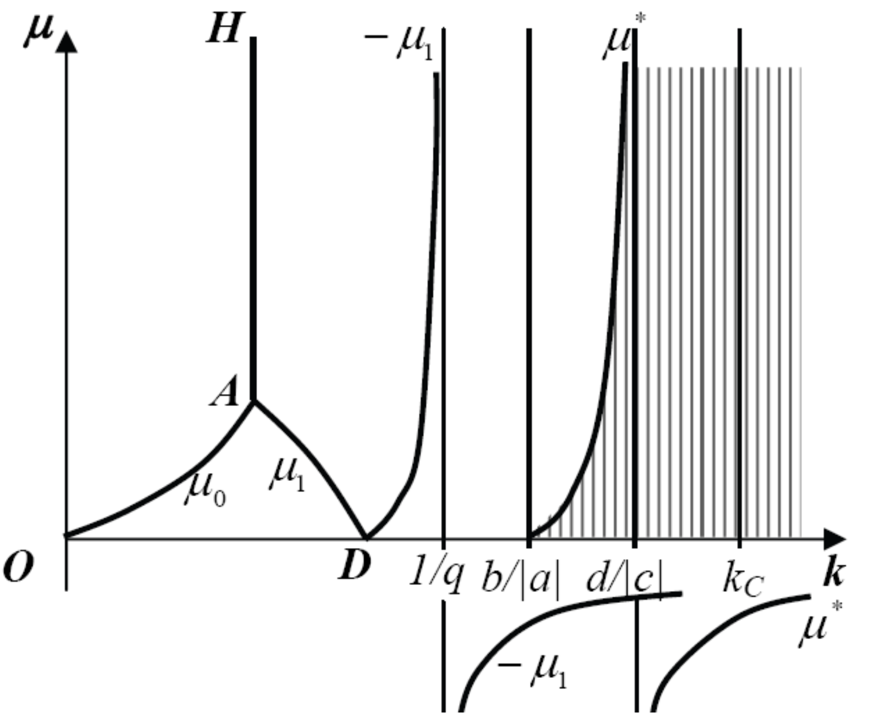

Fig. 44a Region of $\ddot{x}_O \geq 0$ for slide-rock about point O mode (SRO_+), case VI1,1 ($q\gamma \geq 3k', e \leq 0, e' \geq 0$)

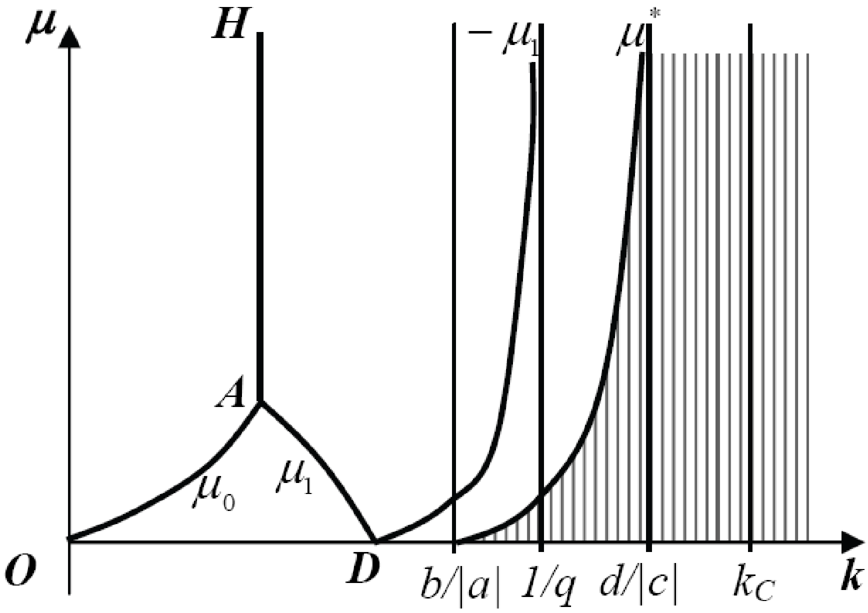

Fig. 44b Region of $\ddot{x}_O \geq 0$ for slide-rock about point O mode (SRO_+), case VI2,1 ($q\gamma \geq 3k', e \leq 0, e' \leq 0$)

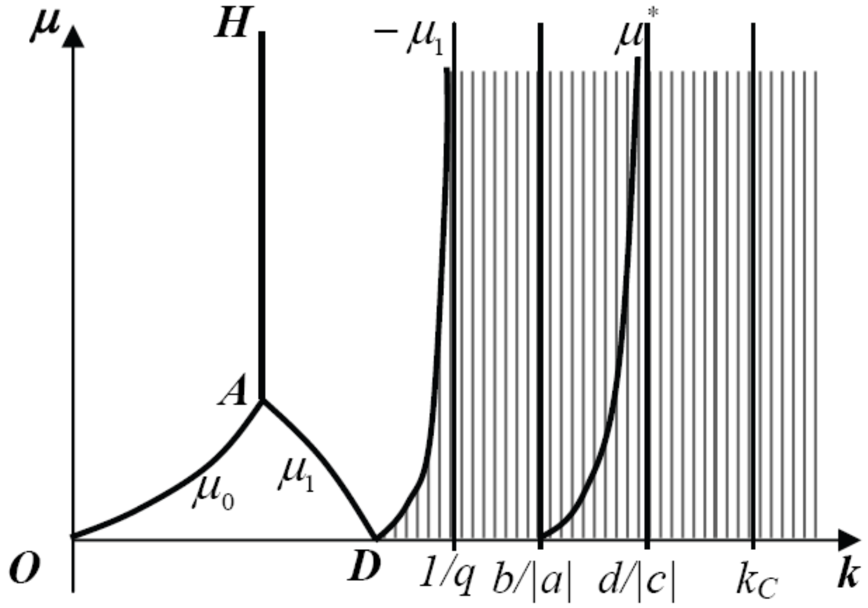

Fig. 45a Region of $\ddot{\theta} \geq 0$ for slide-rock about point O mode (SRO_+), case VI1,1 ($q\gamma \geq 3k', e \leq 0, e' \geq 0$)

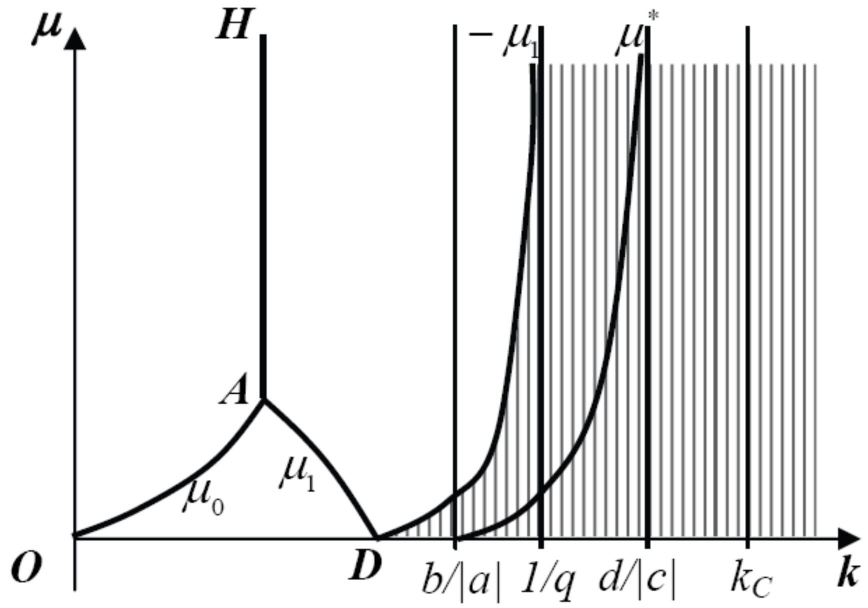

Fig. 45b Region of $\ddot{\theta} \geq 0$ for slide-rock about point O mode (SRO_+), case VI2,1 ($q\gamma \geq 3k', e \leq 0, e' \leq 0$)

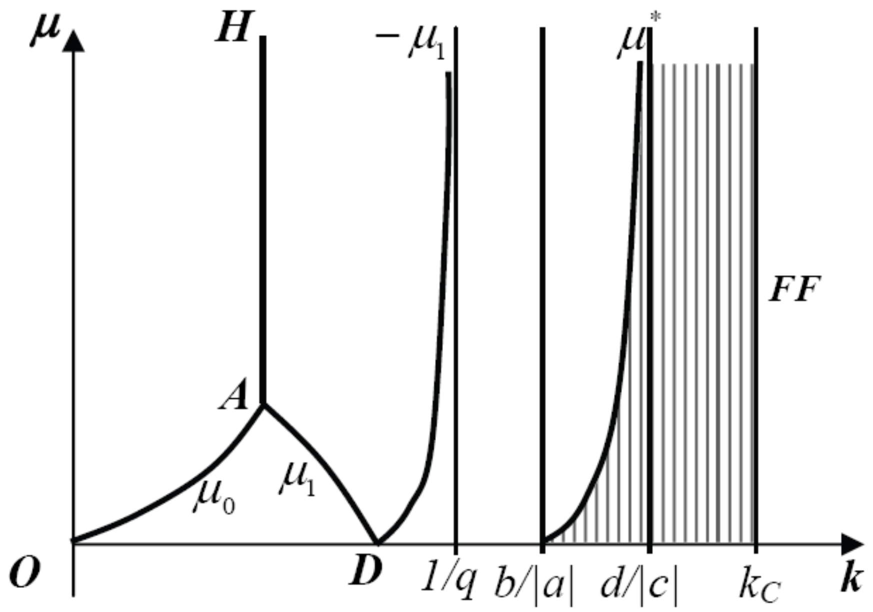

Fig. 46a Region of slide-rock about point O mode (SRO_+), case VI1,1
($q\gamma \geq 3k', e \leq 0, e' \geq 0$)

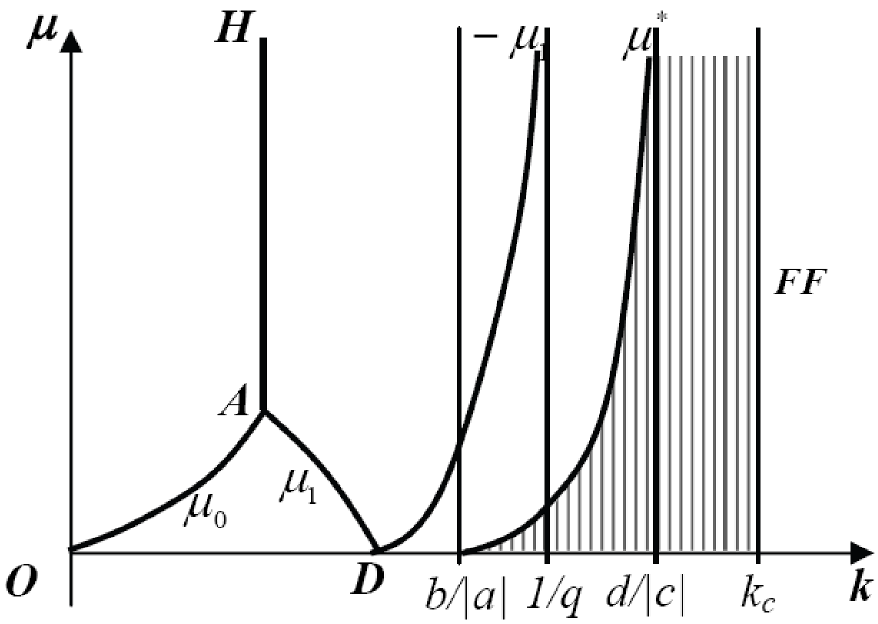

Fig. 46b Region of slide-rock about point O mode (SRO_+), case VI2,1
($q\gamma \geq 3k', e \leq 0, e' \leq 0$)

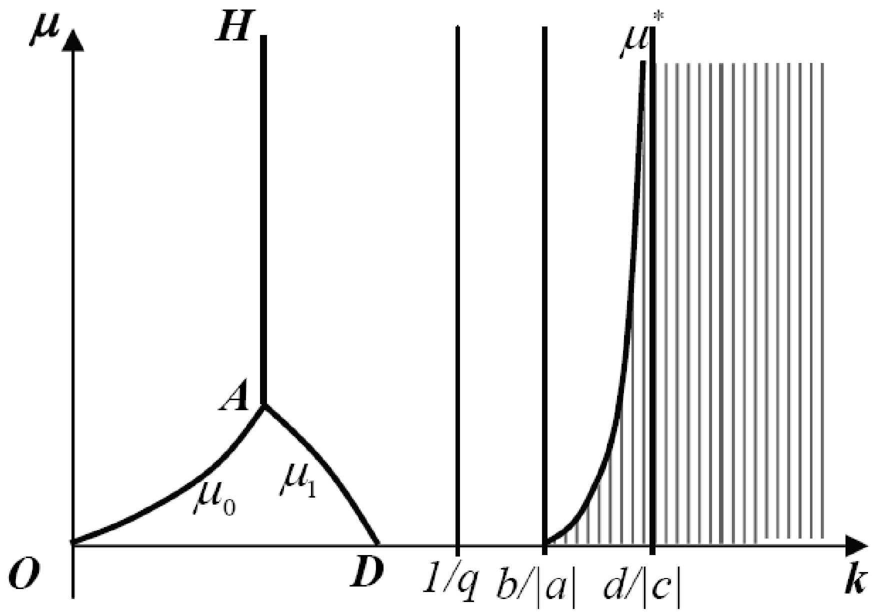

Fig. 47a Region of slide-rock about point O mode (SRO_+), case VI1,2
($q\gamma \le 3k'$, $e \le 0$, $e' \ge 0$)

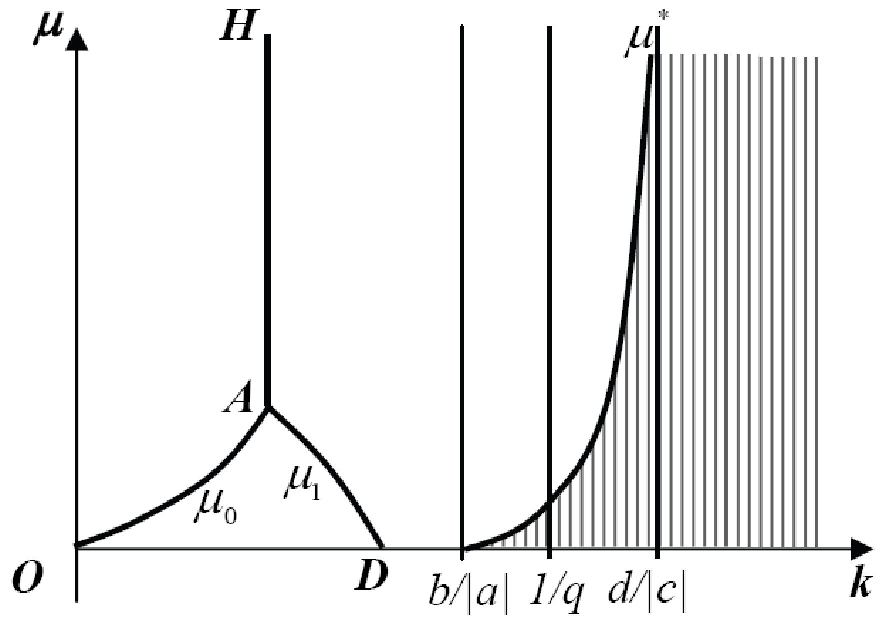

Fig. 47b Region of slide-rock about point O mode (SRO_+), case VI1,2
($q\gamma \le 3k'$, $e \le 0$, $e' \le 0$)

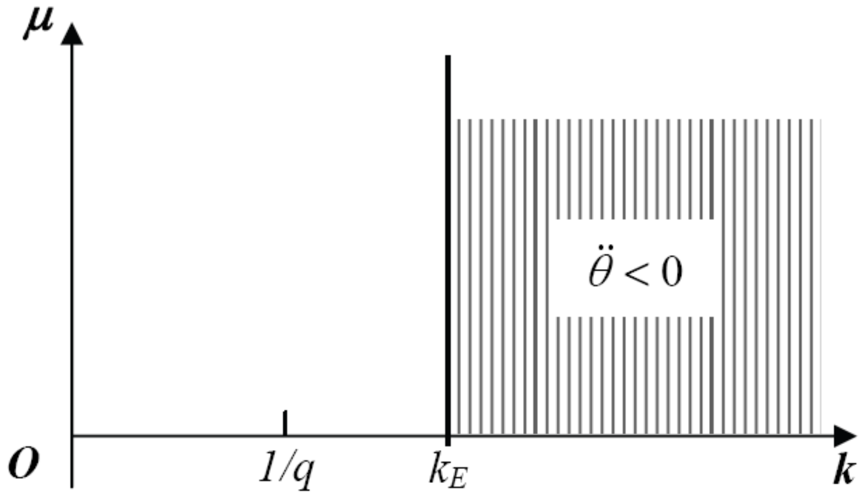

Fig. 48 Region of $\ddot{\theta} \leq 0$ for rock about point O' mode (RO')

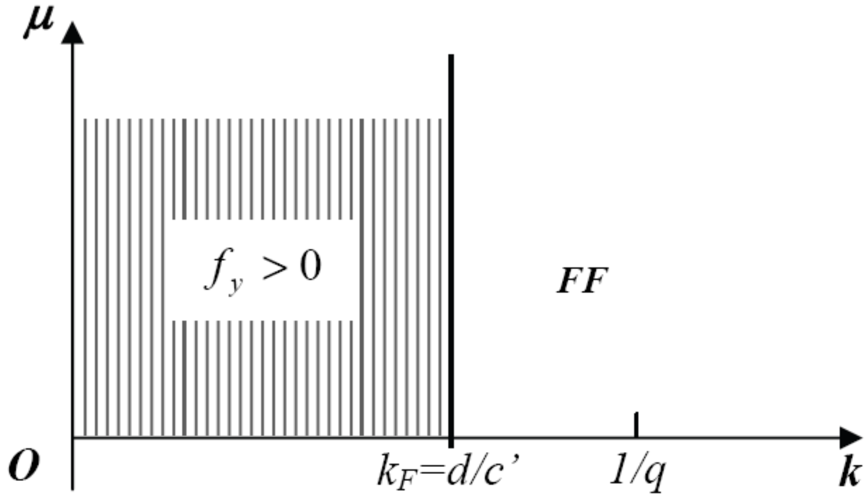

Fig. 49 Region of $f_y \geq 0$ for rock about point O' mode (RO')

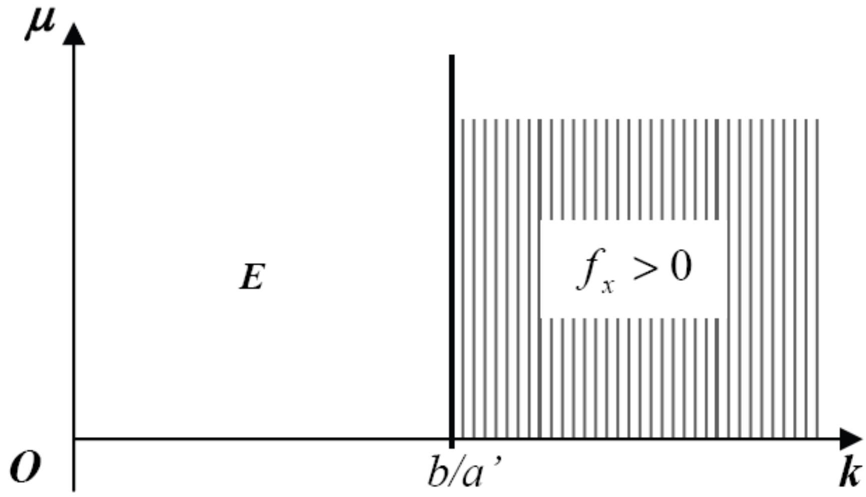

Fig. 50 Region of $f_x \geq 0$ for rock about point O' mode (RO')

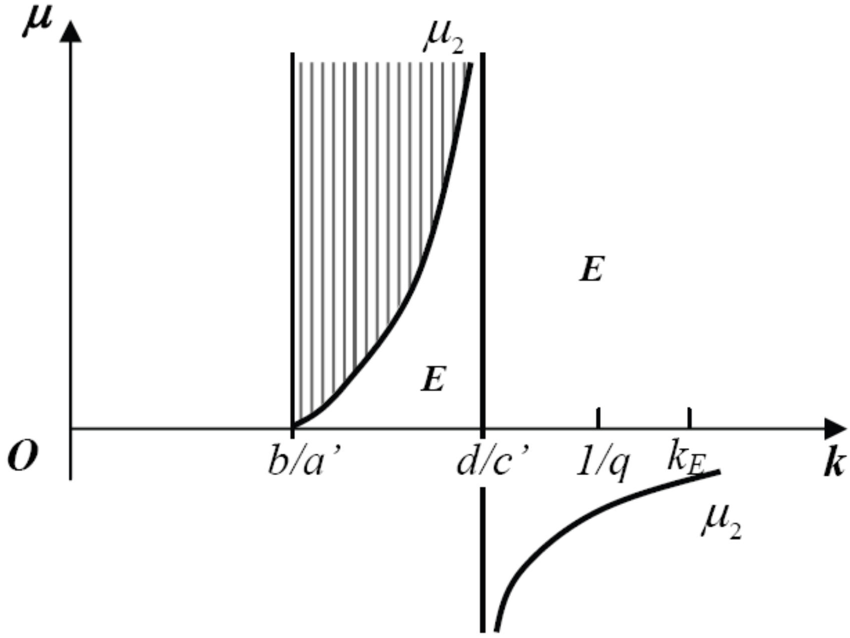

Fig. 51 Region of $\mu \geq f_x / f_y$ for rock about point O' mode (RO')

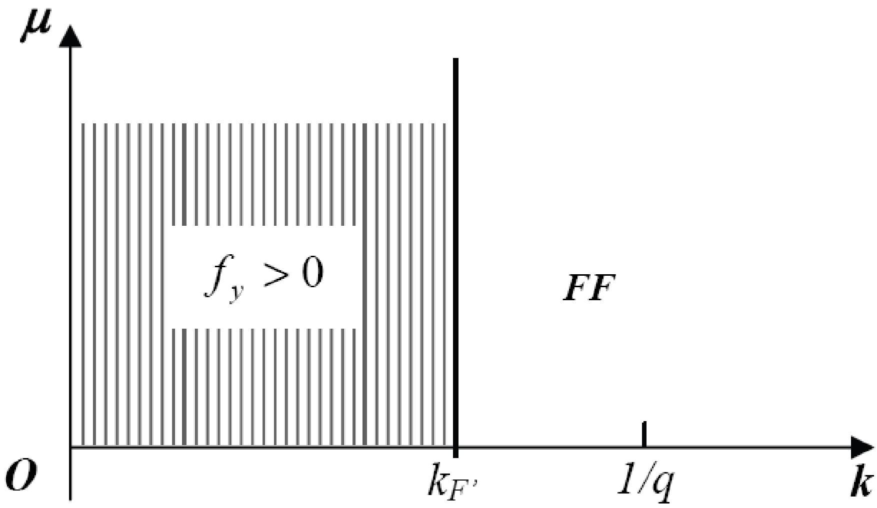

Fig. 52 Region of $f_y \geq 0$ for slide-rock about point O' mode (SRO'_-)

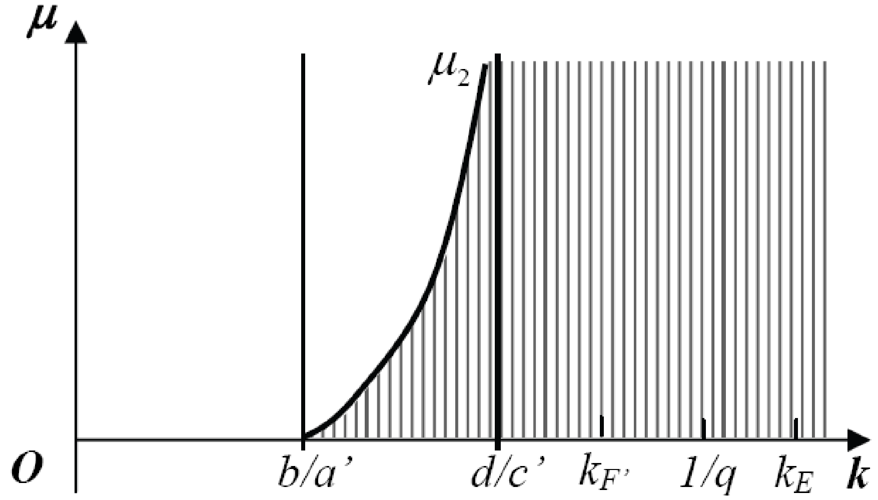

Fig. 53a Region of $\ddot{x}_O \leq 0$ for slide-rock about point O' mode $(SRO'_-)(e \geq 0)$

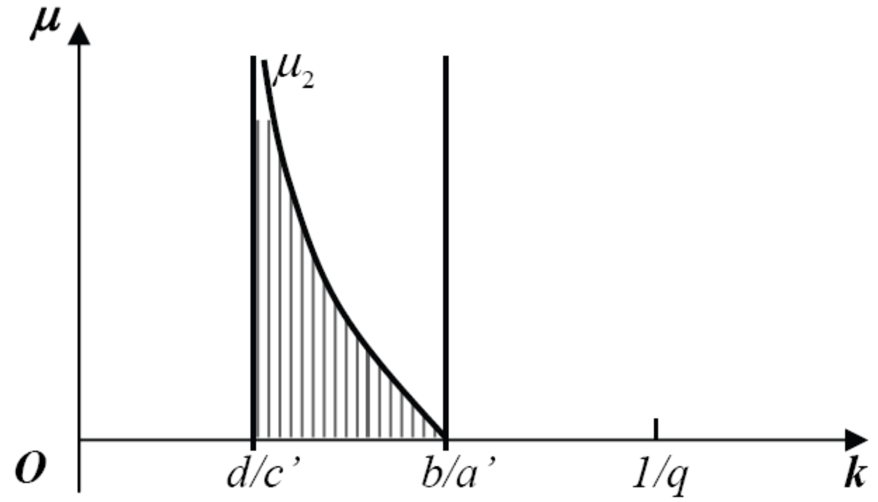

Fig. 53b Region of $\ddot{x}_O \leq 0$ for slide-rock about point O' mode $(SRO'_-)(e \leq 0)$

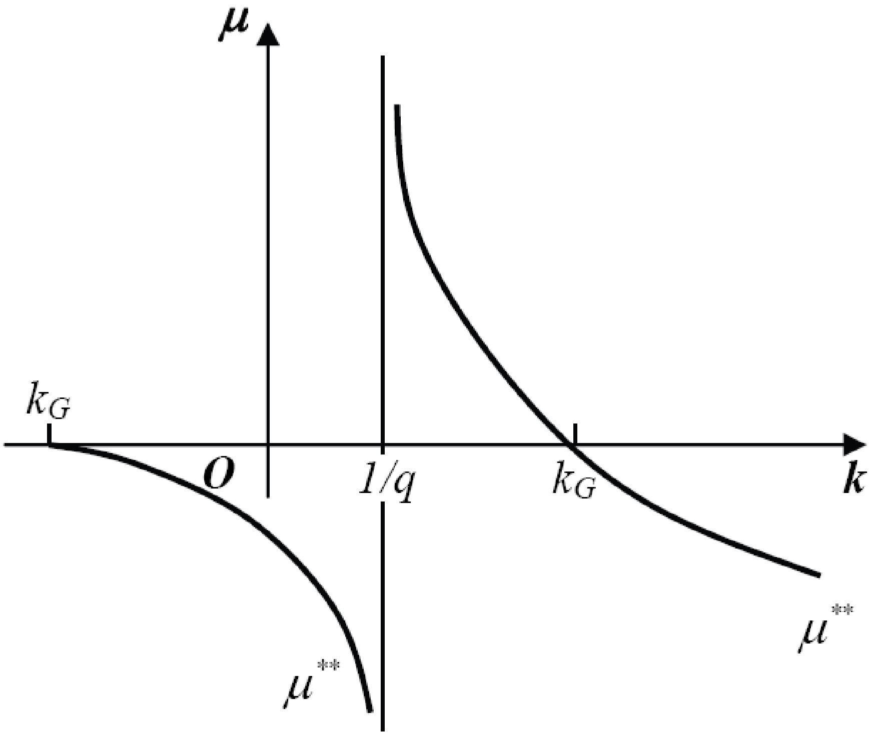

Fig. 54 Sketch of μ^{**} relevant to slide-rock about point O' mode (SRO'_-)

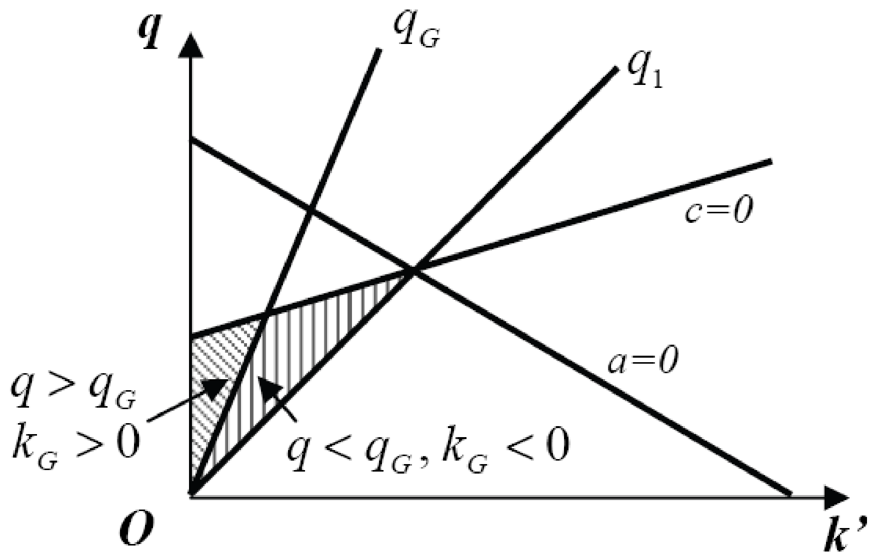

Fig. 55a Region of case I1,1 in $k'-q$ plane showing line $q = q_G$ for $\gamma \geq \sqrt{2}$

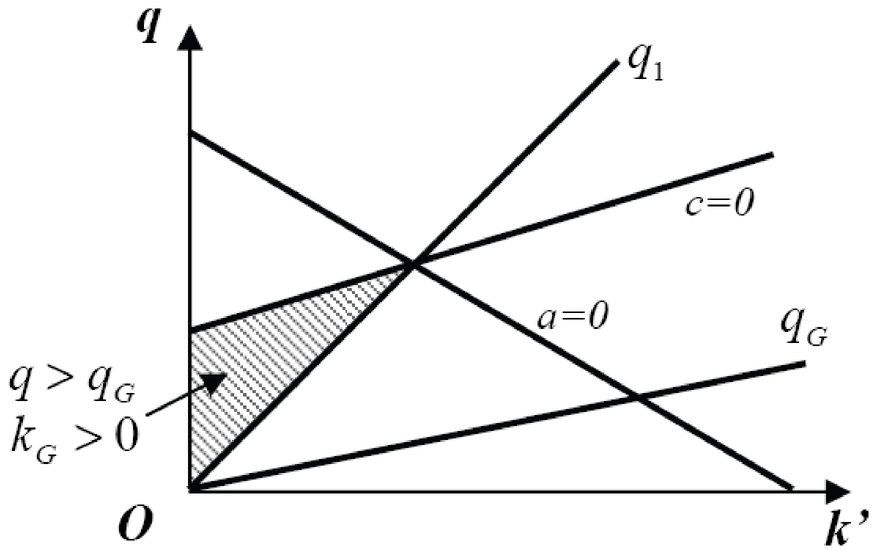

Fig. 55b Region of case I1,1 in $k'-q$ plane showing line $q = q_G$ for $\gamma \leq \sqrt{2}$

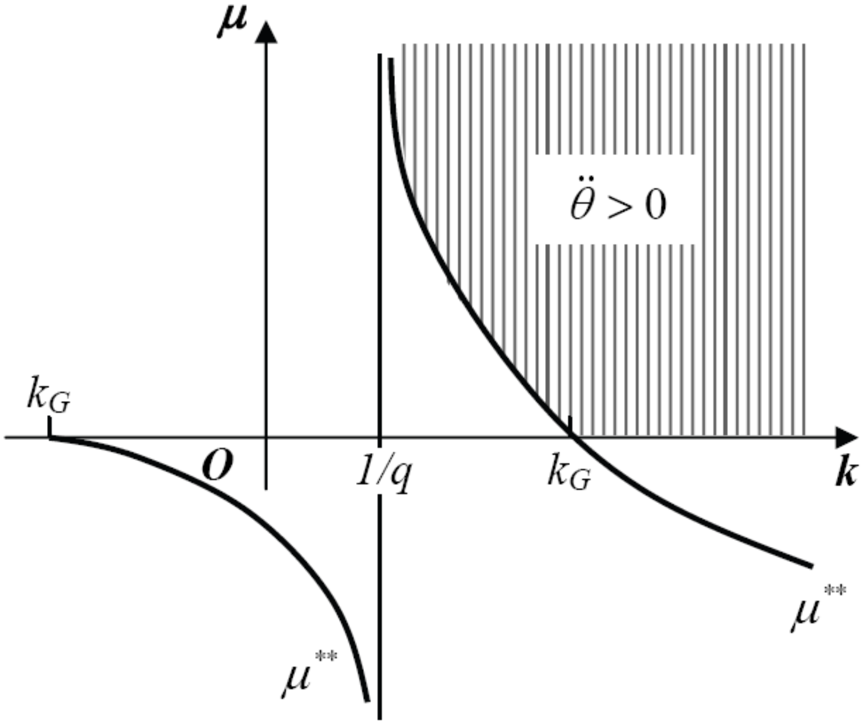

Fig. 56 Region of $\ddot{\theta} \le 0$ for slide-rock about point O' mode (SRO'_-)

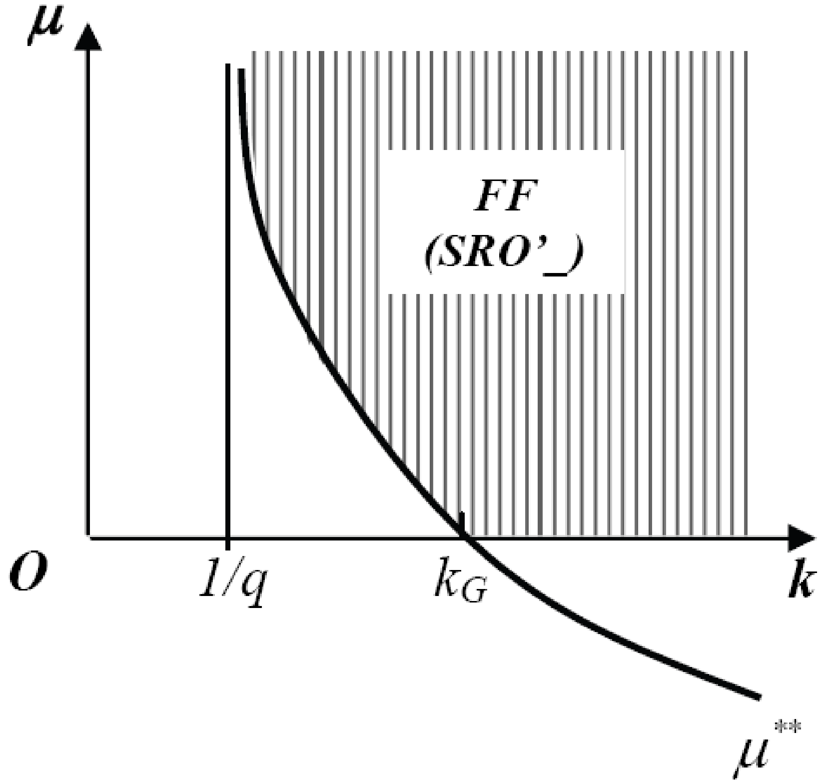

Fig. 57 Region of slide-rock about point O' mode (SRO'_-)

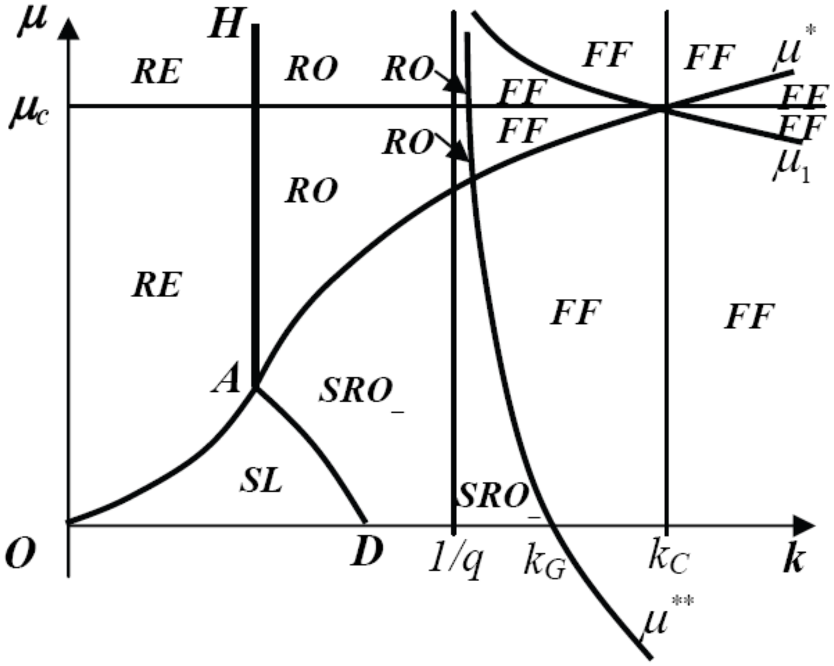

Fig. 58 Regions of all modes for case I1,1 ($\gamma \le \sqrt{2}$)

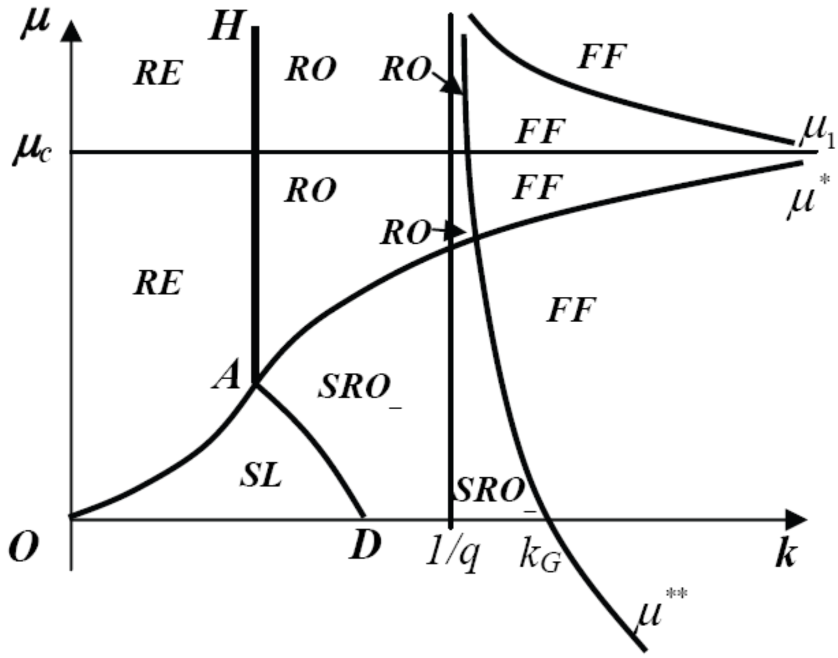

Fig. 59 Regions of all modes for case I1,2

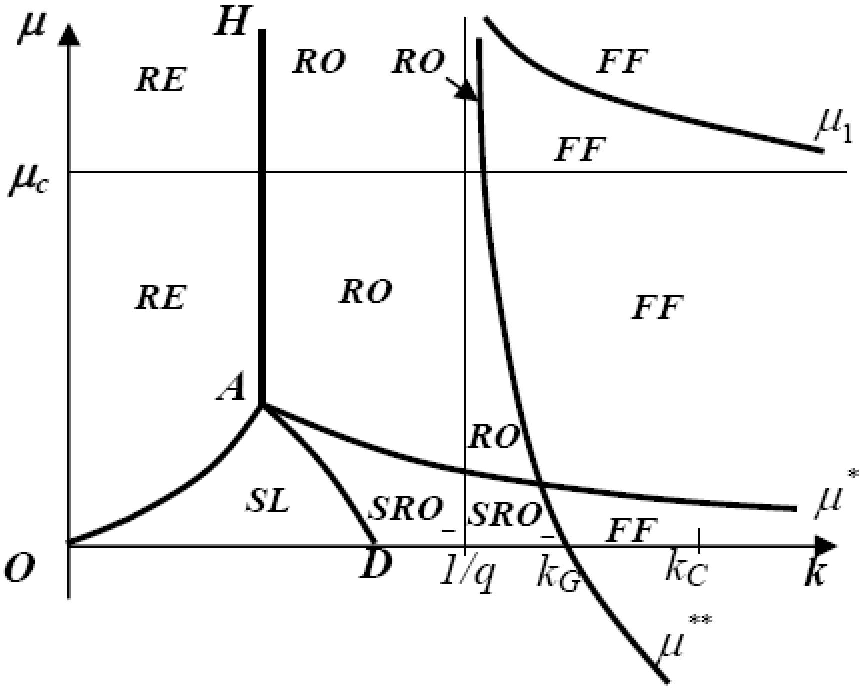

Fig. 60 Regions of all modes for case I2 ($\gamma \le \sqrt{2}$)

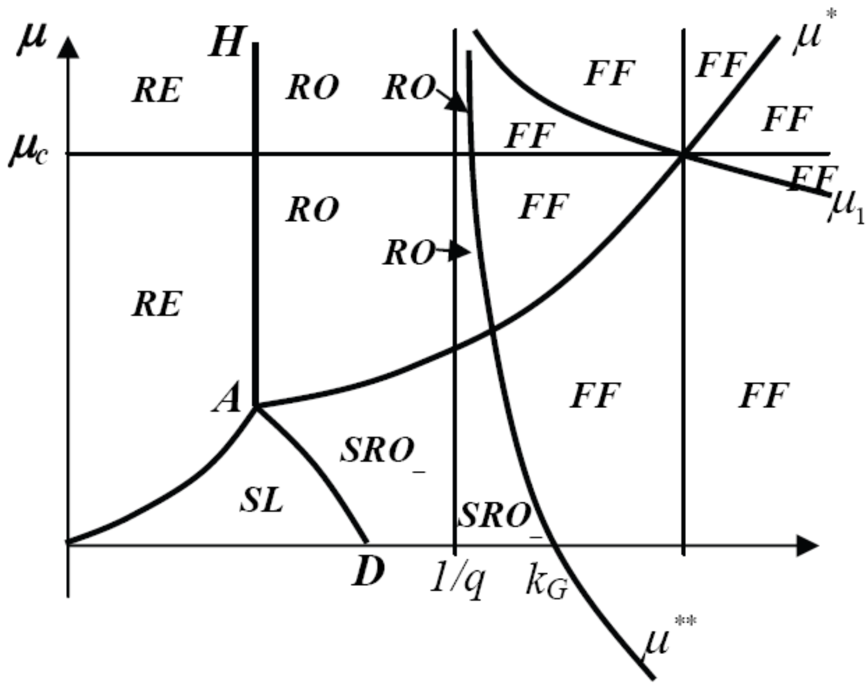

Fig. 61 Regions of all modes for case II ($\gamma \le \sqrt{2}$)

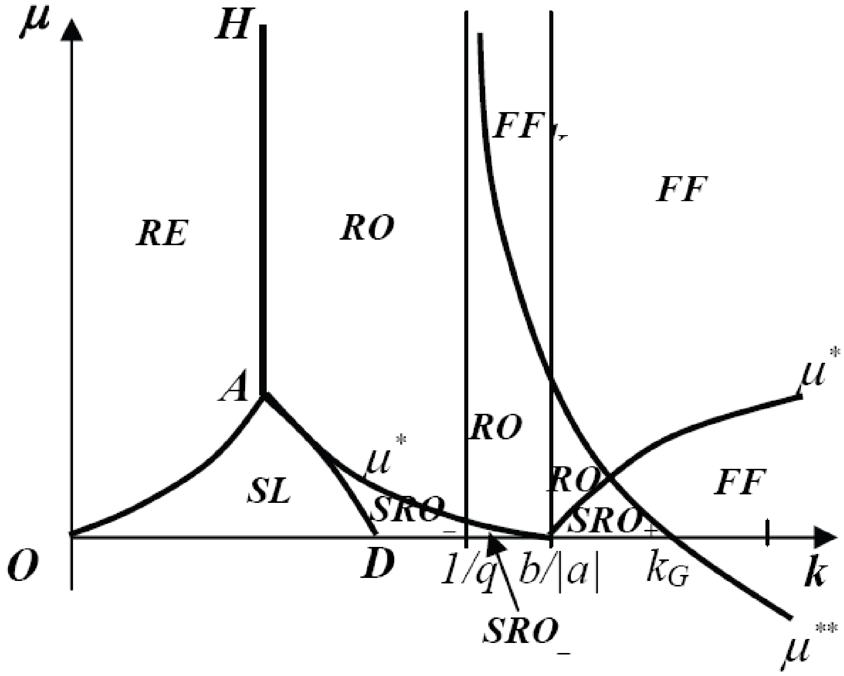

Fig. 62 Regions of all modes for case III1 paired with case V1 ($q\gamma \le 3k'$)

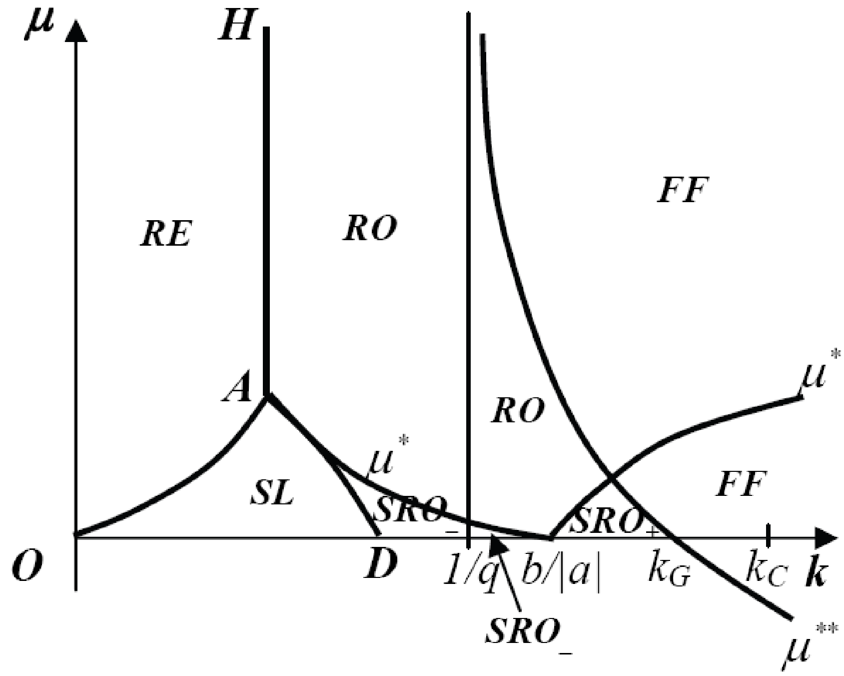

Fig. 63 Regions of all modes for case III1 paired with case V1
($q\gamma \ge 3k', \gamma \le \sqrt{2}$)

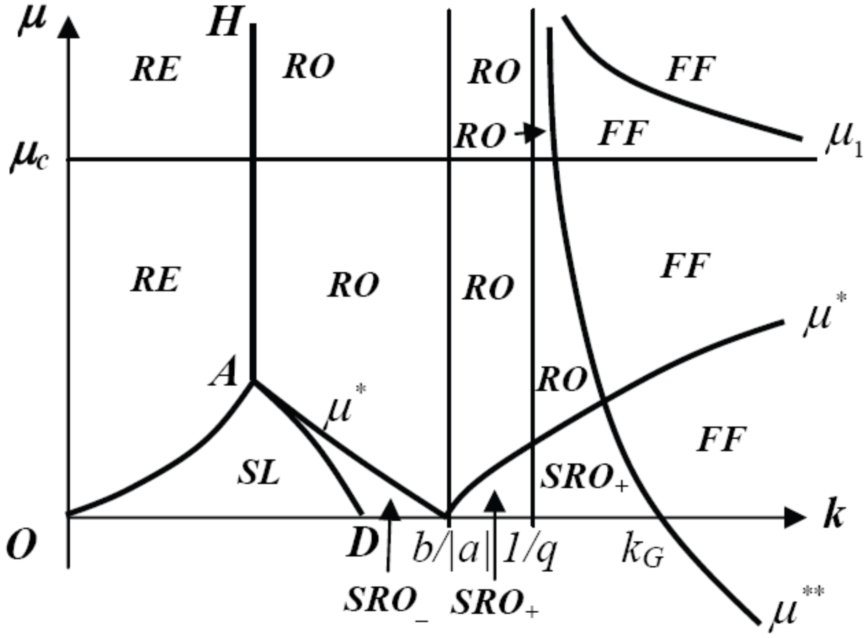

Fig. 64 Regions of all modes for case III2 paired with case V2 ($q\gamma \le 3k'$)

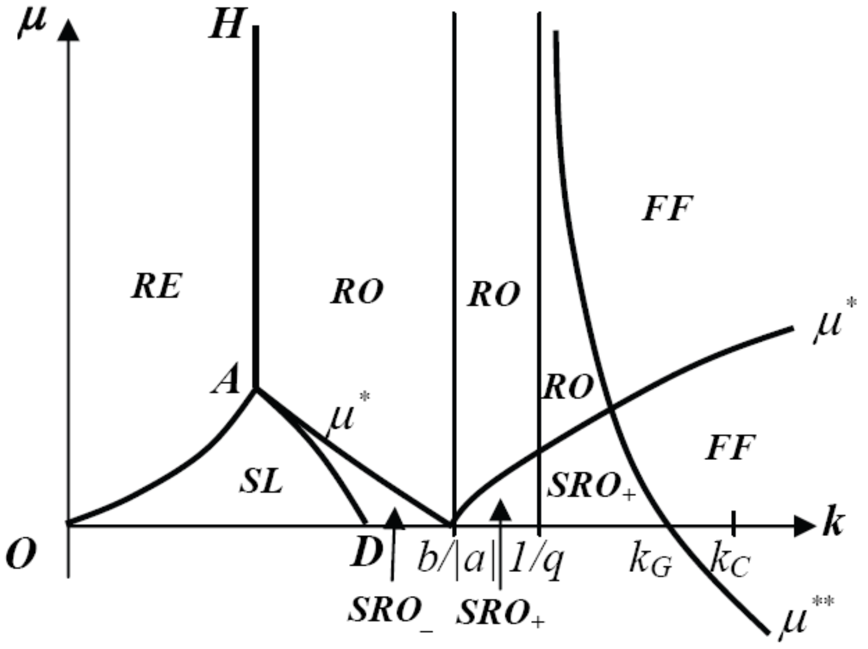

Fig. 65 Regions of all modes for case III2 paired with case V2 ($q\gamma \ge 3k', \gamma \le \sqrt{2}$)

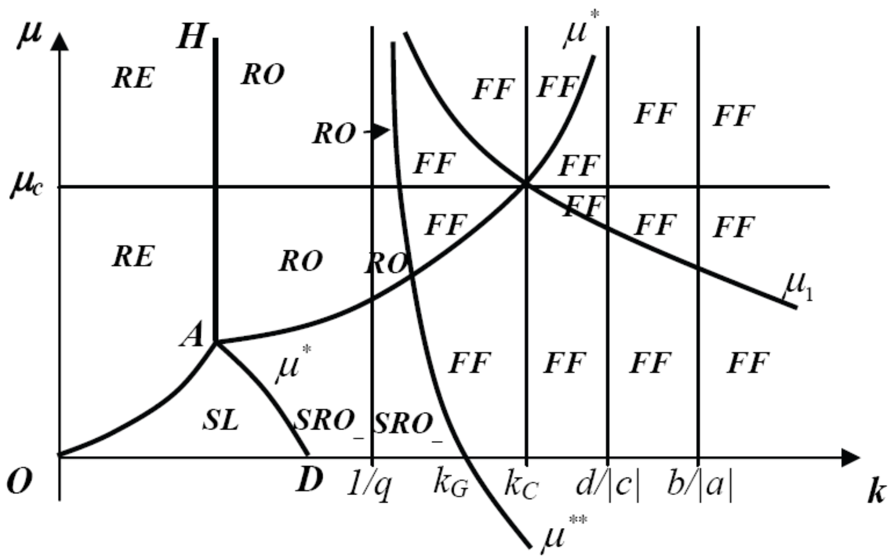

Fig. 66 Regions of all modes for case IV1 ($q\gamma \geq 3k', \gamma \leq \sqrt{2}$**)**

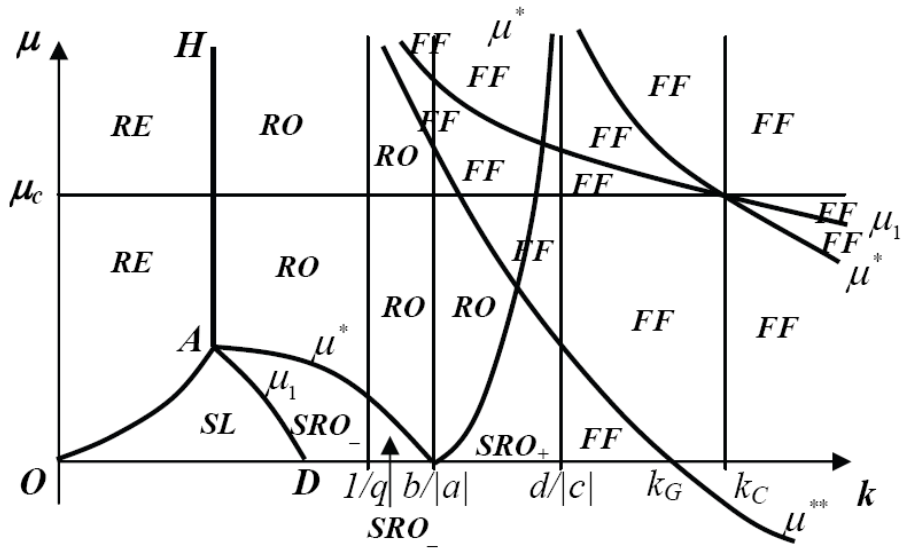

Fig. 67 Regions of all modes for case IV2 paired with case VI1
($q\gamma \geq 3k', \gamma \leq \sqrt{2}$**)**

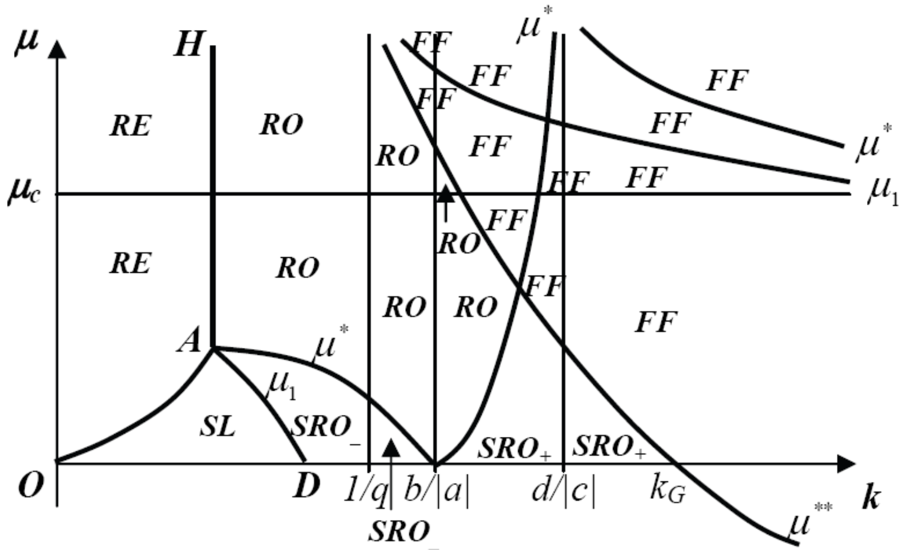

Fig. 68 Regions of all modes for case IV2,2 paired with case VI1,2
($q\gamma \le 3k'$ **)**

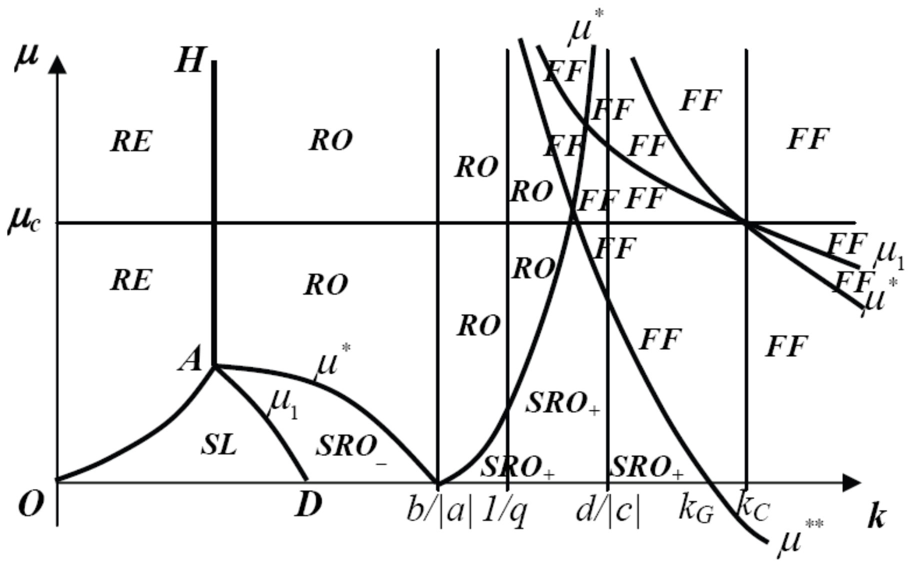

Fig. 69 Regions of all modes for case IV3 paired with case VI2,1
($q\gamma \ge 3k', \gamma \le \sqrt{2}$ **)**

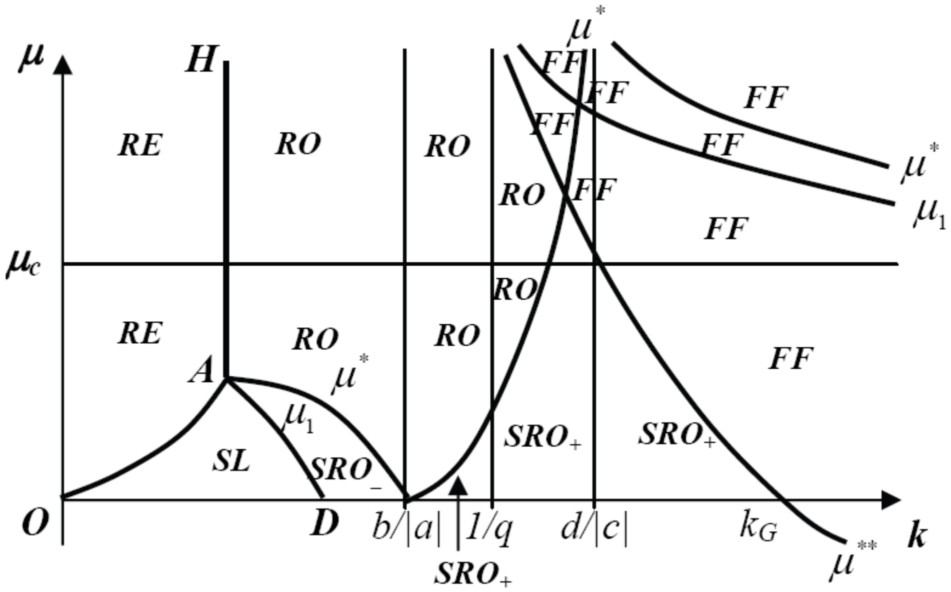

Fig.70 Regions of all modes for case IV3,2 paired with case VI2,2
($q\gamma \le 3k'$)